Universidade Federal de Minas Gerais
Escola de Engenharia
Programa de Pós-Graduação em Engenharia Elétrica

Arthur Noronha Montanari

OBSERVABILITY AND SYNCHRONIZATION OF DYNAMICAL NETWORKS: A NUMERICAL STUDY

Belo Horizonte
2018

Universidade Federal de Minas Gerais

Escola de Engenharia

Programa de Pós-Graduação em Engenharia Elétrica

OBSERVABILITY AND SYNCHRONIZATION OF DYNAMICAL NETWORKS: A NUMERICAL STUDY

Arthur Noronha Montanari

Dissertação de Mestrado submetida à Banca Examinadora designada pelo Colegiado do Programa de Pós-Graduação em Engenharia Elétrica da Escola de Engenharia da Universidade Federal de Minas Gerais, como requisito para obtenção do Título de Mestre em Engenharia Elétrica.

Orientador: Prof. Luis Antonio Aguirre

Belo Horizonte - MG

Agosto de 2018

Montanari, Arthur Noronha.
M764o Observability and synchronization of dynamical networks [recurso eletrônico] : a numerical study / Arthur Noronha Montanari. – 2018.
1 recurso online (xxiii, 100 f. : il., color.) : pdf.

Orientador: Luis A. Aguirre.

Dissertação (mestrado) - Universidade Federal de Minas Gerais, Escola de Engenharia.

Apêndices: f. 97-100.

Bibliografia: f. 87-95.
Exigências do sistema: Adobe Acrobat Reader.

1. Engenharia elétrica - Teses. 2. Estabilidade de Lyapunov - Teses. 3. Filtro de partículas - Teses. 4. Sincronização - Teses. I. Aguirre, Luís Antônio. II. Universidade Federal de Minas Gerais. Escola de Engenharia. III. Título.

CDU: 621.3(043)

Ficha catalográfica: Biblioteca Profº Mário Werneck, Escola de Engenharia da UFMG.

UNIVERSIDADE FEDERAL DE MINAS GERAIS
ESCOLA DE ENGENHARIA
Programa de Pós-Graduação em Engenharia Elétrica

ATA DA 1078ª DEFESA DE DISSERTAÇÃO DE MESTRADO
DO PROGRAMA DE PÓS-GRADUAÇÃO EM ENGENHARIA ELÉTRICA

ATA DE DEFESA DE DISSERTAÇÃO DE MESTRADO do aluno **Arthur Noronha Montanari** - registro de matrícula de número 2017664779. Às 09:30 horas do dia 24 do mês de agosto de 2018, reuniu-se na Escola de Engenharia da UFMG a Comissão Examinadora da DISSERTAÇÃO DE MESTRADO para julgar, em exame final, o trabalho intitulado **"Observability and Synchronization of Dynamical Networks"** da Área de Concentração em Sinais e Sistemas, Linha de Pesquisa Modelagem, Análise e Controle de Sistemas Não Lineares. O Prof. Luis Antonio Aguirre, orientador do aluno, abriu a sessão apresentando os membros da Comissão e, dando continuidade aos trabalhos, informou aos presentes que, de acordo com o Regulamento do Programa no seu Art. 8.16, será considerado APROVADO na defesa da Dissertação de Mestrado o candidato que obtiver a aprovação unânime dos membros da Comissão Examinadora. Em seguida deu início à apresentação do trabalho pelo Candidato. Ao final da apresentação seguiu-se a arguição do candidato pelos examinadores. Logo após o término da arguição a Comissão Examinadora se reuniu, sem a presença do Candidato e do público, e elegeu o Prof .Luis Antonio Aguirre..... para presidir a fase de avaliação do trabalho, constituída de deliberação individual de APROVAÇÃO ou de REPROVAÇÃO e expedição do resultado final. As deliberações individuais de cada membro da Comissão Examinadora foram as seguintes:

Membro da Comissão Examinadora	Instituição de Origem	Deliberação	Assinatura
Prof. Dr. Luis Antonio Aguirre - Orientador	DELT (UFMG)	Aprovado	
Prof. Dr. Luciano Cunha de Araújo Pimenta	DELT (UFMG)	APROVADO	
Prof. Dr. Leonardo Antônio Borges Tôrres	DELT (UFMG)	APROVADO	LABT

Tendo como base as deliberações dos membros da Comissão Examinadora a Dissertação de Mestrado foi .....aprovada..... O resultado final de .....aprovação..... foi comunicado publicamente ao Candidato pelo Presidente da Comissão, ressaltando que a obtenção do Grau de Mestre em ENGENHARIA ELÉTRICA fica condicionada à entrega do TEXTO FINAL da Dissertação de Mestrado.O Candidato terá um prazo máximo de 30 (trinta) dias, a partir desta data, para fazer as CORREÇÕES DE FORMA e entregar o texto final da Dissertação de Mestrado na secretaria do PPGEE/UFMG. As correções de forma exigidas pelos membros da Comissão Examinadora deverão ser registradas em um exemplar do texto da Dissertação de Mestrado, cuja verificação ficará sob a responsabilidade do Presidente da Banca Examinadora. Nada mais havendo a tratar o Presidente encerrou a reunião e lavrou a presente ATA, que será assinada pelo Presidente da Comissão Examinadora. Belo Horizonte, 24 de agosto de 2018.

ASSINATURA DO PRESIDENTE DA COMISSÃO EXAMINADORA

This is for you, Camila, Mom and Dad.

"You see, but you do not observe. The distinction is clear."
– *Sherlock Holmes*

Acknowledgements

There are expressions that do not carry the same impact as in your native language. The following words are in my mother tongue, Portuguese, so that everyone who is mentioned below can *feel* my thankfulness.

Ao meu orientador, Luis Aguirre, pelo acolhimento, ensinamentos e investimento em meu crescimento pessoal durante o desenvolvimento deste trabalho. Obrigado pela confiança depositada, sem a qual toda e qualquer liberdade criativa não seria a mesma. Aguardo com expectativa o prosseguimento da nossa colaboração.

À Camila, meu bem, por todo o suporte, encorajamento e, principalmente, amor que me tem dado ao longo de todos estes anos. Obrigado por suportar meus defeitos, tolerar meus humores e permitir-me compartilhar suas experiências de vida. Nada do que foi será do jeito que já foi um dia. Mas com você, só poderá ser melhor.

Aos meus pais, Mara e Beto, pelo amor e apoio incondicional. Vocês me trouxeram essa vida maravilhosa e graças a vocês cresço de forma mais preparada, forte e consciente. Espero que encontrem em mim o orgulho que procuram. Obrigado por todos os recursos que me forneceram ao longo destes anos para que fosse possível chegar onde cheguei. Agradeço também à (enorme) família que nos acompanha e à minha segunda família que me acolheu nestes últimos anos. Obrigado, Rosana, Ernani e Bi.

Ao meu anterior tutor, Everthon, cujo papel foi além de um tutor acadêmico, me ajudando a encontrar um caminho no qual todo dia de trabalho se torna um dia de prazer.

Aos meus amigos do CPH pelo belo ambiente de trabalho, amizade e ideias que propiciam tantas discussões únicas, sejam produtivas ou completamente inúteis. Trabalhar aqui neste último ano tem sido uma experiência inspiradora.

Aos meus amigos do CEFET-MG, Vitor, Leo, Guilherme, Cléber e todos os outros, que permanecem inseparáveis, não importa a distância física, seja de Pedro Leopoldo a Belo Horizonte, ou do Brasil a Alemanha.

Aos meus amigos do CSA, por cada um dos inumeráveis momentos dos nossos longos anos de amizade, experiências, erros e acertos. Amamos e brigamos como irmãos. Saibam que minha casa sempre estará aberta para todos vocês. Obrigado,

Pedro, Igor, Rosca, Didi, Thz, Biano, Chiquinho, Neman, Few e, por último mas não menos importante, Hugo.

À UFMG, seus professores e funcionários, por disponibilizarem a infraestrutura e conhecimento necessário para a realização deste trabalho. E à CAPES pelo suporte financeiro ao longo de meu programa de Mestrado.

Abstract

Fundamental properties and classic methods of control theory, such as the computation of the observability matrix of a dynamical system or the stability analysis by Lyapunov direct method, faces serious numerical and scalability issues before high-dimensional systems. This led to a renewed interest in literature under the context of large and complex network systems. In this work, we focus on the observability and synchronization properties of dynamical networks—that is, interconnected systems where each node is modeled as an individual dynamical system. For instance, the traditional problem of sensor (actuator) placement in a network can be assessed as an observability (controllability) problem: the choice of the optimal subset of nodes under which a given observability (controllability) metric of the network is maximized. The contributions of this work in the context of observability of network systems are twofold: we review several proposed metric to quantify in a gradual manner the observability of dynamical and network systems; and, noticing a lack of validation in most works, we develop a Bayesian filtering framework, based on particle filtering, for application as a benchmark in observability studies. As shown, the particle filtering can also be used as a means to investigate the interplay between nodal dynamics and the network topology. Numerical results shows the effectiveness of this framework as performance metric for observability in network systems. On the other hand, in the context of synchronization, we investigate the theoretical sufficient conditions for phase synchronization between two interconnected "bridge oscillators" from different clusters of Kuramoto oscillators. In contrast to most graph-theoretical methods in literature, we take a reductionist approach that does not rely on full information of the adjacency matrix—which might be useful since this information is unavailable in some applications. The derived theoretical conditions are compared to numerical simulations. Finally, a brief insight for observability quantification in network systems is suggested in the conclusion.

Keywords: Observability, synchronization, dynamical network, particle filter, cluster synchronization, Lyapunov stability.

Resumo

Propriedades fundamentais e métodos clássicos da teoria de controle, como a computação da matriz de observability ou a análise de estabilidade pelo método direto de Lyapunov, encaram sérios problemas numéricos e de escalabilidade diante de sistemas de alta-dimensão. Isso levou a um interesse renovado na literatura sob o contexto de grandes e complexos sistemas em rede. Neste trabalho, nós focamos nas propriedades de observabilidade e sincronização de redes dinâmicas—isto é, sistemas interconectados em que cada nó é modelado como um sistema dinâmico individual. Por exemplo, o tradicional problema de locação de sensores (atuadores) em uma rede pode ser avaliado como um problema de observabilidade (controlabilidade): a escolha do subconjunto ótimo de nós sob o qual uma dada métrica de observabilidade (controlabilidade) é maximizada. Nossas contribuições sob o contexto de observabilidade em redes dinâmicas são: nós revisamos diversas métricas na literatura que quantificam de maneira gradual a observabilidade de sistemas e redes dinâmicas; e, notando uma absência de validação na grande maioria dos trabalhos, nós desenvolvemos uma metodologia de filtragem Bayesiana, baseada no filtro de partículas, para redes dinâmicas como uma ferramenta de validação de estudos de observabilidade. Conforme demonstrado, o filtro de partículas pode ser usado também como um meio de investigação das interações entre as dinâmicas nodais e a topologia da rede. Resultados numéricos mostram a efetividade deste método como métrica de desempenho para observabilidade de redes. Já em um contexto de sincronismo, nós investigamos as condições suficientes teóricas para sincronismo de fase entre dois interconectados "osciladores ponte" alocados em agrupamentos diferentes de osciladores de Kuramoto. Em contraste com a maioria dos métodos propostos na literatura baseados em teoria de grafos, nós tomamos uma abordagem reducionista que não depende da informação completa da matriz de adjacência—o que pode ser útil uma vez que esta informação é inacessível em determinadas aplicações. As condições teóricas desenvolvidas são comparadas com simulações numéricas. Finalmente, uma breve introspecção para quantificação de observabilidade em redes é sugerida na conclusão.

Palavras-chave: Observabilidade, sincronização, rede dinâmica, filtro de partículas, sincronismo de *clusters*, estabilidade de Lyapunov.

Table of contents

List of figures

List of abbreviations and acronyms

CS	Complete synchronization
GA	Liu and coworkers' graph approach
GS	Generalized synchronization
IPS	Intermittent phase synchronization
LS	Lag synchronization
NRMSE	Normalized root-mean-square error
ODE	Ordinary differential equation
PDF	Probability density function
PF	Particle filter
PS	Phase synchronization (synchronize)
SCC	Strongly connected components
SVD	Singular value decomposition

List of symbols

A	Dynamic matrix. Matrix of dimension $\mathbb{R}^{n\times n}$.
$\bar{A}$	Dynamic matrix of full network. Matrix of dimension $\mathbb{R}^{N\times N}$.
a_i; b_i; c_i	Bifurcation parameters of Rössler system at node v_i.
A_{adj}	Adjacency matrix. Matrix of dimension $\mathbb{R}^{n\times n}$.
b	Ultimate bound.
B	Input (control) matrix. Matrix of dimension $\mathbb{R}^{n\times p}$.
C	Output (measurement) matrix. Matrix of dimension $\mathbb{R}^{q\times n}$.
$C(\mathcal{G})$	Condensation digraph of $\mathcal{G}$.
D	Domain set of interest.
$k_{i,\text{in}}$	In-degree measure of node v_i.
$\mathcal{D}$	Set of driver nodes.
δ	Upper bound of perturbed system.
δ_o	Observability rank.
e_i	Edge.
ϵ; N_t	Arbitrary threshold.
$\boldsymbol{e}$	Dynamic error.
η	Performance index of the particle filter estimates.
$\boldsymbol{f}(\cdot)$	Nonlinear function of the dynamical model. Maps $\mathbb{R}^n \mapsto \mathbb{R}^n$.
$\boldsymbol{F}(\cdot)$; $\boldsymbol{G}(\cdot)$	Arbitrary nonlinear functions.
$\boldsymbol{g}(\cdot)$	Nonlinear function of perturbation model.
$\mathcal{G}$	Graph.
$\mathcal{E}$	Set of edges.
$\mathcal{G}'$	Subgraph of $\mathcal{G}$.
$g_{\max}$	Upper bound of $\|\|\boldsymbol{g}(\cdot)\|\|$.
$\boldsymbol{h}(\cdot)$	Nonlinear function of the output model. Maps $\mathbb{R}^n \mapsto \mathbb{R}^q$.
I_r	Identity matrix. Matrix of dimension $\mathbb{R}^{r\times r}$.
K	Coupling strength.
k_0; c_{1-4}; α	Positive constants.

k	Discrete time instant.
L	Laplacian matrix. Matrix of dimension $\mathbb{R}^{n\times n}$.
$\boldsymbol{\lambda}$	Eigenvalues. Vector of dimension $\mathbb{R}^n$.
$\bar{L}$	Laplacian matrix of full network. Matrix of dimension $\mathbb{R}^{N\times N}$.
$\mathcal{L}_{\boldsymbol{f}}\boldsymbol{h}(\boldsymbol{x})$	Lie derivative of $\boldsymbol{h}(\boldsymbol{x})$ along a vector field $\boldsymbol{f}$.
m	Number of nodes.
$\mathcal{M}$	Maximum matching set.
N	Cardinality of set of nodes in $\mathcal{G}_{\text{full}}$.
n	State variable dimension.
n_{D}	Number of driver nodes.
N_p	Number of particles.
$\mathcal{O}$	Observability matrix. Matrix of dimension $\mathbb{R}^{nq\times n}$.
$\boldsymbol{\omega}$	Oscillator natural frequency. Vector of dimension $\mathbb{R}^n$.
p	Input variable dimension.
$p(a\|b)$	Probability of a given b.
$\mathcal{P}$	Disjoint set.
ϕ	Phase angle.
q	Output variable dimension.
r	Arbitrary radius.
$\mathbb{R}$	Set of real numbers.
Ω	Instantaneous frequency. Vector of dimension $\mathbb{R}^n$.
$\rho(\cdot)$	Rank of a matrix.
$\kappa(\cdot)$	Condtinioning number of a given square matrix.
J	Objective function.
$\boldsymbol{s}$	Output (measurement) variables. Vector of dimension $\mathbb{R}^q$.
$\mathcal{S}$	Set of sensor nodes.
Σ_r	Covariance matrix. Matrix of dimension $\mathbb{R}^{r\times r}$.
T	Time period.
t	Continuous time instant.
t_0	Initial time instant.
θ	Phase difference.
$\bar{\theta}$	Phase difference equilibrium point.
$\boldsymbol{u}$	Input (control) variables. Vector of dimension $\mathbb{R}^p$.
v_i	Node.
$\mathcal{V}$	Set of nodes. Cardinality m.
$\boldsymbol{v}_k$	Measurement noise at time instant k. Vector of dimension $\mathbb{R}^q$.

$V(\cdot)$	Lyapunov function.
$\bar{W}_k^{(p)}$	Normalized importance weight of the pth particle at time instant k.
$\boldsymbol{w}_k$	Process noise at time instant k. Vector of dimension $\mathbb{R}^n$.
W_o	Observability gramian. Matrix of dimension $\mathbb{R}^{n\times n}$.
$W_k^{(p)}$	Importance weight of the pth particle at time instant k.
$\mathcal{X}_i$	Set of vertices at node v_i. Cardinality n_i.
$\boldsymbol{x}$	State variables. Vector of dimension $\mathbb{R}^n$.
$\bar{\boldsymbol{x}}$	Equilibrium point. Vector of dimension $\mathbb{R}^n$.
$\hat{\boldsymbol{x}}$	Estimate of true value $\boldsymbol{x}$.
x_{ij}	Vertex that represents ith state variable at jth node. Element of $\mathcal{X}$.
$\boldsymbol{x}_k$	State variable $\boldsymbol{x}$ at discrete time instant k. Vector of dimension $\mathbb{R}^n$.
$\boldsymbol{x}_k^{(p)}$	pth particle of state variable $\boldsymbol{x}$ at time instant k.
$\boldsymbol{y}_k$	Output variable $\boldsymbol{y}$ at discrete time instant k. Vector of dimension $\mathbb{R}^q$.

Chapter 1

Introduction

1.1 Context and Motivation

The mathematical modeling of *dynamical systems* is a fundamental framework in engineering. Governed by a set of differential equations that simulate the real system behaviour, a mathematical model provides a mean to analyze an existing process, such as its stability, controllability or observability, and thereafter design control techniques for practical applications [19, 56, 59].

Although efficient to systems of low-dimensional order, classic control theory methods are not feasible, for the most part, to high-dimensional systems due to heavy computational burden. For instance, the computation time involved when testing a nonlinear system observability [106], or even calculating its eigenvalues via algorithms based on singular-value decomposition (SVD) techniques, quickly scale if the dynamical system dimension overcome the first few orders of tens [57]. This practical limitation has led control theory notions to be adapted, optimized, or even redefined, in literature for high-dimensional applications [22].

A specific, but recurrent, type of high-dimensional system can be defined as *networks*. A network is a set of nodes interconnected by edges, in which information flows among its elements through pairwise interactions. It can be mathematically modeled by graph structures, which allows a wide range of useful metrics and algorithms of graph theory [91, 21, 8, 14]. For instance, the quantification of a node centrality in a network, or the "amount" of local and global clustering over a network, can be used to assess a power system [134, 135] or biological network [105, 45] robustness to spreading failures.

Up to the end of the twentieth century, it was believed that real-world interconnected systems, such as neuronal, social, communication, traffic, and energy networks, and

even the Internet, were composed of stochastic connections among its nodes. However, recent works over the last decade highlighted that most of real-world networks share recurrent topological characteristics—not being purely random, nor purely regular [6]. *Complex networks*, therefore, is a subclass of mathematical models derived from graph theory, in which topological structures (graphs) shows recurrent patterns that are found in the most diverse real networks present in nature and engineering [21, 8]. Based on these findings, the last years have been flooded by studies about complex networks models, highlighting the *scale-free networks* [7] and *small-world networks* [127].

The study of complex networks is essential to increase the knowledge level of this field about the structural characteristics and recurrent patterns that govern real networks—even when nodal dynamics are disregarded in favor to a higher focus on the graph properties. It is a first step in a long ladder whose final goal is to develop control techniques to *dynamical complex networks* [126]. Dynamical networks are defined by a set of dynamical systems that, when analyzed individually, describes relatively simpler behaviours, but, when interconnected, develops interactions that considerably raises the system complexity [82, 14, 4]. This is a consequence of a twofold interaction between local properties (nodal dynamics between neighbours) and global properties (network structure).

Naturally, in order to improve reliability, many systems were expanded to include complex networks that describe the spatial relations and interactions among their elements. Among the numerous examples are: models of infectious diseases [85, 105], reaction-diffusion systems [129] (e.g. predator-prey models [88]), and boolean systems [44].

In the field of nonlinear dynamics, the study of synchronization in networks of oscillators stands out [11]. In this case, each node is composed of an individual dynamical system, a nonlinear oscillator, and its interactions are determined by couplings among its state variables. Usually, the main goal is to determine under which conditions the synchronization manifold of a dynamical network of oscillators becomes stable. These conditions can be related to the network structure [125, 84], the coupling method [111], or the nonlinear oscillator model—from the well-studied Kuramoto phase oscillator [58, 29] to chaotic ones [11]. Although there are important practical applications to the study of synchronization, such as in power systems [30] or in biological networks [49], it is also possible to consider this field as an approach to investigate and validate nonlinear tools for modeling, analysis and control.

"The ultimate proof of our understanding of natural or technological systems is reflected in our ability to control them", said Liu *et al.* [72]. In 2011, these authors presented a pioneer work on the controllability of network systems. The controllability of a network system is defined as the minimum set of nodes, referred to as *driver nodes*, in which a control signal must be applied in order to conduct the network from any initial state to any desired final state in finite time. They comment on the obstacles of applying brute-force methods from control theory to high-dimensional systems. In that work, an alternative is provided to determine the network controllability with a different definition of controllability grounded on graph theory, the *structural controllability* [70].

Indeed, these fundamental properties of control theory arouse new interest under the context of high-dimensional systems interconnected by networks [115]. Topics such as the study of synchronization, controllability and observability of networks gathered several, but not yet consolidated, results in literature. Liu *et al.* pioneering work created a new branch for research in network systems [72]. However, their results did not considered the nodal dynamics present on a network system, which has led to recurrent criticism on the true applicability of their work [26, 44, 61, 123]. The interplay between the graph structure and nodal dynamics, therefore, remains an open subject to study in network systems.

1.2 Contributions

The focus of this work is to investigate the interplay between the dynamical network nodal dynamics, its coupling methods and the corresponding network structure. Two topics are of main concern: the synchronization stability and the observability of a dynamical network. The contributions of this dissertation are threefold:

Firstly, we thoroughly review the fundamental properties of observability—and by duality controllability—of low-dimensional dynamical systems. We explore the importance of using not only a *crisp* (yes or no) classification of observability, but also one that gradually quantifies *how good* a system observability really is under a specific set of measures. These notions are extended to a network context, where different metrics need to be developed due to high-dimensionality issues. An extensive review and criticism is developed regarding observability metrics based on the network topology properties as represented by its the adjacency matrix. We conclude the review with some interesting guidelines of research in observability and controllability of network systems.

Secondly, following the developed review on observability in network systems, we argue that there is a lack of validation towards novel metrics proposed in literature. To circumvent this problem, using a nonlinear Bayesian filtering method, the particle filtering, we provide an alternative framework to validate observability studies and investigate the interplay between nodal dynamics and network topology [79].

Thirdly, we provide a theorem that determines the sufficient conditions under which a pair of oscillators phase synchronize in a given scenario of interest [80]. This case study consist of two isolated and clustered networks of Kuramoto oscillators being interconnected by a "bridge" among them. If certain conditions are met, a particular reductionist approach can be taken, in which we focus only on the "bridge connection", modeling the other connections as perturbations. This simplified model allows a feasible analysis of the system stability by Lyapunov direct method. Although the studied problem is restrictive, this framework can be generalized to different networks and oscillators.

1.3 Outline

The dissertation is subdivided in six chapters. Chapter 2 presents the used theoretical foundation and notation of system theory and graph theory applied to network systems modeling, while Chapter 3 thoroughly reviews observability of dynamical and network systems. Following the previous discussion, Chapter 4 provides a nonlinear Bayesian filtering class application, the particle filtering, to investigate the importance of nodal dynamics and topology to a network system observability as well as to be used as a benchmark for observability studies in literature. Changing the topics from observability to synchronization, a reductionist framework for analysis of synchronism in a specific case-study of two interconnected clustered networks is provided in Chapter 5. Finally, Chapter 6 concludes the work with its contributions and future works proposals.

Chapter 2

Dynamical Networks Modeling

A *dynamical network* can be studied in three levels: i) the *node dynamics*, described by a dynamical system; ii) the *network topology*, described by a graph; and iii) the *full network*, a combination of both aforementioned levels [4]. The interconnection among independently and comparatively simpler dynamical systems in a network unravels different kinds of interactions that considerably raises the system complexity [82, 14]. Thus, to investigate a full network three components must be considered: i) the graph, which describes the interconnection structure along the network; ii) the coupling method, which describes how these interconnections unfold; and iii) the node dynamics, which describes the isolated nodes behaviour and interactions with its neighbourhood.

This chapter is organized as follows. Section 2.1 formalizes the adopted notation for dynamical systems representation in this work. Section 2.2 reviews fundamental properties of graph theory and some of its most recurrent metrics. And Section 2.3 mathematically defines a dynamical network based on the three aforementioned levels of definition.

2.1 Dynamical Systems Notation

Consider the following state-space representation of a linear continuous time-invariant dynamical system:

$$\begin{cases} \dot{\boldsymbol{x}} = A\boldsymbol{x} + B\boldsymbol{u} \\ \boldsymbol{s} = C\boldsymbol{x} + D\boldsymbol{u} \end{cases}, \tag{2.1}$$

where $\boldsymbol{x} \in \mathbb{R}^n$ is the state vector, $\boldsymbol{u} \in \mathbb{R}^p$ is the input (control) vector, $\boldsymbol{s} \in \mathbb{R}^q$ is the output (measurement) vector, and (A, B, C, D) are matrices of consistent dimensions

known as, respectively, the dynamic matrix, input (control) matrix, output (measurement) matrix and feedforward matrix. Time t dependence is omitted for compactness of notation, only for the system variables $\boldsymbol{x}$, $\boldsymbol{u}$ and $\boldsymbol{s}$. Vectors are defined as column vectors, denoted by bold lower-case letters, and matrix by upper-case letters.

The state-space representation (2.1) can be generalized as a nonlinear continuous time-invariant dynamical system as follows:

$$\begin{cases} \dot{\boldsymbol{x}} = \boldsymbol{f}(\boldsymbol{x}, \boldsymbol{u}) \\ \boldsymbol{s} = \boldsymbol{h}(\boldsymbol{x}) \end{cases} , \tag{2.2}$$

where $\boldsymbol{f} : \mathbb{R}^n \to \mathbb{R}^n$ and $\boldsymbol{h} : \mathbb{R}^n \to \mathbb{R}^q$ are nonlinear functions.

It is assumed that the reader is already familiar with linear and nonlinear system theory. For more details, the reader is referred to [19, 93] for linear systems theory, and to [56, 122] for fundamentals of nonlinear systems. Specific theorems and properties applied throughout this work are revised in their respective chapters. For instance, Section 5.2.2 presents Lyapunov stability theorem, while Chapter 3 reviews observability (and controllability) methods for linear and nonlinear systems.

2.1.1 Oscillators

Among the vast range of nonlinear phenomena to be studied, in this work we are particurlaly interested in oscillatory behaviours—mainly due to its ubiquitous ocurrence in real dynamical networks, as it will be addressed later. A dynamical system is classified as an *oscillator* if its phase portrait contains a stable and isolated *periodic orbit* or, mathematically, if it has a *stable nontrivial solution* satisfying

$$\boldsymbol{x}(t) = \boldsymbol{x}(t+T), \quad \forall t \geq t_0, \quad \text{for some } T > 0 \quad . \tag{2.3}$$

where t_0 is the initial time instant.

A linear system is an oscillator if all its eigenvalues are strictly imaginary conjugate pairs. However, a linear oscillator faces two major problems: i) it is not *structurally stable*, in a sense that any small perturbation to its parameters can break the oscillatory motion and render its equilibrium point stable or unstable; and ii) the amplitude of oscillation is dependent on initial conditions [56].

A nonlinear oscillator, on the other hand, is structurally stable and has periodic orbits whose amplitudes are independent of initial conditions. Thus, a nonlinear system can have a single periodic orbit whose trajectories either converge or diverge in relation

to this set. This periodic orbit is addressed as a *limit cycle*, a type of ω-limit set [56, 59].

A ω-limit set is an *attractor* A if: (i) it is an invariant set (a trajectory $\boldsymbol{x}(t)$ in A never leaves A); (ii) there exists a neighbourhood of A, called as *basin of attraction* $B(A)$, where any initial condition $\boldsymbol{x}(t_0)$ in B converges to A for $t \to \infty$; and (iii) A is minimum, there is no proper subset of A that satisfies the two previous conditions simultaneously. The following ω-limit sets are attractors: equilibrium points, limit cycles, toroidal surfaces and strange attractors [81].

2.1.2 Chaos

A nonlinear dynamical system (2.2) whose trajectories are bounded asymptotically by a *strange attractor* has chaotic dynamics. Among the various definitions of chaos, we state the following [28, 81]. A dynamical system $\boldsymbol{f}$ is chaotic if: (i) $\boldsymbol{f}$ has topological transitivity, i.e. $\|\boldsymbol{x}(t_1) - \boldsymbol{x}(t_2)\| < \epsilon$ for any threshold $\epsilon > 0$ and a sufficient long time t_2; (ii) periodic orbits of $\boldsymbol{f}$ are dense in A; and (iii) $\boldsymbol{f}$ presents sensitive dependence on initial conditions.

In a chaotic system, there is a innumerable set of bounded non-periodic orbits. Since all periodic orbits in A are unstable, a chaotic system *never* completes an orbit in the sense of (2.3). Thus, in a chaotic system context, a system is said to have completed an orbit when

$$\|\boldsymbol{x}(t) - \boldsymbol{x}(t+T)\| < \epsilon, \quad \forall t \geq t_0, \quad \text{for some } T > 0, \quad \text{for a small } \epsilon > 0. \tag{2.4}$$

Therefore, a chaotic orbit is determined by a recurrence in the state-space which occurs at the time instant where a trajectory passes within the vicinity ϵ of a previous point. A common nonlinear tool designed to experimentally assess recurrences in nonlinear systems are recurrence plots [76, 77].

The study of chaotic systems, their behaviour, observability and synchronization is a topic of interest in this work. Others nonlinear concepts, specially Lyapunov exponents and embedding theory, are assumed to be known by the reader.

2.2 Graph Theory

Graph theory provides mathematical definitions, properties and metrics for analysis and design of network systems and even algorithms. This section presents key aspects of graph theory applied throughout the work.

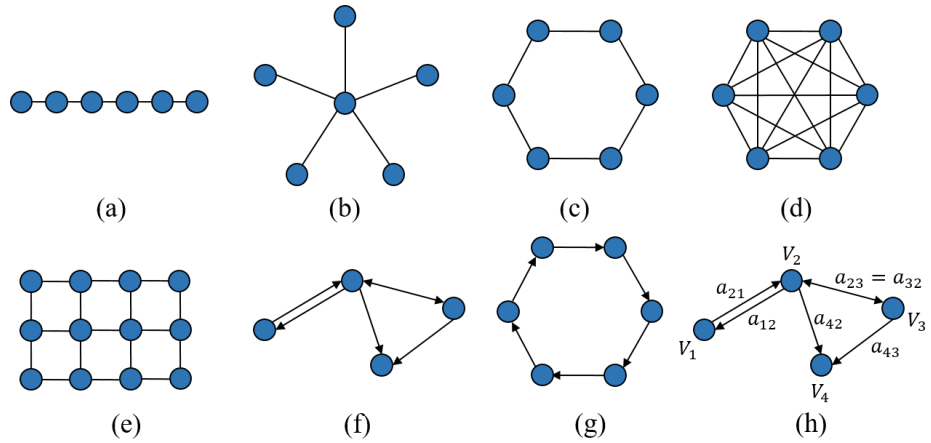

Figure 2.1: Graph examples. (a) Chain or path graph. (b) Star graph. (c) Ring or cycle graph. (d) Complete or fully connected graph. (e) Cartesian grid graph. (f) Digraph. (g) Cycle digraph. (h) Weighted graph.

A *graph* is defined as $\mathcal{G} = \{\mathcal{V}, \mathcal{E}, A\}$, where $\mathcal{V} = \{v_1, v_2, \ldots, v_m\}$ and $\mathcal{E} \subseteq \mathcal{V} \times \mathcal{V} = \{e_1, e_2, \ldots, e_r\}$ are finite sets of m nodes and r edges, respectively. The *adjacency matrix* $A_{\text{adj}} = [a_{ij}]$ is a mapping which associates elements (edges) of $\mathcal{E}$ to a pair of elements (nodes) of $\mathcal{V}$.

We define the following conventions [21, 14]. The reader is referred to [91, 21, 14] for further details. Figure 2.1 illustrates the following types of graph and exemplifies some recurrent graph structures in literature:

- *Undirect and direct graphs.* If (v_i, v_j) are undirectedly linked, then $a_{ij} = a_{ji} > 0$, and A is a symmetric matrix. If (v_i, v_j) are not linked, then $a_{ij} = 0$. This adjacency matrix is denoted as *undirected*. If it is a *directed* graph, or *digraph* for short, then a_{ij} corresponds to an edge connecting node v_j to node v_i [91], but not necessarily contrariwise. If $a_{ii} > 0$, then node i has an edge connecting itself, denoted as *self-loop*.

- *Binary and weighted graphs.* If $A_{\text{adj}} \in \{0, 1\}^{m \times m}$, then the graph is *binary* or *unweighted*. And if $A_{\text{adj}} \in [0, \infty)^{m \times m}$, then the graph is *weighted*.

- *Paths.* A *path* is an ordered sequence of nodes, interconnected by direct edges (if it is a digraph), between a given pair of nodes. A *simple path* has no repeated node in its sequence, except possibly for the initial and final node.

- *Cycle.* A *cycle* is a simple path where the final node equals the inital one, and it has at least 3 nodes. Otherwise, it is *acyclic*.

- *Connected.* A graph is *connected* if there exists a path between any pair of nodes.
- *Subgraph.* A digraph $\mathcal{G}' = \{\mathcal{V}', \mathcal{E}'\}$ is a subgraph of $\mathcal{G}$ if $\mathcal{V}' \subseteq \mathcal{V}$ and $\mathcal{E}' \subseteq \mathcal{E}$.

The aforementioned definitions are the most common classifications of a graph in literature. Based on the type of graph in study, several interesting conclusions can be derived from the graph connectivity properties or some graph metrics[1] [21]. In a dynamical system context, the Laplacian matrix is very useful for modelling of networks of coupled oscillators [14]. These concepts are reviewed as follows.

2.2.1 Connectivity properties

The following connectivity properties are defined as in [14]:

1. $\mathcal{G}$ is *strongly connected* if there exists a directed path between any pair of nodes;
2. $\mathcal{G}$ is *weakly connected* if the undirected version of a digraph is connected;
3. A *globally reachable node* is a node that can be reached from any node by a direct path; and
4. A *directed spanning tree* is a subgraph where a node is the root of directed paths to all other nodes.

A particular definition of interest is the *strongly connected components* (SCC). A subgraph $\mathcal{G}'$ is a SCC if $\mathcal{G}'$ is strongly connected and any subgraph of $\mathcal{G}$ strictly containing $\mathcal{G}'$ is not strongly connected. A *root SCC* is a SCC with no incoming edges. A *condensation digraph* $C(\mathcal{G})$, in turn, is defined as a graph in which its nodes are SCC of $\mathcal{G}$, and there exists a directed edge from node formed by $\mathcal{G}'_1$ to a node formed by $\mathcal{G}'_2$ if there exists a node from $\mathcal{G}'_1$ connected to a node from $\mathcal{G}'_2$. Figure 2.2 illustrates these concepts.

The Laplacian matrix $L = [l_{ij}]$ is defined as follows:

$$L = D_{\text{diag}} - A_{\text{adj}}, \tag{2.5}$$

where $D_{\text{diag}} = \text{diag}(\text{k}_{1,\text{in}}, \text{k}_{2,\text{in}}, \ldots, \text{k}_{\text{m,in}})$ and $k_{i,\text{in}} = \sum_{j=1}^{m} a_{ij}$ is the in-degree of node v_i. Some useful properties of the Laplacian matrix are:

1. L is always symmetric and positive semidefinite.

[1] For the brevity of this text, graph and complex network metrics were omitted. The reader is referred to [25, 21] for further details.

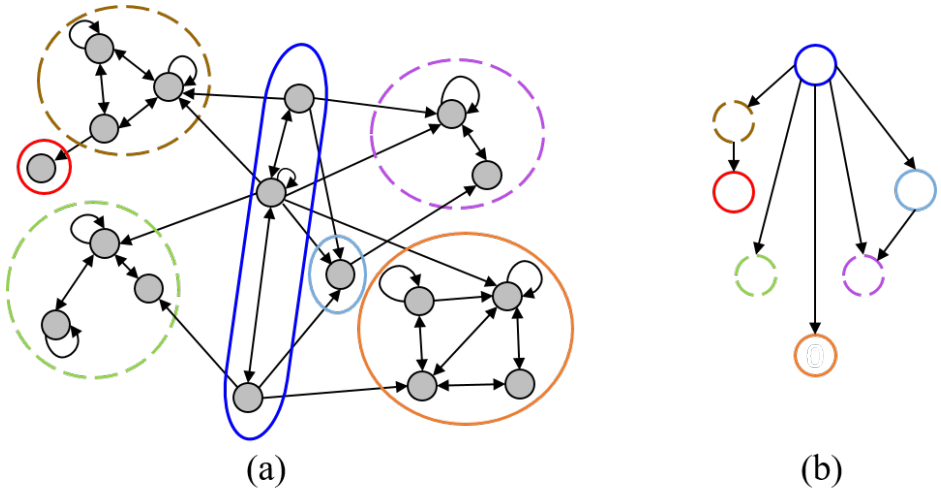

Figure 2.2: (a) SCC (in dashed circles) and root SCC (in solid circle) of a digraph. (b) Condensation graph of (a). [14]

2. Given that $\lambda_1 \leq \lambda_2 \leq \ldots \lambda_m$ are eigenvalues of L, if $\lambda_2 > 0$ (implying $\lambda_1 = 0$), then the network is connected [12].

The Laplacian matrix is specially interesting for oscillators networks modelled in a state-space representation, as it is presented in Example 2.1.

2.3 Dynamical Networks

A dynamical network is a set of dynamical systems—possibly oscillators—interconnected according to a network topology described by an adjacency matrix. Although these dynamical systems are relatively simple when analyzed individually, it is the interactions among those oscillators dynamics and their local and global neighbourhood that considerably raises the network system complexity. This interplay is not only governed by the nodal dynamics and the adjacency matrix, but also by the coupling method.

In this section, we investigate dynamical networks, or networks for short, from two points of view: (i) a graph approach, and (ii) a dynamic systems approach.

2.3.1 Graph theory approach

We follow the paradigm exposed in [4] for a "graph theory approach" to model dynamical networks, extending it mathematically to a more generic case. Overall, a dynamical network is described by a network topology $\mathcal{G}$ which determines the interconnection structure among every element of $\mathcal{V}$. However, in a dynamical network, every node v_i

is composed of a dynamical system (A_i, B_i, C_i, D_i). In order to include the effects of nodal dynamics, we represent the dynamical system (A_i, B_i, C_i, D_i) of a given node v_i by its corresponding graph $\mathcal{G}_i$. Thus, every node in $\mathcal{G}$ is expanded as subgraph $\mathcal{G}_i$. The "expanded" network is the full network graph $\mathcal{G}_{\text{full}}$. We detail the approach formally as follows.

Consider a network of m nodes whose topology is described by a graph $\mathcal{G} = \{\mathcal{V}, \mathcal{E}, A_{\text{adj}}\}$. Consider that each node $v_i \in \mathcal{V}$ represents a n_i-dimensional linear dynamical system, as in (2.1). Hence, each multi-dimensional system placed in a node v_i can be described by a graph $\mathcal{G}_i = \{\mathcal{V}_i, \mathcal{E}_i, A_i\}$. Note that, assuming $B = C = D = 0$, the dynamical matrix A_i of a dynamical system in node v_i is the adjacency matrix of graph $\mathcal{G}_i$.

Basically, each node v_i is dismembered as an individual graph $\mathcal{G}_i$ that are, in turn, interconnected among themselves by the graph $\mathcal{G}$ (the network topology). In order to distinguish the nomenclature between the nodes of the network topology from the nodes of a nodal dynamical system, we define that: a *set of nodes* $\mathcal{V} = \{v_1, v_2, \ldots, v_m\}$ refers to the *network topology graph* $\mathcal{G} = \{\mathcal{V}, \mathcal{E}, A_{\text{adj}}\}$, while a *set of vertices* $\mathcal{X}_i = \{x_{1i}, x_{2i}, \ldots, x_{n_i i}\}$ refers to the *nodal dynamic system graph* $\mathcal{G}_i = \{\mathcal{X}_i, \mathcal{E}_i, A_i\}$, of a dynamic system (A_i, B_i, C_i, D_i) present in node v_i.

Graphs $\{\mathcal{G}_1, \mathcal{G}_2, \ldots, \mathcal{G}_m\}$ are, therefore, subgraphs of a bigger graph $\mathcal{G}_{\text{full}}$ that represents the *full network* graph. Graph $\mathcal{G}$, in turn, is only a subgraph of $\mathcal{G}_{\text{full}}$ if the oscillators are coupled by the *same* variable among themselves[2]. Full network $\mathcal{G}_{\text{full}}$ has, therefore, $N = \sum_{i=1}^{m} n_i$ nodes, or $N = nm$ nodes if all nodal systems share the same dimension $n_1 = n_2 = \ldots = n_m = n$. These concepts are illustrated in Fig. 2.3. Note that $\mathcal{G}_{\text{full}}$ describes not only the interconnections among the dynamical systems, but also which variable is interconnected.

This notation is only valid for linear dynamical matrices coupled by a linear graph (i.e. a linear coupling method). For nonlinear dynamical systems (2.2), or nonlinear couplings between the nodes, we use the following representation [4]: linear connections are represented by solid lines, while nonlinearities are represented by dashed lines. This convention is a reminder that nonlinear connections are not anymore constant and might vanish under specific circumstances. The nonlinear graph now faces singularity issues that can have a huge impact for the "information flow" between two nodes, or vertices, interconnected by a nonlinear connection. See Example 2.2 for further details. This representation has great value for symbolic analysis, as presented in an observability context [63, 10, 4].

[2]This is later examplified in Example 2.2.

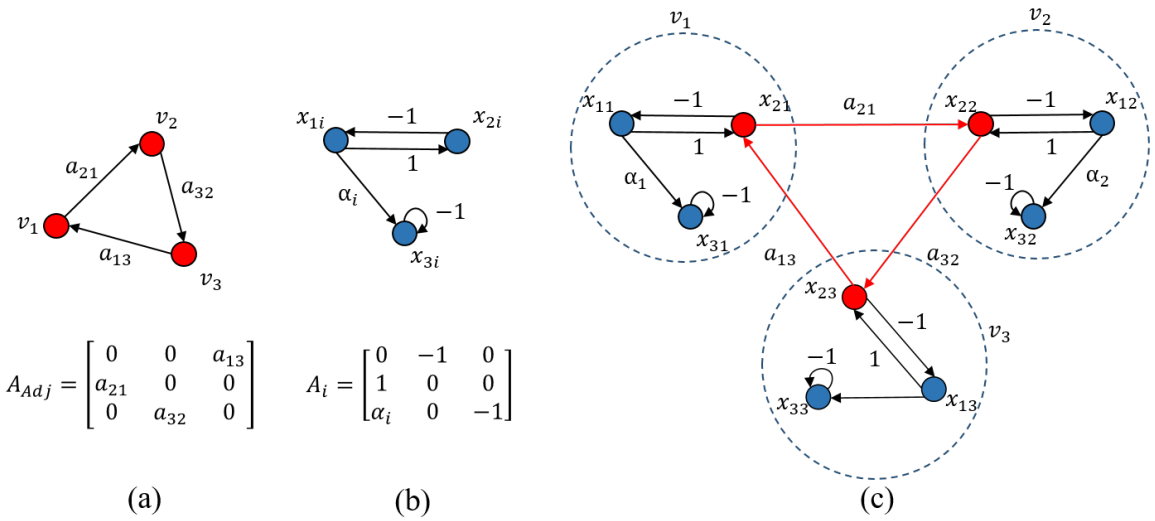

Figure 2.3: (a) Network topology graph, and respective adjacency matrix. (b) Nodal dynamical system graph of a 3-dimensional linear oscillator $\mathcal{X}_i = \{x_{1i}, x_{2i}, x_{3i}\}$, and respective dynamic matrix. (c) Full network graph of a network topology graph described in (a) where each node is composed of a linear oscillator presented in (b) coupled by the x_{2i} variable.

2.3.2 System theory approach

Naturally, a dynamical network can be represented as a larger dynamical system[3] (2.2), where $\boldsymbol{x} = \begin{bmatrix} \boldsymbol{x}_1^\mathsf{T} & \boldsymbol{x}_2^\mathsf{T} & \dots & \boldsymbol{x}_m^\mathsf{T} \end{bmatrix}^\mathsf{T} \in \mathbb{R}^N$, $\boldsymbol{x}_i = \begin{bmatrix} x_{1i} & x_{2i} & \dots & x_{n_i i} \end{bmatrix}^\mathsf{T} \in \mathbb{R}^{n_i}$ and $\boldsymbol{f} : [t_0, \infty) \times \mathbb{R}^N \to \mathbb{R}^N$. Thus, x_{ji} is the j-th state variable of the dynamical system present in node v_i, and $\boldsymbol{x}_i$ is the column vector of state variables in node v_i.

The linear counterpart of (2.2) is:

$$\dot{\boldsymbol{x}} = \bar{A}\boldsymbol{x}, \tag{2.6}$$

where $\bar{A} \in \mathbb{R}^{N \times N}$ is the dynamical matrix of the full network $\mathcal{G}_{\text{full}}$.

The usual high dimensionality of (2.2) and (2.6) turns traditional methods for system analysis and control design rather unfeasible[4]. It can be argued that this generic representation of any N-dimensional dynamical system is not suitable for a network context because it does not highlight the main properties of a dynamical network and, therefore, provides little insight to the analysis.

[3] For the sake of simplicity, no input or output is considered in what follows.

[4] Some examples are the application of Lyapunov theorem [56], the computation of the controllability (observability) matrix rank [72], or the computation of the dynamical matrix eigenvalues through SVD techniques [57].

As stated in [4], a full dynamical network is composed of an interplay of two levels: (i) the nodal dynamics, described by the dynamical system state-space representation $\boldsymbol{f}(\cdot)$ (or A_i in linear applications); and (ii) the topological structure, described by the adjacency matrix A_{adj} and the Laplacian matrix L. In a linear graph composed of linear dynamical systems in its nodes, this can be shown explicitely due to the superposition principle:

$$\begin{bmatrix} \dot{\boldsymbol{x}}_1 \\ \dot{\boldsymbol{x}}_2 \\ \vdots \\ \dot{\boldsymbol{x}}_m \end{bmatrix} = \left(\begin{bmatrix} A_1 & 0 & \dots & 0 \\ 0 & A_2 & \dots & 0 \\ \vdots & \vdots & \ddots & \vdots \\ 0 & 0 & \dots & A_m \end{bmatrix} + \bar{L} \right) \cdot \begin{bmatrix} \boldsymbol{x}_1 \\ \boldsymbol{x}_2 \\ \vdots \\ \boldsymbol{x}_m \end{bmatrix} \tag{2.7}$$

where $\bar{L}$ the Laplacian matrix of the full network graph, describing the connection among all the network system state variables (including nodes and vertices). For instance, the dynamical network (2.7) can be represented by a "full graph" as in the example of Fig. 2.3. In this case, the nodal dynamics $A_1 = A_2 = A_3 = A$ are represented by the corresponding graph in (b), and the coupling dynamics dictated by $\bar{L}$ is represented by the graph of the network topology in (a). Since in Fig. 2.3 the coupled variables are the same among the network nodes, the Laplacian matrix L of the network topology is identical to the Laplacian matrix $\bar{L}$ of the "full network", i.e. $L \equiv \bar{L}$. This is not true if the coupled variables are not the same, as in Fig. 2.5b.

Although a system of high-dimension, the dynamical matrix $\bar{A}$ of a dynamical network, specially if the graph is not completely connected, is rather sparse. Moreover, if the network is composed of similar oscillators (with parametric differences), then several patterns and properties can be explored. Representation (2.7) provides further insight on how the interactions of a network system unfold from its nodal dynamics and topology.

In this work, two specific oscillators are taken as benchmark examples for theoretical and numerical analysis in dynamical networks: the Kuramoto phase oscillator [58] and the Rössler attractor [102]. The former for its rich dynamic behaviour with the added advantage of being described by rather simple equations. The latter for its chaotic behaviour, wide knowledge in literature and interesting observability properties. The state space representations of both oscillators are presented in the following examples.

Example 2.1. Network of Kuramoto phase oscillators.

The Kuramoto phase oscillator is a linear dynamical system defined as [58]:

$$\dot{x} = \omega, \tag{2.8}$$

where $x \in \mathbb{R}$ is the oscillator state variable, its phase angle, and ω is the oscillator natural frequency.

Although described by a rather simple equation, the Kuramoto oscillator show a rich dynamical behaviour when interconnected in a network by a sinusoidal coupling [29]. Consider a network $\mathcal{G} = \{\mathcal{V}, \mathcal{E}, A_{\text{adj}}\}$ of Kuramoto oscillators where each oscillator $v_i \in \mathcal{V}$ is represented by the phase angle $x_i \in \mathbb{R}$ (i.e. $v_i \equiv x_i$). The dynamical benchmark network can be represented by the following continuous state-space model [125, 84, 21, 29]:

$$\dot{x}_i = \omega_i + \sum_{j=1}^{N} a_{ij} \sin(x_j - x_i), \quad i = 1, 2, \ldots, m, \tag{2.9}$$

where $\boldsymbol{x} = \begin{bmatrix} x_1 & x_2 & \ldots & x_N \end{bmatrix}^{\mathsf{T}} \in \mathbb{R}^N$, m is the network size (and number of states n of the dynamical network, in this case), and $A_{\text{adj}} = [a_{ij}]$. Note that the coupling among the oscillators is additive, diffusive[5] and proportional to the coupling strength a_{ij}.

Alternatively, (2.9) can be rewritten as a function of the Laplacian matrix:

$$\dot{\boldsymbol{x}} = \boldsymbol{\omega} + \sum_{j=1}^{N} L \odot \sin\left(\mathbf{1}\boldsymbol{x}^{\mathsf{T}} - \boldsymbol{x}\mathbf{1}^{\mathsf{T}}\right), \tag{2.10}$$

where $\boldsymbol{\omega} = \begin{bmatrix} \omega_1 & \omega_2 & \ldots & \omega_N \end{bmatrix}^{\mathsf{T}}$, $\mathbf{1} \in \{1\}^N$ (N-dimensional column vector of "ones"), $\odot$ denotes the Hadammard product (element-wise product).

If x is bounded in a small region of the equilibrium point[6], it is possible to linearize (2.10) with a reasonable accuracy, yielding the following linear representation

$$\dot{\boldsymbol{x}} = \boldsymbol{\omega} - L\boldsymbol{x}. \tag{2.11}$$

△

[5] A diffusive coupling is defined through the weighted difference between state variables belonging to different nodes.

[6] Usually, $\|x\| \leq 5°$, since in this region $\sin x \approx x$.

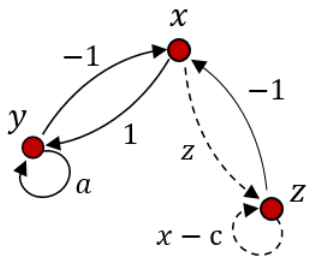

Figure 2.4: Nonlinear graph of Rössler system.

Example 2.2. Network of Rössler systems.

The well-known Rössler system is given by the following set of ordinary differential equations (ODE) [102]:

$$\begin{cases} \dot{x} &= -y - z \\ \dot{y} &= x + ay \\ \dot{z} &= b + z(x - c) \end{cases} \tag{2.12}$$

where (a, b, c) are bifurcation parameters. A typical set of parameters considered in this work is $(b, c) = (2, 4)$ and $a \in [0.3, 0.55]$.

Figure 2.4 illustrates how a nonlinear system such as the Rössler system can be represented as a "nonlinear graph" using the Jacobian matrix $D\boldsymbol{f}$ of (2.12):

$$D\boldsymbol{f} = \begin{bmatrix} 0 & -1 & -1 \\ 1 & a & 0 \\ z & 0 & x - c \end{bmatrix}. \tag{2.13}$$

Note that edges $a_{33} = x - c$ and $a_{31} = z$ might vanish under certain conditions ($x(t) = c$ and $z(t) = 0$), interrupting the flow of information.

Consider now a network of Rössler oscillators coupled by the y variable [96, 11]. Hence, in each node $v_i \in \mathcal{V}$ there is a system with three state variables $\boldsymbol{x}_i = \begin{bmatrix} x_i & y_i & z_i \end{bmatrix}^\intercal$. The dynamical network can be represented by the following state-space model:

$$\begin{cases} \dot{x}_i &= -y_i - z_i \\ \dot{y}_i &= x_i + a_i y_i + \sum_{j=1}^{N} a_{ij}(y_j - y_i)\,, \quad i = 1, 2, \ldots, m. \\ \dot{z}_i &= b_i + z_i(x_i - c) \end{cases} \tag{2.14}$$

where m is the network size, (a_i, b_i, c_i) are the parameters of the ith Rössler system, and $A = [a_{ij}]$ is the network adjacency matrix. This is a state-space model of dimension

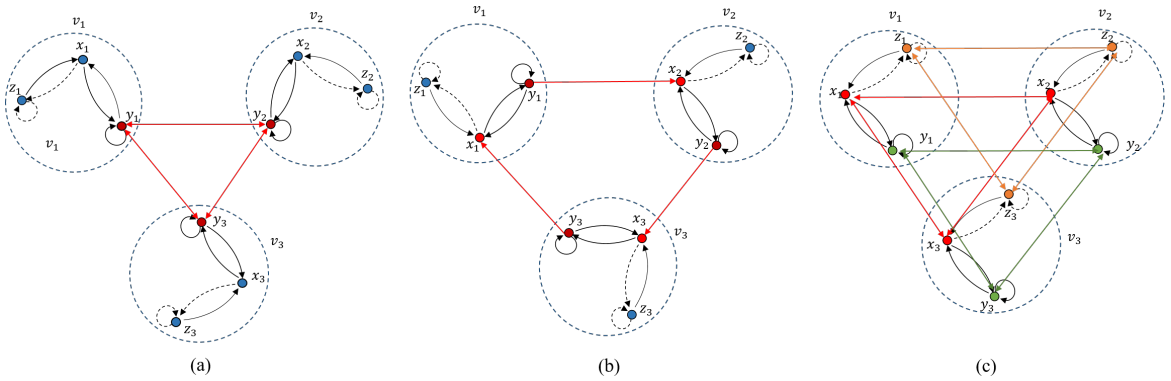

Figure 2.5: Full network of Rössler systems coupled (a) undirectedly by y variable, (b) directly from variable y to x, and (c) undirectedly between all respective variables. For simplification purposes, the network topology is a chain graph.

$n = 3m$. Note that, differently from the Kuramoto network, the coupling method is linear. Equations (2.15) and (2.16) exemplifies two occasions where the network of Rössler systems are interconnected by a direct couple from y to x, or undirectedly coupled by all variables (also known as "network of networks" [18]):

$$\begin{cases} \dot{x}_i &= -y_i - z_i + \sum_{j=1}^{N} a_{ij}(y_j - x_i) \\ \dot{y}_i &= x_i + a_i y_i \\ \dot{z}_i &= b_i + z_i(x_i - c) \end{cases} , \quad i = 1, 2, \ldots, N, \quad \text{and} \tag{2.15}$$

$$\begin{cases} \dot{x}_i &= -y_i - z_i + \sum_{j=1}^{N} a_{ij}(x_j - x_i) \\ \dot{y}_i &= x_i + a_i y_i + \sum_{j=1}^{N} a_{ij}(y_j - y_i) \\ \dot{z}_i &= b_i + z_i(x_i - c) + \sum_{j=1}^{N} a_{ij}(z_j - z_i) \end{cases} , \quad i = 1, 2, \ldots, N. \tag{2.16}$$

Dynamical networks (2.14), (2.15) and (2.16) are illustrated as full networks in Fig. 2.5. Note that the network topology graph $\mathcal{G}$ is not a subgraph of $\mathcal{G}_{\text{full}}$ in (2.15). The presented examples are only illustrations of how a full network, with different coupling methods, can be represented by a set of ODEs and its corresponding graphs. We are not concerned with the "physical" feasibility of these interconnected systems. △

Although this work mainly studies the nonlinear oscillators of Kuramoto and Rössler, during our review of literature, several others dynamical networks have been used as benchmarks in literature to study controllability and observability properties. Some examples that we find interesting ones are found in chemical reactions [73], food web [26], power systems [95, 115], social networks [95], epidemic spreading [95],

and combustion networks [48]. Several real network topologies have been used as benchmarks in [72] and subsequent works, although in this case none have its nodal dynamics modeled.

Chapter 3

A Review on Observability of Network Systems

Observability is a measure that determines if the trajectory temporal evolution of the internal states of a dynamical system can be reconstructed based on knowledge of the inputs and outputs, as introduced by R.E. Kalman [54]. The classic concept of observability, addressed in this work as *structural observability*, is based on a *crisp* definition, i.e. the system is or is not observable [19]. This concept can be extended by metrics that quantify observability in a gradual or continuous manner, i.e. measuring *how well* the system trajectory can be reconstructed [40, 1], which we address as *dynamical observability*. Sections 3.1 and 3.2 reviews both approaches to quantify the observability of a linear and nonlinear dynamical system.

In a network systems context, it is a reasonable assumption that not all nodes are available for measurement. Thus, two important goals for network systems are: i) to determine if a given set of sensor nodes[1] renders the network observable, a problem that can be assessed by *structural observability* metrics; and ii) to determine the *best* (or minimum) set of sensor nodes from different configurations, a problem that can only be solved by *dynamical observability* metrics.

However, the observability metrics presented in Sections 3.1 and 3.2 are unfeasible for high-dimensional systems [106], including dynamical networks. A recurrent approach in literature to assess a network observability is to refer to its respective graph representation. This approach is addressed in this work as *topological observability*, reviewed in Section 3.3. Since the concept of *topological* analysis was born in a con-

[1] A common jargon in literature is to refer to nodes available for measurement (output signals) as *sensor nodes*, and control nodes as *driver nodes*.

trollability context, some discussion might be focused on controllability rather than observability, relying on the duality between both concepts.

Finally, Section 3.4 briefly comments on some other proposals to quantify a (network) system observability.

We refer to [4] for the adopted nomenclature and classification of observability metrics in this chapter.

3.1 Structural Observability

3.1.1 Linear dynamical systems

The classic concepts of observability for linear systems were introduced by Rudolf E. Kalman [54]. The following definition and theorem is further discussed and proven in many textbooks in linear systems theory such as [19].

Definition 3.1. *[19, Definition 6.O1] The linear system (2.1) or the pair $(\boldsymbol{A}, \boldsymbol{C})$ is said to be observable if for any unknown initial state $\boldsymbol{x}(t_0)$, there exists a finite time $t_1 > 0$ such that the knowledge of the input $\boldsymbol{u}$ and the output $\boldsymbol{y}$ over $t \in [t_0, t_1]$ suffices to determine uniquely the initial state $\boldsymbol{x}(t_0)$. Otherwise, (2.1) is said to be unobservable.*

Theorem 3.1. *[19, Theorem 6.O1] The following statements are equivalent.*

1. *The n-dimensional pair (A, C) is observable.*
2. *The matrix $W_o(t) \in \mathbb{R}^{n \times n}$*

$$W_o(t) = \int_{t_0}^{t} e^{A^\mathsf{T}\tau} C^\mathsf{T} C e^{A\tau} d\tau \tag{3.1}$$

   is nonsingular for any $t > t_0$.

3. *The observability matrix $\mathcal{O} \in \mathbb{R}^{nq \times n}$*

$$\mathcal{O} = \begin{bmatrix} C \\ CA \\ CA^2 \\ \vdots \\ CA^{n-1} \end{bmatrix} \tag{3.2}$$

   has full column rank $\rho(\mathcal{O}) = n$.

4. *The matrix* $\begin{bmatrix} A - \lambda I & C \end{bmatrix}^{\mathsf{T}}$ *has full column rank at every eigenvalue* λ_i *of* A*, for* $i = 1, 2, \ldots, n$.

5. *If all eigenvalues* $\lambda_i < 0$*, for* $i = 1, 2, \ldots, n$*, then the unique solution, called observability Gramian, of*

$$A^{\mathsf{T}} W_o + W_o A = -C^{\mathsf{T}} C \tag{3.3}$$

is positive definite. It can be expressed as

$$W_o = \int_{t_0}^{\infty} e^{A^{\mathsf{T}} \tau} C^{\mathsf{T}} C e^{A\tau} d\tau \tag{3.4}$$

■

Equivalence between statements (1)-(5) is proven in [19]. We state an alternative view on the equivalence between statements (1) and (3). According to Definition 3.1, suppose that the input $\boldsymbol{u}$ and output $\boldsymbol{s}$ are known over $t \in [t_0, t_1]$. The ability to determine uniquely the initial state $\boldsymbol{x}(t_0)$ is related to the possibility of determining the values of its derivatives $\{\boldsymbol{x}^{(1)}, \boldsymbol{x}^{(1)}, \ldots, \boldsymbol{x}^{(n-1)}\}$ from knowledge of $\{\boldsymbol{s}, \boldsymbol{s}^{(1)}, \ldots, \boldsymbol{s}^{(n-1)}\}$. Thus:

$$\begin{aligned}
\begin{bmatrix} \boldsymbol{s} \\ \boldsymbol{s}^{(1)} \\ \vdots \\ \boldsymbol{s}^{(n-1)} \end{bmatrix} &= \begin{bmatrix} C\boldsymbol{x} + D\boldsymbol{u} \\ C(A\boldsymbol{x} + D\boldsymbol{u}) + D\boldsymbol{u}^{(1)} \\ \vdots \\ C(A \ldots (A\boldsymbol{x} + B\boldsymbol{u})) + D\boldsymbol{u}^{(n-1)} \end{bmatrix} \\
\begin{bmatrix} \boldsymbol{s} \\ \boldsymbol{s}^{(1)} \\ \vdots \\ \boldsymbol{s}^{(n-1)} \end{bmatrix} &= \begin{bmatrix} C \\ CA \\ \vdots \\ CA^{n-1} \end{bmatrix} \boldsymbol{x}(t_0) + \begin{bmatrix} D & 0 & \ldots & 0 \\ CB & D & \ldots & 0 \\ \vdots & \vdots & \ddots & \vdots \\ CA^{n-2}B & CA^{n-3}B & \ldots & D \end{bmatrix} \begin{bmatrix} \boldsymbol{u} \\ \boldsymbol{u}^{(1)} \\ \vdots \\ \boldsymbol{u}^{(n-1)} \end{bmatrix}.
\end{aligned} \tag{3.5}$$

The second term on the right, the control input, is known. Subtracting it from the measured output $\boldsymbol{s}$ vector and its derivatives yields

$$\bar{\boldsymbol{s}} = \begin{bmatrix} C \\ CA \\ \vdots \\ CA^{n-1} \end{bmatrix} \boldsymbol{x}(t_0) \equiv \mathcal{O}\boldsymbol{x}(t_0). \tag{3.6}$$

Since $\bar{\boldsymbol{s}}$ is known, the initial state $\boldsymbol{x}(t_0)$ can be determined (i.e. the system is observable) if $\bar{\boldsymbol{s}}$ is within the image of $\mathcal{O}$—which is always true if the dimension of the null space of $\mathcal{O}$ is zero, implying $\rho(\mathcal{O}) = n$. Because, from Cayley-Hamilton Theorem [19, Theorem 3.4], CA^n is a linear combination of its lower degree terms $\{C, CA, \ldots, CA^{n-1}\}$, the rank of $\mathcal{O}$ stops growing if terms CA^t, for $t \geq n$, were added to it—which implies that the dimension of the image space of $\mathcal{O}$ stops growing too.

Theorem 3.2. *[19, Theorem 6.O2] The observability property is invariant under equivalence transformation.*

Remark 3.1. Although $W_o \neq \mathcal{O}$, the following equality holds, $\text{rank}(W_o) = \text{rank}(\mathcal{O}) = n_o$, where n_o is the dimension of the observable subspace.

Note that Definition 3.1 only classifies the pair (A, C) as observable or unobservable. Thus, we refer to Theorem 3.1 as a *structural observability* index. This *crisp* classification of observability is due to the observability index being based on a *discrete* rank condition of (3.2). Consequently, the index of observability is a discontinuous function of the system parameters such that, in the borderline, a small change in the parameter space of (2.6) can move a dynamical system from unobservable to observable.

Suppose that matrix W_o is nonsingular, but *ill-conditioned*. For practical purposes, W_o can become *almost* singular since the computation of its inverse is prone to large numerical errors. Thus, W_o is almost *not* full rank and, following Remark 3.1, neither is $\mathcal{O}$. One might argue that in this case, a pair (A, C) is *almost unobservable*—or rather unobservable for practical purposes—and, therefore, the structural observability index of Theorem 3.1 is not suitable for certain applications due to its sensitivity to an ill-conditioned matrix [40]. Moreover, although Theorem 3.2 holds for this crisp classification, an observable system can still be driven to an almost unobservable condition under certain transformations [1]. This problem is further explored in Section 3.2.

3.1.2 Nonlinear dynamical systems

The concept of observability was extended by [50] to nonlinear systems (2.2) according to the definition of *locally weakly observable*, presented as follows. In this subsection, considering the nonlinear system (2.2), or the pair $[\boldsymbol{f}, \boldsymbol{h}]$, , let $\boldsymbol{x}$ be restricted to the state-space set M rather than R^n, i.e. $\boldsymbol{x} \in M$. Thus:

Definition 3.2. *Given a subset $U \subseteq M$, $\boldsymbol{x}_1$ is U-accessible from a given state $\boldsymbol{x}_0$ if there is a bounded control $\boldsymbol{u}$ for $t \in [t_0, t_1]$ such that the corresponding solution of $\boldsymbol{x}$*

in $t \in [t_0, t_1]$ *of* (2.2) *satisfies* $\boldsymbol{x}(t_0) = \boldsymbol{x}_0$, $\boldsymbol{x}(t_1) = \boldsymbol{x}_1$ *and* $\boldsymbol{x} \in U$ *for all* $t \in [t_0, t_1]$. $A_U(\boldsymbol{x}_0)$ *is the set of accessible points from* $\boldsymbol{x}_0$ *in subset* U. *If there is an unique smallest equivalence relation on* U *which contains all* U*-accessible points from* $\boldsymbol{x}_0$, *then this is a weak* U*-accessibility, denoted by* $WA_U(\boldsymbol{x})$.

Definition 3.3. *The nonlinear system* (2.2), *or the pair* $[\boldsymbol{f}, \boldsymbol{h}]$, *is locally observable at* $\boldsymbol{x}$ *if for every neighbourhood* U *of* $\boldsymbol{x}$, $A_U(\boldsymbol{x})$ *is also a neighbourhood of* $\boldsymbol{x}$. *The pair* $[\boldsymbol{f}, \boldsymbol{h}]$, *is locally observable if it is locally observable at every* $\boldsymbol{x} \in \mathbb{R}^n$.

Definition 3.4. *The nonlinear system* (2.2), *or the pair* $[\boldsymbol{f}, \boldsymbol{h}]$, *is locally weakly observable at* $\boldsymbol{x}$ *if for every neighbourhood* U *of* $\boldsymbol{x}$, $WA_U(\boldsymbol{x})$ *is also a neighbourhood of* $\boldsymbol{x}$. *The pair* $[\boldsymbol{f}, \boldsymbol{h}]$, *is locally weakly observable if it is locally weakly observable at every* $\boldsymbol{x} \in \mathbb{R}^n$.

Theorem 3.3. *The nonlinear system* (2.2), *or the pair* $[\boldsymbol{f}, \boldsymbol{h}]$, *is locally weakly observable if the observability matrix* $\mathcal{O}(\boldsymbol{x}) \in \mathbb{R}^{nq \times n}$

$$\mathcal{O}(\boldsymbol{x}) = \begin{bmatrix} \dfrac{\partial \mathcal{L}_{\boldsymbol{f}}^0(\boldsymbol{h}(\boldsymbol{x}))}{\partial \boldsymbol{x}} \\ \dfrac{\partial \mathcal{L}_{\boldsymbol{f}}^1(\boldsymbol{h}(\boldsymbol{x}))}{\partial \boldsymbol{x}} \\ \vdots \\ \dfrac{\partial \mathcal{L}_{\boldsymbol{f}}^{n-1}(\boldsymbol{h}(\boldsymbol{x}))}{\partial \boldsymbol{x}} \end{bmatrix}. \tag{3.7}$$

is full rank, i.e. $\rho(\mathcal{O}(\boldsymbol{x})) = n$, $\forall \boldsymbol{x} \in \mathbb{R}^n$. ■

Proof. Proof is analogue to the stated view on equivalence (1)-(3) of Theorem 3.1. As in (3.5), we have

$$\begin{bmatrix} \boldsymbol{s} \\ \boldsymbol{s}^{(1)} \\ \vdots \\ \boldsymbol{s}^{(n-1)} \end{bmatrix} = \begin{bmatrix} \boldsymbol{h}(\boldsymbol{x}) \\ \dfrac{\mathrm{d}\boldsymbol{h}(\boldsymbol{x})}{\mathrm{d}t} \\ \vdots \\ \dfrac{\mathrm{d}^{n-1}\boldsymbol{h}(\boldsymbol{x})}{\mathrm{d}t^{n-1}} \end{bmatrix}. \tag{3.8}$$

Differentiating $\boldsymbol{s}(t)$ yields

$$\dot{\boldsymbol{s}}(t) = \begin{bmatrix} \frac{\mathrm{d}}{\mathrm{d}t} h_1(\boldsymbol{x}) \\ \frac{\mathrm{d}}{\mathrm{d}t} h_2(\boldsymbol{x}) \\ \vdots \\ \frac{\mathrm{d}}{\mathrm{d}t} h_q(\boldsymbol{x}) \end{bmatrix} = \begin{bmatrix} \frac{\partial h_1}{\partial \boldsymbol{x}} \dot{\boldsymbol{x}} \\ \frac{\partial h_2}{\partial \boldsymbol{x}} \dot{\boldsymbol{x}} \\ \vdots \\ \frac{\partial h_q}{\partial \boldsymbol{x}} \dot{\boldsymbol{x}} \end{bmatrix} = \begin{bmatrix} \frac{\partial h_1}{\partial \boldsymbol{x}} \boldsymbol{f}(\boldsymbol{x}) \\ \frac{\partial h_2}{\partial \boldsymbol{x}} \boldsymbol{f}(\boldsymbol{x}) \\ \vdots \\ \frac{\partial h_q}{\partial \boldsymbol{x}} \boldsymbol{f}(\boldsymbol{x}) \end{bmatrix} = \begin{bmatrix} \mathcal{L}_{\boldsymbol{f}}(h_1(\boldsymbol{x})) \\ \mathcal{L}_{\boldsymbol{f}}(h_2(\boldsymbol{x})) \\ \vdots \\ \mathcal{L}_{\boldsymbol{f}}(h_q(\boldsymbol{x})) \end{bmatrix} = \mathcal{L}_{\boldsymbol{f}}(\boldsymbol{h}(\boldsymbol{x})), \tag{3.9}$$

where $\mathcal{L}_{\boldsymbol{f}}(h_i(\boldsymbol{x})) = \frac{\partial h_i}{\partial \boldsymbol{x}} \boldsymbol{f}(\boldsymbol{x})$ is the Lie derivative of h_i along the vector field $\boldsymbol{f}$. Thus, the time derivatives of $\boldsymbol{s}$ can be written in terms of Lie derivatives as follows:

$$\boldsymbol{s}^{(j)} = \mathcal{L}_{\boldsymbol{f}}^{j}(\boldsymbol{h}(\boldsymbol{x})) = \frac{\partial \mathcal{L}_{\boldsymbol{f}}^{j-1}(\boldsymbol{h}(\boldsymbol{x}))}{\partial \boldsymbol{x}} \cdot \boldsymbol{f}(\boldsymbol{x}), \tag{3.10}$$

where $\mathcal{L}_{\boldsymbol{f}}^{0} h_i(\boldsymbol{x}) = h_i(\boldsymbol{x})$. Note that, as $\boldsymbol{x} \in \mathbb{R}^n$ and $\boldsymbol{f} : [t_0, \infty) \times \mathbb{R}^n \to \mathbb{R}^n$, the 1st-order Lie derivative $\mathcal{L}_{\boldsymbol{f}}^{j}(h_i(\boldsymbol{x}))$ yields, for example,

$$\mathcal{L}_{\boldsymbol{f}}^{1}(h_i(\boldsymbol{x})) = \begin{bmatrix} \frac{\partial h_i(\boldsymbol{x})}{\partial x_1} & \frac{\partial h_i(\boldsymbol{x})}{\partial x_2} & \cdots & \frac{\partial h_i(\boldsymbol{x})}{\partial x_n} \end{bmatrix} \cdot \begin{bmatrix} f_1(\boldsymbol{x}) \\ f_2(\boldsymbol{x}) \\ \vdots \\ f_n(\boldsymbol{x}) \end{bmatrix}. \tag{3.11}$$

Substituting (3.9) and (3.10) in (3.8), we derive the observability matrix (3.7):

$$\begin{bmatrix} \boldsymbol{s} \\ \boldsymbol{s}^{(1)} \\ \vdots \\ \boldsymbol{s}^{(n-1)} \end{bmatrix} = \begin{bmatrix} \frac{\partial \mathcal{L}_{\boldsymbol{f}}^{0}(\boldsymbol{h}(\boldsymbol{x}))}{\partial \boldsymbol{x}} \\ \frac{\partial \mathcal{L}_{\boldsymbol{f}}^{1}(\boldsymbol{h}(\boldsymbol{x}))}{\partial \boldsymbol{x}} \\ \vdots \\ \frac{\partial \mathcal{L}_{\boldsymbol{f}}^{n-1}(\boldsymbol{h}(\boldsymbol{x}))}{\partial \boldsymbol{x}} \end{bmatrix} \equiv \mathcal{O}(\boldsymbol{x}). \tag{3.12}$$

□

Remark 3.2. The observability matrix (3.7) is a generalization of (3.2) for the nonlinear case.

The discussion in Section 3.1.1 regarding this crisp classification of observability and the effects of ill-conditioning of $\mathcal{O}$ holds for the nonlinear case. Naturally, computational burden is aggravated for the nonlinear case, since computation of (3.7) can be more computationally intensive than (3.2).

The following theorem states the relation between observability and embedding theory [65].

Theorem 3.4. *Consider a nonlinear system (2.2) where $s(t) \in \mathbb{R}$, i.e. $h : [t_0, \infty) \times \mathbb{R}^n \to \mathbb{R}$. The pair $[\boldsymbol{f}, h]$ is locally observable if the Jacobian matrix of the map $\boldsymbol{\Phi} : \mathbb{R}^n(\boldsymbol{x}) \to \mathbb{R}^n(s, s^{(1)}, \ldots, s^{(n-1)})$ is locally nonsingular.* ■

Proof. If $s(t) \in \mathbb{R}$, i.e. $h : [t_0, \infty) \times \mathbb{R}^n \to \mathbb{R}$, then (3.7) reduces to

$$\mathcal{O}(\boldsymbol{x}) = \begin{bmatrix} \dfrac{\partial \mathcal{L}_{\boldsymbol{f}}^0(h(\boldsymbol{x}))}{\partial \boldsymbol{x}} \\ \vdots \\ \dfrac{\partial \mathcal{L}_{\boldsymbol{f}}^{n-1}(h(\boldsymbol{x}))}{\partial \boldsymbol{x}} \end{bmatrix}. \tag{3.13}$$

which in fact is the Jacobian matrix of the map $\boldsymbol{\Phi}$ between the original and the n-dimensional differential embedding space [65][2]. Because the condition for invertibility of $\boldsymbol{\Phi}$ at $\boldsymbol{x}_0$ is

$$\rho\left(\frac{\partial \boldsymbol{\Phi}}{\partial \boldsymbol{x}}\bigg|_{\boldsymbol{x}=\boldsymbol{x}_0}\right) = n, \tag{3.14}$$

then the invertibility of $\boldsymbol{\Phi}$ guarantees full rank of $\mathcal{O}(\boldsymbol{x})$ at $\boldsymbol{x}_0$. *Therefore, the system is locally observable if $\boldsymbol{\Phi}$ is locally nonsingular.* □

Remark 3.3. If $\boldsymbol{\Phi}$ is nonsingular for all $\boldsymbol{x}$, then there is global diffeomorphism and the pair $[\boldsymbol{f}, h]$ is fully (globally) observable [65] .

Remark 3.4. According to Takens' theorem [117], if the dimension of the reconstructed space is increased, that is $\boldsymbol{\Phi} : \mathbb{R}^n(\boldsymbol{x}) \to \mathbb{R}^n(s, s^{(1)}, \ldots, s^{(d-1)})$, with $d > n$ usually, then any singularities of $\boldsymbol{\Phi}$ may vanish (only if the system is structurally observable) and the pair $[\boldsymbol{f}, h]$ gradually becomes observable [65] .

This explains how loss of *local observability* is related to local singularities that $\boldsymbol{\Phi}$ may have —a consequence of nonlinearities. An example with Rössler system is provided for further understanding.

[2]The relation between the observability matrix and the Jacobian matrix of map $\boldsymbol{\Phi}$ was investigated for multivariate embedding ($\boldsymbol{h} : \mathbb{R}^n \to \mathbb{R}^q$) in [2]

Example 3.1. Structural observability of Rössler system.

Consider Rössler system (2.12).If $s = y$, then the observability matrix $\mathcal{O}_y(\boldsymbol{x})$ (or the Jacobian of the map $\boldsymbol{\Phi}_y^3 : \mathbb{R}^3(\boldsymbol{x}) \to \mathbb{R}^3(y, \dot{y}, \ddot{y})$) is

$$\frac{\partial \boldsymbol{\Phi}_y^3}{\partial \boldsymbol{x}} \equiv \mathcal{O}_y(\boldsymbol{x}) = \begin{bmatrix} 0 & 1 & 0 \\ 1 & a & 0 \\ a & a^2 - 1 & -1 \end{bmatrix}. \tag{3.15}$$

Since $\mathcal{O}_y(\boldsymbol{x})$ is constant and nonsingular, from Remark 3.3, the Rössler system is observable from the y variable at any point of the state space.

If $s = z$, then the observability matrix $\mathcal{O}_z(\boldsymbol{x})$ (or the Jacobian of the map $\boldsymbol{\Phi}_z^3 : \mathbb{R}^3(\boldsymbol{x}) \to \mathbb{R}^3(z, \dot{z}, \ddot{z})$) is

$$\frac{\partial \boldsymbol{\Phi}_z^3}{\partial \boldsymbol{x}} \equiv \mathcal{O}_z(\boldsymbol{x}) = \begin{bmatrix} 0 & 0 & 1 \\ z & 0 & x - c \\ b + 2z(x - c) & -z & (x - c)^2 - y - 2z \end{bmatrix}. \tag{3.16}$$

Since $\mathcal{O}_z(\boldsymbol{x})$ is not constant, we refer to Theorem 3.4. Note that $\mathcal{O}_z(\boldsymbol{x})$ is singular for $z = 0$, since $\det(\mathcal{O}_z(\boldsymbol{x})) = -z^2$. Thus, considering the definition of structural (crisp) observability, the Rössler system is unobservable for $z = 0$ and observable for $z \in \mathbb{R}\backslash\{0\}$.

This raises the following question. How good is the trajectory reconstruction from observations on z in the vicinity of $z = 0$? This question is further explored with the definition of dynamical (gradual) observability in Section 3.2. △

3.2 Dynamical Observability

3.2.1 Linear dynamical systems

As detailed in Section 3.1, the structural classification of observability faces several practical problems, such as the feasibility of reconstructing a dynamical system trajectory from a set of output signals whose observability matrix is ill-conditioned (sensitive to small changes). In other words, for practical purposes, it is relevant to classify a system not only as observable or not, but also to establish a continuous quantification of observability levels so that a system can be distinct between conditions of poor and rich observability. Indexes that quantify observability in a continuous manner, rather than discrete, are referred in this work as *dynamical observability* indexes [4].

As the problem of investigating dynamical observability seems to be related with the conditioning of matrix $\mathcal{O}$, Friedland [40] proposes the *conditioning number* as an alternative:

$$\kappa(A) = \left\|A^{-1}\right\|\|A\| = \frac{\sigma_{\max}(A)}{\sigma_{\min}(A)} \tag{3.17}$$

where we have used the l_2-norm (Euclidean norm), and $\sigma_{\max}(A)$ and $\sigma_{\min}(A)$ refer, respectively, to the maximum and minimum singular values of the square matrix A. The higher $\kappa(A)$, the less conditioned is A.

Friedland adapted the conditioning number for a more intuitive quantification of observability as follows.

Definition 3.5. *[40] The degree of (dynamical) observability of a pair (A, C) is defined as*

$$\delta_o = \left|\frac{\lambda_{\min}(F)}{\lambda_{\max}(F)}\right| \tag{3.18}$$

where $F = \mathcal{O}^\intercal\mathcal{O}$ or $F = W_o$, $\lambda_{\max}(A)$ and $\lambda_{\min}(A)$ refer, respectively, to the maximum and minimum eigenvalues[3] of F, and $0 \leq \delta_o \leq 1$.

The higher δ_o, the more observable is (A, C). Even when $\mathcal{O}$ (or W_o) is full rank, a small value of coefficient δ_o points to a *poor observability*. If $\delta_o = 0$, (A, C) is unobservable.

Remark 3.5. The ranking allows one to compare observable pairs. For instance, suppose that two pairs (A, C_1) and (A, C_2) are structurally observable, where $\boldsymbol{s}_i = C_i\boldsymbol{x}$, for $i = 1, 2$. Evaluating the dynamical observability, one might find that $0 < \delta_{o1} < \delta_{o2}$. Thus, (A, C_1) is less observable than (A, C_2) and, therefore, we state $s_2 \triangleright s_1$. Moreover, this ranking allows one to compare observable pairs with different dynamic matrices, i.e. (A_1, C_1) and (A_2, C_2). This is quite useful to compare a system observability rank under linear transformations [1].

Remark 3.6. Although the structural observability definition is invariant under similarity transformations (Theorem 3.2), the dynamical observability index δ_o is sensitive to similarity transformations [1].

While the conditioning metric δ_o is related to the observable subspace dimension, it is worth mentioning that other indexes for quantifying observability have been proposed in literature [115], such as: i) the trace of the Gramian, related to average observation energy in all directions of the observable subspace; ii) the determinant of

[3]Since F is symmetric, its singular values are equal to the absolute values of its eigenvalues.

the Gramian, which is a volumetric measure of the set of spaces which can be observed within one unit of energy [53]; and iii) the smallest eigenvalue of the Gramian, which is a worst-case metric related to the amount of energy required to observe the most difficult state [95].

3.2.2 Nonlinear dynamical systems

The concept of Definition 3.5 was extended to nonlinear dynamical systems in [66, 62].

Definition 3.6. *The degree of (dynamical) observability of a pair* $(\boldsymbol{f}, \boldsymbol{h})$ *is defined as*

$$\delta_o(\boldsymbol{x}) = \left| \frac{\lambda_{\min}(\mathcal{O}^\top \mathcal{O}, \boldsymbol{x}(t))}{\lambda_{\max}(\mathcal{O}^\top \mathcal{O}, \boldsymbol{x}(t))} \right| \tag{3.19}$$

where $0 \leq \delta_o(\boldsymbol{x}) \leq 1$.

Definition 3.6 still follows Remarks 3.5 and 3.6, although any comparison or analysis of $\delta_o(\boldsymbol{x})$ is only valid at a local point $\boldsymbol{x} = \boldsymbol{x}_0$. To assess a *global dynamical observability* index, Letellier and Aguirre [62] proposed to evaluate the average of (3.7) along a trajectory $\boldsymbol{x}(t)$, for $t \in [t_0, t_1]$ as follows.

$$\delta_o = \frac{1}{t_1 - t_0} \int_{t_0}^{t_1} \delta_o(\boldsymbol{x}(\tau)) \mathrm{d}\tau. \tag{3.20}$$

Remark 3.7. The nonlinear observability rank in (3.20) is not normalized to a $[0, 1]$ scale. It is not possible to compare the observability rank between variables of different systems, only between variables of the same system. It must be noted that the comparison is relative.

Remark 3.8. In this work, it was observed that the computation of (3.20) usually requires long data series to converge numerically.

Example 3.2. Dynamical observability of Rössler system

Consider Rössler system (2.12), where $(a, b, c) = (0.398, 2, 4)$, and its observability matrices $\mathcal{O}_y(\boldsymbol{x})$ in (3.15). Since $\mathcal{O}_y$ is constant for any point the state space, using (3.19) yields $\delta_y = 0.133$.

On the other hand, consider $\mathcal{O}_z(\boldsymbol{x})$ in (3.16). As explained in Example 3.1, since $\det(\mathcal{O}_z(\boldsymbol{x})) = -z^2$, the system is considered to be unobservable for $z = 0$ and, from a dynamical observability point of view, is also poorly observable in the vicinity of $z = 0$. For instance, for $z = 0.3$, using (3.19) yields $\delta_z(z = 0.3) = 1.32{\cdot}10^{-6}$. However, equation (3.19) only provides a *local* quantification of the variable z observability. For a more

global quantification, we refer to the average (3.20), which yields $\delta_z = 0.006$—indicating, nonetheless, the poor observability of z when compared to y.

For the Rössler system, the following values were computed using (3.20): $\delta_x = 0.022, \delta_y = 0.133, \delta_z = 0.006$ [62], yielding $y \triangleright x \triangleright z$. △

3.3 Topological Observability

Sections 3.1 and 3.2 focused the study of observability from a system theory point of view. However, the developed methods are not particularly efficient for high-dimensional dynamical systems such as networks. Indeed, even if the full network dynamics were known, to find a set of sensor nodes that render a full network observable would require a brute force computation of $\mathcal{O}$ over 2^N distinct combinations [73], where $N = \sum_{i=1}^{m} n_i$—which is not feasible [106]. This process would be even more demanding if computation of eigenvalues in (3.18) or Lie derivatives in (3.7) were involved.

Faced to these challenges, a possible strategy to study the observability of a network system is to investigate it from a graph approach, which we refer as *topological observability*. In this case, the topological observability is usually assessed solely from the network topology graph, although some works [26, 61, 4] argue that the results are more representative when the topological observability is assessed from the full network graph, as detailed in Section 2.3.1.

Most studies developed over this idea follow the pioneer line of work of Liu *et al.* [72, 73], grounded on the structural observability definition of Lin [70]. We review both main works and refer some extended works and similar proposals, discussing its possible outcomes and misleadings.

3.3.1 Lin's method: Structural controllability and observability

In 1974, Lin proposed a novel concept of structural controllability for linear systems [70], which was later extended to observability [17].

Definition 3.7. *Two pairs* (A_0, C_0) *and* (A_1, C_1) *are of the same structure if: (i)* $\dim A_0 = \dim A_1$ *and* $\dim C_0 = \dim C_1$*, and (ii) for every fixed zero entry of* (A_0, C_0)*, the corresponding entry of* (A_1, C_1) *is also zero, and vice-versa.*

Definition 3.8. *The pair* (A_0, C_0) *is structurally observable if and only if there exists an observable pair* (A_1, C_1) *of the same structure of* (A_0, C_0) *such that* $\|A_0 - A_1\| < \epsilon$ *and* $\|C_0 - C_1\| < \epsilon$*, for some* $\epsilon > 0$.

Remark 3.9. Definition 3.7 is grounded on the assumption that, in real applications, the true entries of (A, B, C, D) are usually contaminated by uncertainties, while zero entries are somewhat guaranteed [70]. Thus, one might argue that if a system is structurally observable, then it is observable for a wide range of parameters except for a *proper algebraic variety* in the parameter space which renders it unobservable [72].

Remark 3.10. A possible interpretation to Definition 3.7 grounded on graph theory is that two pairs (A_0, C_0) and (A_1, C_1) are of the same structure if their corresponding graphs share the same structure, i.e. the same set of nodes $\mathcal{V}$ and edges $\mathcal{E}$, although the edge weights do not need to share the same values—provided that they are different from zero.

Remark 3.11. Note that Lin's definition of structural observability is structural in two senses: (i) it is a crisp definition, as detailed in Section 3.1; and (ii) it is independent of the specific entries of (A, B, C, D)—relying only on the fact that zero entries are specifically known. A pair that is "structurally observable (controllable)" in Lin's sense (Definition 3.8) is not guaranteed to be observable (controllable) in Kalman's sense (Definition 3.1).

Definition 3.8 has been given an insightful analysis by Lin to determine structurally controllability by drawing a graph associated with the pair (A, B). Lin states that a pair (A, B) is uncontrollable if its respective graph has *non-accessible* nodes from the driver nodes. In this section, since our main concern is with observability, we present and detail an extension of Lin's work for determination of structurally observability following the *duality theorem* [19, Theorem 6.5] as presented by [4]. Thus, (A, C) is structurally observable if and only if $(A^\mathsf{T}, C^\mathsf{T})$ is structurally controllable.

Let a linear system (2.1), or a pair (A, C), be expressed as

$$A = \begin{bmatrix} a_{11} & a_{12} & 0 \\ a_{21} & a_{22} & 0 \\ a_{31} & a_{32} & a_{33} \end{bmatrix}, \quad C = \begin{bmatrix} 0 & 0 & c_3 \end{bmatrix}. \tag{3.21}$$

Following nomenclature established in Section 2.3.1, pair (A, C) can be represented by a graph $\mathcal{G}(A, C) = \{\mathcal{X}, \mathcal{E}, A_{\text{adj}}\}$, where the system state variables $\boldsymbol{x}$ are designated as a set of vertices $\mathcal{X} = \{x_1, \ldots, x_n\}$. Likewise, the output variables $\boldsymbol{s}$ can be designated

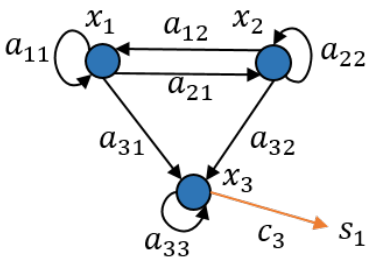

Figure 3.1: Graph representation of (3.22).

to a *set of sensor nodes* $\mathcal{S} = \{s_1, \ldots, s_q\}$. A graph of (3.21) can be drawn from

$$A_{\text{adj}} = \left[\begin{array}{c|c} A & C^{\mathsf{T}} \end{array}\right] = \left[\begin{array}{cccc|c} a_{11} & a_{12} & 0 & \cdots & 0 \\ a_{21} & a_{22} & 0 & \cdots & 0 \\ a_{31} & a_{32} & a_{33} & \cdots & c_3 \end{array}\right] \tag{3.22}$$

as shown in Fig. 3.1. A pair (A, C) is structurally unobservable if there is *non-accessible nodes* to the sensor nodes. In other words, (A, C) is structurally observable if there exists a directed path from all vertices in $\mathcal{X}$ to any sensor node in $\mathcal{S}$. Since all nodes $\mathcal{X} = \{x_1, x_2, x_3\}$ are accessible from s_1, we note that the graph in Fig. 3.1 is structurally observable in Lin's definition.

Remark 3.12. If A or C are transposed, the directions of the corresponding edges (that is, the direction of the arrows) in $\mathcal{G}(A, C)$ should be reversed.

Remark 3.13. As stated before, Lin's definition follows the concept of structural observability, where his results extend those of Kalman's rank condition (Section 3.1.1) to necessary, although not sufficient, graph properties of a given linear system.

From this graph approach to determine structural observability, the following theorem holds.

Theorem 3.5. *[70, See equivalent theorem and proof for controllability] The following statements are equivalent*[4]*.*

1. *The pair (A, C) is structurally observable by Definition 3.8.*
2. *The respective graph $\mathcal{G}(A, C)$ contains no non-accessible nodes.* ■

[4]The original theorem involves further equivalences that are omitted in this work since it would require the introduction of new graph concepts such as *dilatation* and *cactus* that are not further relevant.

3.3.2 Liu and coworkers' method for controllability: Maximum matching

Following ground-breaking results relating (complex) network topologies to the dynamical process on it, from dynamics spreading [85, 134] to synchronization phenomenon [119, 29], Liu *et al.*, in 2011, presented a pioneer work for controllability of *complex networks* [72][5]. The main goal is to identify the *minimum set of driver nodes* $\mathcal{D} = \{d_1, d_2, \ldots, d_p\}$ which can guide a (linear) network system entire dynamics, and understand the relations between controllability and the complex network (topology) properties.

Liu *et al.* argue that others pioneering works on controllability of network systems [120, 74, 101] are based on a weak assumption that, in a network system, the network topology and nodal dynamics are entirely known and mapped. This assumption allowed to explore the spectral graph properties, such as the spectrum of the Laplacian matrix [101]. However, even in the face of recent developments in modeling of complex networks, allowing one to assess reliably a network topology, the accurate estimation of edge weights is not realistic yet. Indeed, if biological or social networks are taken under consideration, not even the nodal dynamics are known.

Thus, in order to study controllability of complex networks, Liu *et al.* turned to Lin's structural controllability definition (dual to Definition 3.8) since: i) Lin's structural controllability has a convenient interpretation grounded on a theoretical graph approach, which is very useful for network systems where the network topology modeling is reliable; and ii) following Remark 3.9, Lin's structural controllability is not sensitive to parameter fluctuations, also a convenient feature since parameter estimation is very unreliable in large network systems.

The authors show that Lin's structural controllability problem maps into an equivalent graph problem where one can gain full control over a directed network[6] $\mathcal{G}(A, B)$ if and only if each unmatched node is directly connected to a driver node, and there are direct paths from any input signal to all matched nodes. A *matching* is formally defined as

Definition 3.9. *[72, Definition 8 of Supplementary Information] An edge subset $\mathcal{M}$ is a matching if no two edges of $\mathcal{M}$ share a common starting node or a common ending*

[5] Although the main focus of this chapter is dedicated to observability of network systems, the review of Liu *et al.* proposal for controllability is still relevant to this work due to the duality between controllability and observability.

[6] Definition of $\mathcal{G}(A, B)$ is analogous to that of $\mathcal{G}(A, C)$. $\mathcal{G}(A, B)$ is the corresponding graph of pair (A, B).

node. A node is matched if it is an ending node of an edge in the matching. Otherwise, it is unmatched.

This leads to the following theorem.

Theorem 3.6. *[72, Theorem 2 of Supplementary Information] The minimum number of driver nodes n_{D} needed to render $\mathcal{G}(A, B)$, or the pair (A, B), controllable, is defined by*

$$n_{\mathrm{D}} = \max\{m - |\mathcal{M}|, 1\} \tag{3.23}$$

where m is the number of nodes in $\mathcal{G}(A, B)$, and $|\mathcal{M}|$ is the cardinality (number of elements) of $\mathcal{M}$.

If there is a perfect matching in $\mathcal{G}(A, B)$, $n_{\mathrm{D}} = 1$—which, in this case, $\mathcal{D}$ is formed by any single node. Otherwise, n_{D} equals the number of unmatched nodes with respective to any maximum matchings—which, in this case, $\mathcal{D}$ is formed by just the unmatched nodes. ■

Remark 3.14. Adding more edges on $\mathcal{G}(A, B)$ will never weaken a system structural controllability by Definition 3.8 [70], which is not necessarily true for Definition 3.1. This feature makes Theorem 3.6 meaningful in dealing with missing links in network topology modeling [72].

Remark 3.15. Differently from a brute force search for a minimum $\mathcal{D}$, which is of order $\mathcal{O}(2^N)$, the maximum matching algorithm allows $\mathcal{D}$ to be identifiable with at most $\mathcal{O}(m^{1/2}|\mathcal{E}|)$ steps [72].

From these results, Liu *et al.* reach several conclusions regarding complex networks properties and controllability. The most interesting ones are: i) controlling heterogeneous and sparse networks is harder than controlling homogeneous and dense ones, and ii) the counterintuitive notion that driver nodes tend to avoid high-degree nodes[7]. Some other conclusions, such as the correlation between the n_{D} and the network degree distribution are arguable considering the applied methodology and assumptions [26].

Figure 3.2 illustrates $\mathcal{D}$ selection by maximum matching in rather simple networks. Section 3.3.4 presents some pertinent criticism of this technique.

3.3.3 Liu and coworkers' method for observability: SCC search

Despite the duality property of controllability and observability, Liu *et al.* decided to take an alternative route to depict the observability of complex networks [73], rather

[7] This is further explored in this work in Section 3.3.4, "Control via *control hubs*".

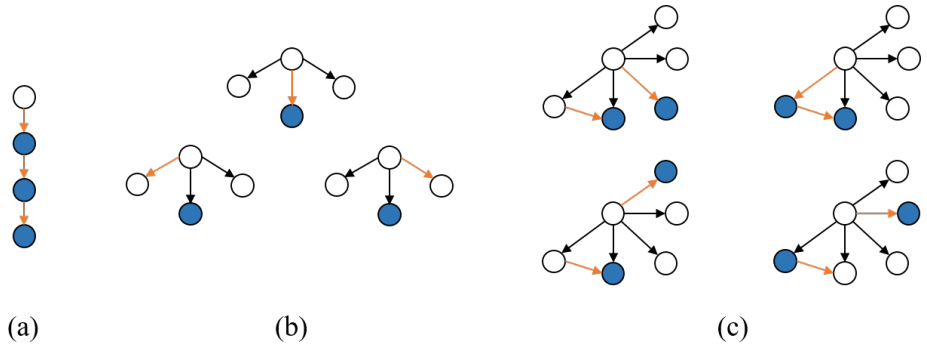

Figure 3.2: Maximum matching of simple networks. Set $\mathcal{M}$ is composed of orange edges. Unmatched and matched nodes are represented, respectively, in white and blue colors. To render the graph structurally observable, all unmatched nodes must have an input signal. [72]

than adapting Theorem 3.6. Motivation is similar to Section 3.3.2, whereas the main goal of Liu *et al.* is to determine the *minimum set of sensor nodes* $\mathcal{S} = \{s_1, s_2, \ldots, s_q\}$ which can reconstruct the entire trajectory of a network system.

Since the maximum matching approach is restrained to linear networks, Liu *et al.* developed a novel methodology, also grounded on Lin's structural observability (Definition 3.8), but adjusted to nonlinear polynomial networks, such as chemical reactions. Entitled *graph approach* (GA), the procedure to achieve observability in a network system consists of: i) drawing an inference diagram, a graph $\mathcal{G}$, from (2.2) according to Section 2.3.1[8,9]; ii) decomposing $\mathcal{G}$ in SCCs (see Section (2.2.1)); iii) determine the *root SCC*, i.e. SCC with no incoming edges; and iv) attribute a sensor node s_i to at least one node of each root SCC.

Remark 3.16. By the duality theorem [19, Theorem 6.5], the observability problem $\mathcal{G}(A, C)$ solved by GA can be mapped into a controllability problem as $\mathcal{G}(A, B)$ [73].

Remark 3.17. If no node from all root SCC are observed, then one or more columns of $\mathcal{O}(\boldsymbol{x})$ in (3.7) are zero and, therefore, $\text{rank}(\mathcal{O}(\boldsymbol{x})) < n$. A more physical interpretation is that if there is no incoming path from a given node to a sensor node (which always happens if no sensor node is placed in a root SCC), then the information from this state cannot be inferred from any sensor node [73].

Remark 3.18. The detailed procedure is only a *sufficient condition* for nonlinear polynomial systems. If all sensor nodes selected from GA are measured, then $\mathcal{O}(\boldsymbol{x})$

[8]Note that in [73], the inference diagram $\mathcal{G}$ drawn from a (2.2) does not distinguish between linear (continuous) and nonlinear (dashed) interconnections. The problem of singularities is not explored as in [4].

[9]For a linear system 2.6, this is similar to referring of a graph $\mathcal{G}(A, C)$ from a pair (A, C).

has no zero columns [73]. Nevertheless, there is no guarantee that $\mathcal{O}(\boldsymbol{x})$ columns are linearly independent, i.e. $\mathcal{O}(\boldsymbol{x})$ is full rank.

Following Remark 3.18, Liu *et al.* argue from an empirical analysis of multiple randomly generated chemical reactions that although there can be correlation among the columns of $\mathcal{O}(\boldsymbol{x})$, the probability is rather small, if not zero due to the "complicated polynomials" entries of $\mathcal{O}(\boldsymbol{x})$ [73]. Indeed, if there are symmetries in a dynamical network that render the state derivatives invariant, this will render the system unobservable, leading GA to underestimate $\mathcal{S}$. This is shown by [73] when comparing the (sufficient) lower bound of $\mathcal{S}$ provided by GA to the (sufficient and necessary) one provided by maximum matching.

Finally, we highlight that GA is a methodology developed exclusively for nonlinear systems described by polynomial functions and, therefore, is not directly[10] applicable to other nonlinear systems, such as networks of Kuramoto oscillators (see Example 2.1 and Chapter 5). Moreover, as acknowledged by the authors, GA cannot identify the best sensors in a root SCC, i.e. the observability of different $\mathcal{S}$ selected by GA is not ranked.

3.3.4 Criticism and related works

This section reviews the extensions and criticism in literature regarding methods of *topological observability*. Most earlier discussions in the study of controllability and observability of network systems focused mainly on the former property rather than the latter. However, due to the duality of these properties, there is no harm or loss of generality in comparing and discussing methods designed for controllability and observability. Therefore, the terms controllability and observability are used or compared indistinctly according to the related referred work.

It is important to state that, in this review on observability of networked systems, we are more interested in a broader class of works that propose metrics designed for what we call *generalized networks*—that is, no specific network topology or nodal dynamics (only linear and nonlinear distinctions). Nevertheless, several works have been proposed in literature on their own merits that explore the relation of observability and the graph properties of certain types of network topologies, including Cartesian grid graph [92], chain and cycle graph [94], clustered networks [103], and specific complex network models, such as the scale-free network [41]. The discussion of observability has

[10]There exist "universal" representations for nonlinear systems as polynomial systems (i.e. polynomial vector fields) at the expense of augmenting the number of states and considering only predefined initial conditions ("consistent" inital conditions) [55].

also been directed to networks of specific dynamics and applications, such as boolean networks [20, 44, 60], chemical reactions [73], traffic networks [16], biological systems (e.g. neuronal networks [46, 114]) and power systems [83, 5].

Lin's structural definition of controllability. As reviewed in details in Sections 3.3.1, Lin's definition of structural controllability [70] allows an intuitive analysis of a given linear dynamical system via its respective graph representation. This approach, which we refer to as topological controllability (observability), is not concerned with the specific entries of system matrices (A, B, C, D) such as the Kalman rank condition in Theorem 3.1, but rather if the those matrices present a structure that *might* allow controllability under the correct and arbitrary choice of parameters. Lin argue that, in a mathematical model of a real process, the parameters estimations are contaminated by uncertainties whereas "zero" entries are practically guaranteed. Thus, a first step towards deciding if a system is controllable or not, is to perceive if it is structurally controllable or not in his definition.

Liu and coworker's controllability of complex networks. Liu *et al.*, motivated by the fact that complex networks usually have a reliable topological (graph) representation but an unreliable estimation of edges weights, took advantage of Lin's topological approach to investigate controllability in complex networks [72]. Using a method entitled maximum matching, Liu *et al.* identify the "minimum" set of driver nodes $\mathcal{D}$ to render a complex network structurally controllable. However, as one might have noticed, Lin's definition of structural controllability is a *crisp* definition, so how can one assure that this $\mathcal{D}$ provided by the maximum matching is really the minimum set? Indeed, as pointed out by [61], the result of a maximum matching search is not unique. Cowan *et al.* argue that no importance is given by Liu *et al.* to the nonzero entries of (A, B, C, D). Thus, perhaps a more relevant question rather than if a network is structurally controllable is if it is almost uncontrollable [26].

Criticism of benchmark networks used in [72]. A common topic of criticism to Liu *et al.* work is that the networks used as benchmarks for the proposed maximum matching method (see Table 1 of [72]) were only analyzed on an exclusive topological level. In other words, only the network topology is considered, while the internal states that describes an individual nodal behaviour (that is possibly an independent dynamical system) are disregarded. Leitold *et al.* contests that Liu *et al.* uses network systems that are not even dynamical systems[11], such as social networks, the Internet or the World Wide Web [61]. On the other hand, when dealing with networks such

[11]It is arguable that these networks still are dynamical systems, although its dynamics are not entirely known and modeled.

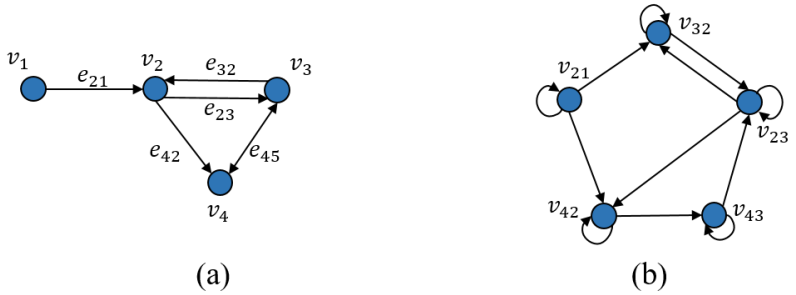

Figure 3.3: Transforming nodal dynamics representation to edge dynamics. (a) Nodal dynamics. (b) Edge dynamics.

as food webs, regulatory networks, power grids, electronic circuits, neuronal networks and metabolic systems, it is expected that the minimum set of driver nodes would be significantly different if all nodes were expanded as individual dynamical systems, taking into considerations its own dynamic responses, time constants and interactions among the nodal state variables [26].

Control via "control hubs". A fundamental result in [72] is that heterogeneous and sparse networks are harder to control than homogeneous and dense ones. This result is based on an analysis of correlation between the number of driver nodes n_{D} required for controllability and the network degree distribution, which was further discussed in [99]. This led to a contra-intuitive notion that high-degree nodes, also called *hubs*, are less desirable to be driver nodes [72]. As discussed by [90, 107], this is a consequence of the fact that, since network models in [72] do not consider nodal dynamics, the control signal injected by driver nodes spread homogeneously among its neighbouring nodes, raising symmetries that restrict the state space exploration.

Nepusz and Vicsek shows that control by nodes of high-degree is also possible if a different paradigm is embraced: to change analysis from nodal dynamics to *edge dynamics* [90]. The argumentation follows that by choosing a hub node as a driver node, if one can control its edge dynamics individually instead of its nodal dynamics, then the spread control signals no longer suffer from symmetries. In case of controlling edge dynamics, homogeneous and dense networks become harder to control than heterogeneous and sparse ones. Moreover, one can benefit from controllability metrics (and other network metrics) designed for nodal analysis by performing a transformation from nodal dynamics representation to edge dynamics (that is, inverting nodes and edges roles). This is exemplified in Fig. 3.3. This approach reduces the number of driver nodes in exchange of a higher control energy cost per driver node.

Contrariwise to [72, 90] judgment, Cowan *et al.* affirms that the minimum number of driver nodes is not mostly dependent of node degrees distributions (at least in linear networks). Once more, Liu and coworker's choice of benchmark networks are criticized for being modeled only on topological level and not including nodal dynamics. Indeed, by [72] network models, the individual nodes of these benchmarks would show no independent behaviour if the network were fully disconnected, acting as pure integrators. This is a consequence of [72] not considering *self-edges*. Thus, a linear dynamical network of form (2.6) can be rewritten as

$$\dot{x}_i = -\lambda_i x_i + \sum_{j=1}^{n} a_{ij} x_j + \sum_{j=1}^{p} b_{ij} u_j, \quad \text{for } i = 1, 2, \ldots, n, \tag{3.24}$$

where x_i is a state at node v_i (only 1-dimensional systems are considered at each node), n is the number of states (nodes), p is the number of inputs, $A_{\text{adj}} = [a_{ij}]$,$B = [b_{ij}]$, and λ_i are eigenvalues of A. This representation is a specific case of the vectorial form in (2.7), while (2.11) is an example of (3.24) for a network of Kuramoto oscillators.

Nevertheless, (3.24) shows that a dynamical network has each of its nodes described by an independent dynamical behaviour (absent of external influences), i.e. an eigenvalue λ_i that determines its time constant. Moreover, each node is influenced by its neighbouring interactions, if $a_{ij} \neq 0$, which includes a potential self-edge a_{ii} related to the network topology (which is usually translated in the Laplacian matrix). Therefore, most, if not all, nodes of a dynamical network are influenced by self-edges from both nodal dynamics and network topology [26]. If all nodes of a dynamical network include self-edges, then all nodes are matched. The network is referred as perfectly matched and, according to Theorem 3.6, the number of driver nodes required to render it structurally controllable is *one*—as long as this unique driver node is attached to *all nodes* [26]. Once more, hub nodes are shown to be fundamental for network control, but they demand higher control energy costs.

Inspired by an example in [61], Fig. 3.4 shows how a tank system was portrayed as a network in [72] (i.e. representing only its network topology) and how it is meant to be when including self-edges [26] and nodal dynamics [61, 4] (i.e. representing the full network). In each case, the necessary set of driver and sensor nodes to render the network structurally controllable and observable is represented. Note that when including the network dynamics, only one driver and sensor is (theoretically) required, as mentioned in [26]. Although Fig. 3.4c is more precise, this full network representation is harder to conceive mathematically, specially in biological systems.

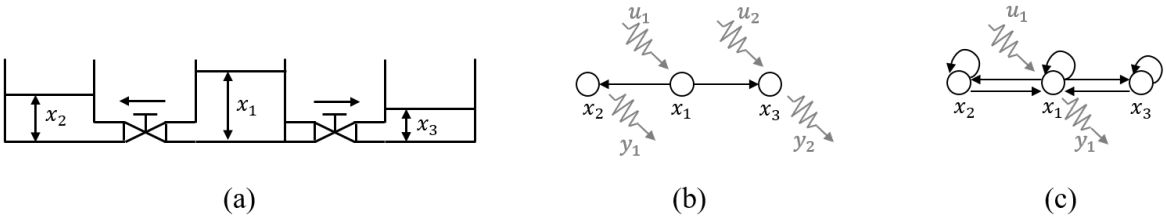

Figure 3.4: (a) Tank system. (b) Liu and coworker's representation based on network topology, exclusively. (c) Full network representation. [61]

Further works related to topological observability. Despite the criticism regarding the limitations of using graph approaches to determine the controllability or observability of a network system, a lot of effort was assigned to this front for two reasons: i) the plainness from which a graph approach such as Lin's [70] extended to the context of network systems, and ii) the fact that the ground-breaking and pioneer result in controllability [72] and observability [73] of network systems involved topological aspects. Several extensions to Liu and coworkers' work led to results on target control [47, 87, 52, 43], study of correlations between controllability and network properties [99], analysis of energy control and the chosen set of driver nodes [133], novel controllability methods based on graph properties [61], and recent developments in network control of neuronal networks [46, 114].

Lack of validation. A common problem in studies involving network systems and novel controllability and observability proposals is the lack of validation. Many algorithms and techniques are applied to network data-bases and compared to other metrics, leading to conclusions regarding which method provide the smaller set of driver (sensor) nodes [72, 90, 73, 136]. However, the relevance of the provided set of driver nodes are not usually questioned. Is it the smaller set of driver nodes really *better* than the the bigger set? This question is a matter resolved by dynamical observability metrics, although most, if not all, are only applicable to systems of lower dimensions.

Using a first-order electronic circuit interconnected by a chain graph as a validation benchmark, Wang *et al.* [123] gives attention to this topic when studying the practical feasibility of two network controllability metrics: the maximum matching and the "exact" controllability [136] (which is discussed later in Section 3.4.1) methods. The authors perceive that, when applying a single control signal in one of the chain extremities, the highest the "control chain", the more singular the controllability Gramian (dual to (3.4)). Thus, the "well-behaviour" and conditioning of the controllability Gramian is related to the practical (entitled physical by the author) capability of a set of driver nodes to drive the system states through the state space. Wang *et al.* provides an

attempt to quantify controllability in a network through the energy costs (or control energy). Nevertheless, it is clear that, in order to quantify controllability of different sets of driver nodes, Wang *et al.* relied on a dynamical controllability approach. One interesting result is that it is possible to raise the controllability index by a slight addition of driver nodes along the chain, "breaking" the long control chain in smaller sections.

Indeed, when validating these metrics, another frequent conclusion is that controllability metrics based on Lin's structural definition usually undershoots or overshoots the minimum set of driver nodes [44, 61, 123]. An interesting approach to validate controllability metrics is to use boolean networks, since it highlights the interaction between the network topology and nonlinear dynamics involving simple binary variables [44]. This conclusion is also present when estimating the minimum set of sensor nodes defined by Liu *et al.* GA procedure [73], as seen in Haber *et al.*'s validation test of observability using Bayesian filtering [48]. Reference [44] shows that the controllability previewed by the maximum matching method might fail even for (linearized) small nonlinear examples. Likewise, Aguirre *et al.* shows that the structural observability defined by GA is susceptible to failures if the procedures do not take the possibility of certain nonlinear edges vanishing due to singularities in the state space [4]. We reproduce their example with a chain graph of Rössler systems in the following example.

Example 3.3. Topological observability of a network of Rössler systems.

We illustrate a potential failure of Liu and coworkers' GA approach with a polynomial nonlinear system, the Rössler system.

As detailed in Section 2.3.1, let the Rössler system be represented by a nonlinear graph where linear and nonlinear connections are represented by full and dashed lines, respectively. Clearly, if z tends to 0 in (2.12), then the nonlinear connection tends to vanish. In Figure 3.5 we represent the root SCC of a Rössler system graph when the nonlinear edge has not vanished and otherwise. If the nonlinear edge vanishes, the z variable (node) is no longer a part of the root SCC. This is related to the poor observability of the z variable of Rössler system.

Although the Liu *et al.* [73] argue that their approach is unable to indicate which variable in a root SCC is the best option, in Rössler system, when $z = 0$, it is important to note that system is indeed unobservable from measurements taken only on z. Therefore, it is important to consider the vanishing effects of nonlinear systems to determine the potential root SCC, specially when the operation point is in the vicinity of the "vanishing region". △

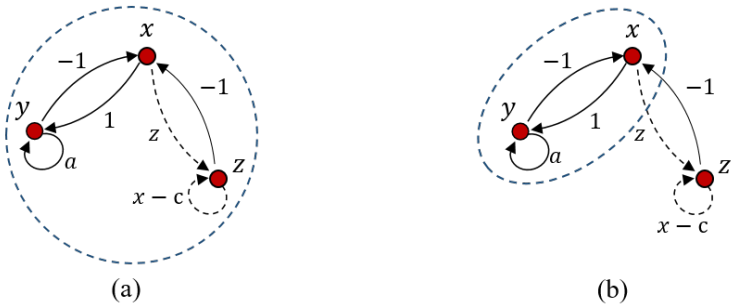

Figure 3.5: Root SCC (dashed circle) of a Rössler system graph. (a) All edges are nonzero constants. (b) The nonlinear edges vanished for $z = 0$, remaining only linear edges.

3.4 Dynamical Observability of Network Systems

As mentioned in Section 3.3.4, most topological observability metrics are mainly concerned with distinguishing what set of sensor nodes render a network system observable or unobservable—a question of *structural* observability. Indeed, most works do not question the practicability of their proposed methods when applied to network systems whose dynamics are usually not modeled. As pointed out by Cowan *et al.* [26], a more important question than if a system is observable or not, is if it is almost unobservable.

Thus, another important goal is to measure if a set of sensor nodes is more or less observable than another set. This is a question of dynamical observability. In the following section, we investigate recent contributions to quantify observability (controllability) of network systems in a computationally feasible way.

3.4.1 Recent contributions

A quantitative approach of controllability and observability of network systems has been discussed in several papers for different purposes [132, 95, 115, 46, 123, 48]. For instance, references [132, 95, 46] adopted the same measure, based on the smallest eigenvalue of the Gramian (see Section 3.2.1), although [132] focused on the study of scaling laws for the control energy as function of the control horizon, while [95], supported by [116], studied the trade-offs between control energy and the number of control nodes. Gu *et al.* [46], on the other hand, direct its study to neuronal network. Summers *et al.* [115] noticed that several controllability measures (including the trace, determinant, rank and smallest eigenvalue of the Gramian, as seen in Section 3.2.1) share submodularity or modularity properties and took advantage to implement

optimization techniques to determine the best set of driver nodes. Analogous discussions to [95] are given for observability and its related trade-offs by using a Bayesian filtering approach [48]. Finally, Aguirre *et al.* [4] reviews some advances in (nonlinear) system theory and observability, showing some possible guidelines for study and quantification of observability in network systems.

What is not a dynamical observability metric for network systems. Before further detailing dynamical observability metrics of network systems, it is important to prevent a possible misconception of "observability" quantification. To that end, we refer to the "exact controllability" proposition of [136] as an example.

In their work, Yuan *et al.* deviated from Liu *et al.*'s topological analysis [72] and, grounded on spectral properties of a dynamical network system[12], provided a paradigm to assess controllability of weighted networks whose parameter entries are known (unlike Lin's structural controllability). By evaluating the maximum geometric multiplicity among all eigenvalues of the network system, an elegant proof provides guarantees of the sufficient number of driver nodes n_{D} that render a system controllable. Moreover, this minimum set of driver nodes $\mathcal{D}$ can be determined by using canonical transformations and setting an input matrix B so that any correlation (linear dependence) in matrix $(A - \lambda I)$ is canceled. This approach has two main problems, however.

First, to quantify the proposed method and compare it to previous works, the authors proposed a measure of controllability which is the ratio of n_{D} and n. *This measure is not a dynamical controllability metric.* It only relates the minimum number of driver nodes to the network size, being still a structural controllability metric (although now in Kalman's sense rather than in Lin's sense as in [72]). There is no guarantees that the minimum set $\mathcal{D}$ is almost unobservable. Indeed, to be defined as a (relevant) controllability measure, this quantity must be able to relate the chosen set of driver nodes to the control energy costs (e.g., via the controllability Gramian) or the controllable subspace dimension (e.g., verifying the controllability matrix conditioning).

Second, although computation of n_{D} is of order $\mathcal{O}(n^2 \cdot \log(n)^2)$, the determination of set $\mathcal{D}$ is done by SVD techniques that do not escalate well with the system dimension [136], specially with networks with a hundred of nodes. This raises the following concern.

Scalability of observability methods for network systems. One of the reasons that led graph-inspired (topological) techniques, such as [72, 73, 61], to dominate this field of work in place of matrix-theoretical ones is the high scalability of graph

[12]More specifically in equivalence (1)-(4) of Theorem 3.1, i.e. changing the main approach from Kalman rank condition of the controllability matrix to an evaluation of Popov-Belevitch-Hautus rank condition.

tools compared to those developed in control theory. Yuan *et al.*, and others [128, 112], whose works are grounded on concepts introduced in control theory, are a victim of the lack of applicability of their methods in large-scale networks. Moreover, when dealing with driver (sensor) node selection, most solutions are compromised in high-dimensional systems [95], since one either based on combinatorial or non-scalable optimization techniques , or heuristic approaches that are limited to the specific studied systems and show no guarantees of control .

The scalability problem is even worse when dealing with dynamical observability metrics, such as those described in Section 3.2. Thus, when dealing with matrix-theoretical frameworks, we discuss two interesting approaches in literature, given by Pasqualetti *et al.* [95] and Summers *et al.* [115], that attempt to circumvent this problem via, respectively, network partitioning and use of scalable optimization technique.

Network partitioning. Formally, network partitioning consists of segregating the set of nodes $\mathcal{V}$ of a given graph $\mathcal{G} = \{\mathcal{V}, \mathcal{E}\}$ into P disjoint sets $\mathcal{P} = \{\mathcal{V}_1, \mathcal{V}_2, \ldots, \mathcal{V}_P\}$, where $\mathcal{G}_i = \{\mathcal{V}_i, \mathcal{E}_i\}$ is the ith subgraph of $\mathcal{G}$, for $i = 1, 2, \ldots, P$.

Clearly, network partitioning methods [38] are a viable alternative in network systems to subdivide a high-order systems into several and, if possible, independent "clusters" of lower dimension. Ideally, the low-order subgraphs could be assessed by traditional methods from control theory. In practice, however, to subdivide a network into independent systems, or even to uncover its remaining dynamical interdependences, might be a challenge. For instance, Liu *et al.* [73] (Section 3.3.3) proposed a sensor selection method based on a network partitioning into SCC. Despite the order reduction in each SCC, the choice of sensor nodes inside each subgraph still remained unsolved. Desynchronized (partitioned) control has also been implemented by [114] to validate its experiments.

By partitioning the network into several SCC, Pasqualetti *et al.* [95] proposed an elegant solution to actuator placement by choosing all nodes at each SCC boundaries[13] as driver nodes. Hence, the authors developed a control law strategy that *decouples* each SCC dynamical interdependences in such a manner that its selected "internal" driver nodes are solely responsible for the SCC steering from the origin to a target state. This practice is only possible by choosing the aforementioned nodes at the SCC boundaries as actuators. In fact, by "forcing" the independences of all SCC, the high-order network problem is reduced to independent low-order dynamical systems ones which can be controlled by local control centers. The authors argue that their method is scalable

[13] See [95] for mathematical definition.

since it depends on the number of partitioning, rather than the network cardinality. To study the viability of the proposed method, the authors recurred to a dynamical controllability metric based on the minimum eigenvalue of the Gramian.

Although the aforementioned method, as well as other network partitioning methods, are tempting, highly centralized networks (see centrality measures in Section **??**) are not suitable to decomposition. In those cases, even if SCC can still be identifiable, their subgraphs might still be very large order systems for traditional techniques of control theory.

Optimization techniques. Summers *et al.* [115] formulates the actuator (sensor) placement problems as a *set function* optimization problem as follows

$$\max_{\mathcal{D}\subseteq\mathcal{V},|\mathcal{D}|=p} J(\mathcal{D}) \tag{3.25}$$

where given a $\mathcal{V} = \{v_1, v_2, \ldots, v_m\}$, the problem is to select a p-element (q-element) subset $\mathcal{D}$ ($\mathcal{S}$) of $\mathcal{V}$ that maximizes an objective set function $J(\mathcal{D}) : 2^m \to \mathbb{R}$—i.e. a function that assigns a real number to each subset $\mathcal{D}$ ($\mathcal{S}$). A good objective function J is one that represents the trade-off between the number of required driver (sensor) nodes and the related control (observation) energy costs. Possible functions are the dynamical controllability (observability) metrics depicted in Section 3.2.1. As one might note, (3.25) is a combinatorial optimization problem that could be solved by brute force search if the network size were of lower order.

The great contribution of [115] is to show that most dynamical network metrics based on the controllability Gramian are *submodular* functions. Thus, although maximization of (3.25) is computationally hard, the optimization problem whose objective function is submodular can be (globally or locally) solved by a greedy algorithm with guaranteed performance [89]. Via numerical simulations, the authors shows that, considering $|\mathcal{V}| = 25$ and $|\mathcal{D}| = 7$, the greedy optimization displays a result better than 99.93% of all other combinations. The method is further validated on a power system and scalability of the greedy algorithm is discussed in details. Haber *et al.* [48] apply, for comparison purposes, Summers and coworkers' approach on nonlinear networks and show that their method perform well, regardless of not providing any mathematical proofs for the nonlinear case.

An analogous study for observability. As perceived, the study of controllability and observability of network systems is more focused on the former property rather than the latter. An observability centered study is provided by Haber *et al.* [48], exploiting analogous characteristics to that described in [95]. Motivated by the lack

of applicability of structural and graph-inspired metrics of observability, the authors derived an "unified" optimization-based framework to both select the sensor nodes and reconstruct the network system trajectories. Instead of [115] approach, the optimization framework is based on a moving horizon technique, a kind of Bayesian filter.

While Pasqualetti *et al.* [95] mathematically studied the trade-off between the number of driver nodes and the required control energy, Haber *et al.* analyzed from empirical data the trade-off between the number of sensor nodes and the observation length against the estimation error of the suggested filter. The authors inquire that, although Liu and coworkers' GA approach [73] seems sufficient from a theoretical point of view, in practice a much larger number of sensor nodes are required to push the filter performance beyond a certain threshold that holds its performance in lower values. This problem seems to be related with the following aspects: model uncertainties, numerical precision, measurement noise and the conditioning of the (linearized) nonlinear system Jacobian. Either the conditioning of the system Jacobian is improved by an unrealistic amount of data, or the number of iterations in the optimization problem remains too large.

As a side note, at least of the considered nonlinear networks in [48], no correlation between the best set of sensor nodes were found with graph centrality measures.

Role of symmetry. Lin's structural analyses [70] (Section 3.3.1) of a pair (A, B) (or (A, C)) is independent from the specific nonzero values of its network parameters. Although his studies did not specifically cover presence of symmetries, Whalen *et al.* points that any pair containing symmetries is subjected to constraints over the nonzero entries of (A, B) [128]. Indeed, symmetries in a network system creates linear dependences over the dynamical matrix columns which restrict the state space exploration for a small set of driver nodes. Through small network motifs (tree interconnected nodes), the authors study the interdependences of observability (controllability), the spatial location of sensor (driver) nodes, the coupling strengths, the system time evolution (dynamics) and the type of symmetry. To quantify the observability found in each motif, the authors referred to (3.19). Some interesting conclusions are that specific types of symmetries, such as rotational ones, do not affect Lin's structural controllability of a network system. Moreover, the authors postulate that the higher the number of direct connections into a sensor node, the higher its observability (and dually for controllability)—although it is still arguably if this feature is restricted to the intrinsic nature of the studied motifs or if it is a more general property.

A possible approach to circumvent the problem caused by symmetries is explored by using group theory to partition a network system into decoupled sets (see [95] for

another interesting strategy). Alternatively, Whalen *et al.* suggests that perturbing the network coupling strengths could break the symmetries. This latter approach, however, can lead to a reverse Hopf bifurcation[14] if the coupling strengths are increased past a threshold. Due to the decrement of "dynamical movement" in stable points, the rate of change of trajectories tends to zero and, consequently, the Lie derivatives in (3.7) become too small, leading to a decrease of observability.

3.4.2 Other observability metrics

As any other review in literature, it is unfeasible to state and discuss thoroughly all related works to the study of observability in network systems. In this review, emphasis was given to graph and system theory-inspired techniques, however others approaches are existent. For instance, to deal with larger systems with more complicated dynamics, Bianco-Martinez *et al.* [63, 10] provided a dynamical symbolic observability metric that does not depend on the specific parameter entries but rather on the presence of nonlinear couplings within the dynamical system. The observability metric is normalized in a $[0, 1]$ range, allowing to compare different dynamical systems [4]—differently from other observability metrics of nonlinear systems based on (3.20). Moreover, this approach seems to be promising for "not very large" dynamical networks [4].

Some other interesting symbolic approaches to quantify observability have been presented in a power system analysis context [108, 13]. The problem of sensor and actuator placement in power systems is a very relevant (and old) one due to emerging and expensive technologies designed to monitor or control the system states [83, 5]. Since it is not feasible to implement these equipments in every single substation (node), one is concerned with which substations are the more relevant ones, including performance and robustness [134, 135, 86].

Finally, although not quite feasible in a network context due to large computational burden and dependence of extensive recorded time series, it is interesting to cite Aguirre and Letellier's approach to indirectly quantify observability using a SVD technique over the reconstructed trajectories of the system state space [3].

[14] Hopf bifurcation is a critical point where a system stable point switch to a limit cycle solution, and contrariwise for the reverse Hopf bifurcation.

Chapter 4

Particle Filtering of Dynamical Networks: A Benchmark for Observability Studies

The motivation of this chapter follows the discussion in Chapter 3. The chapter is organized as follows. Section 4.1 provides the motivations and goals of this chapter. Section 4.2 provides a background on PF, while Section 4.3 describes the PF methodology and numerical setup applied in each network benchmark. Section 4.4 presents the numerical results and Section 4.5 concludes the work.

The contents of this chapter are similar to the manuscript [79].

4.1 Introduction

In network systems, it is practically and numerically unfeasible to perform measurements on every single node, thus a selection of sensor nodes, in which both quantity and positioning must be optimal, is required. This is an observability problem. However, due to high-dimensionality issues, classical observability metrics face serious numerical and scalability issues. For instance, as thoroughly discussed in Section 3.3, topological observability approaches [70, 72, 73] have been shown to underestimate or overestimate the set of sensor nodes needed to render a network observable [26, 44, 61], not being suitable for practical applications [123]. Moreover, the literature has been flooded by several different proposals of observability (controllability) metrics.

Thus, a recurrent goal in literature revolves around two questions: (i) what is the *best* set of sensor nodes; and (ii) which proposed metric really estimates a *better*

set of sensor nodes than other metrics. In order to answer these questions, one can turn to the notions of dynamical observability—discussed in Section 3.2. For instance, references [95, 46, 115] applied "traditional" dynamical observability (controllability) metrics to quantify the selected set of sensor (driver) nodes.

On an exclusively observability context, a second approach can be used: the use of Bayesian filters, a class of methods designed for estimation of a probability density function (PDF) of the dynamical system states based on a a mathematical process model and a sequence of noisy measurements [15, 23]. Since the quality of the filter estimation depends on the "level" of observability provided by the signal (sensors) that drives the filter, *observability can be used as a performance criterion for filters*. Using a moving horizon estimation technique, this concept was explored by [48] to assess the quality of the provided set of sensor nodes as state reconstructors.

In this chapter, we present a Bayesian filter formulation, based on the particle filter[1] (PF), to dynamical network applications as a way to assess its observability properties. This is motivated by the fact that if the measuring signals do not provide relevant information to the filter, i.e. they convey low observability, then the update stage of the filter is compromised and, consequently, the estimates show low performance. Thus, we argue that the provided PF formulation can be used in literature as a mean to validate and compare, on a practical level, different observability metrics and sensor selection methods proposed in literature.

Moreover, via the PF numerical results, we take the opportunity to discuss the observability aspects of a network system based on the interplay between the network topology and the node individual dynamic system. We use two benchmark systems: a network of Kuramoto oscillators and a network of Rössler systems. In the former, in which every node is composed of a 1-dimensional model, we focus exclusively on the observability impacts from the sensor nodes selection of the network system. In the latter, each node has a 3-dimensional model with uttermost observability properties, allowing us to study the correlation among the sensor nodes selection and the chosen variable observabilities.

The chosen method for Bayesian filtering is the PF for convenience purposes. Despite the PF suffering with the inconvenient *curse of dimensionality* [109, 121], we deal only with networks of utmost 45 states. Furthermore, as our second benchmark involves chaotic behaviour, the PF is proven to be a better alternative due to the system several nonlinearities and non-Gaussian uncertainties [24, 71]. We argue that Kalman filter-based estimators are not recommended since its covariance matrix is not

[1] Also known as sequential importance resampling (SIR) filter.

computationally feasible in high-dimensional systems, specially those with high linear dependences among its states, such as network systems.

4.2 Background on Particle Filtering

PF is a suboptimal state estimator based on sequential Monte Carlo methods to solve statistic problems. This method uses an independent number of stochastic samples, so-called *particles*, extracted directly from the state-space, that are recursively located, propagated and weighted accordingly to Bayes' theorem. It describes the states probability density function (PDF) by sampling approximation, not relying on any linearisation method or function approximation. Thus, it is applicable to any nonlinear and non-Gaussian problem, such as systems with several nonlinearities (e.g. chaotic systems) or multi-modal PDFs. The drawback is the computational burden, although the ever-increasing computational power already allows PF to be used on *online* applications [32], specially multi-target tracking [124].

This section provides background on the PF framework. The reader is referred to [31, 23, 32, 15] for details. Let us consider the following discrete-time autonomous nonlinear dynamical system:

$$\begin{aligned} \boldsymbol{x}_k &= f(\boldsymbol{x}_{k-1}) + \boldsymbol{w}_k \qquad \text{state equation} \\ \boldsymbol{y}_k &= h(\boldsymbol{x}_{k-1}) + \boldsymbol{v}_k \qquad \text{observation equation} \end{aligned} \tag{4.1}$$

where $k = 1, 2, \ldots$ are the time indices, $\boldsymbol{x}_k \in \mathbb{R}^n$ is the n-dimensional state at time instant k, $\boldsymbol{y}_k \in \mathbb{R}^q$ is the q-dimensional observation at time instant k, $f : \mathbb{R}^n \mapsto \mathbb{R}^n$ and $h : \mathbb{R}^n \mapsto \mathbb{R}^q$ are nonlinear functions, and $\boldsymbol{w}_k \in \mathbb{R}^n$ and $\boldsymbol{v}_k \in \mathbb{R}^q$ are additive process and observation noises, respectively with known distributions.

Given the system model (4.1) and a sequence of observations $\boldsymbol{y}_{1:k} = \{\boldsymbol{y}_1, \boldsymbol{y}_2, \ldots, \boldsymbol{y}_k\}$, the goal is to estimate the *posterior* distribution $p(\boldsymbol{x}_k|\boldsymbol{x}_{1:k-1}, \boldsymbol{y}_{1:k})$ sequentially, that is, from a *prior* distribution $p(\boldsymbol{x}_{k-1}|\boldsymbol{x}_{1:k-2}, \boldsymbol{y}_{1:k-1})$. It is assumed that model (4.1) is a Markovian process, i.e. future states depend only upon the present state, yielding $p(\cdot|\boldsymbol{x}_{1:k-1}) = p(\cdot|\boldsymbol{x}_{k-1})$ and $p(\cdot|\boldsymbol{y}_{1:k}) = p(\cdot|\boldsymbol{y}_k)$. Recall that the PF approximates a posterior distribution $p(\boldsymbol{x}_k|\boldsymbol{x}_{k-1}, \boldsymbol{y}_k)$ with random samples, which are propagated from time instant $k-1$ to k by a mathematical model. The particles are assigned to weights based on the likelihood of its estimations regarding the acquired observations at time instant k. Finally, the filter output is the weighted average of all particles estimatives. Algorithm 1 summarizes these proceedings.

Algorithm 1 Particle filter

For time steps $k = 1, 2, \ldots$

1. Given a *proposal* distribution q, draw N_p particles (samples)

$$\boldsymbol{x}_k^{(p)} \sim q(\boldsymbol{x}_k^{(p)} | \boldsymbol{x}_{k-1}^{(p)}, \boldsymbol{y}_k), \quad \forall p = 1, 2, \ldots, N_p, \tag{4.2}$$

   where $\boldsymbol{x}_k^{(p)}$ is the p-th particle of $\boldsymbol{x}_k$.
2. Given a *likelihood* distribution $p(\boldsymbol{y}_k | \boldsymbol{x}_k^{(p)})$ and a *transition* distribution $p(\boldsymbol{x}_k^{(p)} | \boldsymbol{x}_{k-1}^{(p)})$, calculate the importance weights $W_k^{(p)}$ of the p-th particle at time instant k:

$$W_k^{(p)} = W_{k-1}^{(p)} \cdot \frac{p(\boldsymbol{y}_k | \boldsymbol{x}_k^{(p)}) \cdot p(\boldsymbol{x}_k^{(p)} | \boldsymbol{x}_{k-1}^{(p)})}{q(\boldsymbol{x}_k^{(p)} | \boldsymbol{x}_{k-1}^{(p)}, \boldsymbol{y}_k)}, \quad \forall p. \tag{4.3}$$

3. Normalize the importance weights

$$\overline{W}_k^{(p)} = \frac{W_k^{(p)}}{\sum_{p=1}^{N_p} W_k^{(p)}}, \quad \forall p. \tag{4.4}$$

4. Calculate the (estimated) effective sample size

$$\hat{N}_{\text{eff}} = \frac{1}{\sum_{i=1}^{N_p} (\overline{W}_k^{(p)})^2}. \tag{4.5}$$

5. If $\hat{N}_{\text{eff}} < N_{\text{t}}$, where N_{t} is a predefined threshold, resample N_p particles and reset weights to $W_k^{(p)} = 1/N_p$.

Some remarks are in order: (i) the estimate $\hat{\boldsymbol{x}}_k$ is given by the weighted average $\hat{\boldsymbol{x}}_k = 1/N_p \sum_p \boldsymbol{x}_k^{(p)} \overline{W}_k^{(p)}$; (ii) for resampling methods details, e.g. multinomial, residual and systematic, see [15]; (iii) a common threshold is $N_{\text{t}} = N_p/2$ or $N_p/3$ [23]; and (iv) weights are usually calculated in logarithmic scale to improve numerical precision. Noise process must be carefully designed: a smaller noise process causes sample impoverishment in very few iterations, while higher noise process can provide estimates with larger deviations [23]. Furthermore, in this paper, we implement exclusively the *bootstrap* PF variant, in which the proposal distributions is assumed to be equal to the transition distribution, yielding $q(\boldsymbol{x}_k^{(p)} | \boldsymbol{x}_{k-1}^{(p)}, \boldsymbol{y}_k) = p(\boldsymbol{x}_k^{(p)} | \boldsymbol{x}_{k-1}^{(p)})$.

4.3 Particle Filtering for Dynamical Networks

In the following experiments, there is a dynamical system at each node. A benchmark network is used to generate the data that will feed a particle filter. A hat, e.g. $\hat{\boldsymbol{x}}$, is used to indicate estimated values.

4.3.1 Network of Kuramoto oscillators

Consider a network of Kuramoto oscillators where each oscillator $v_i \in \mathcal{V}$ is represented by a phase angle $\boldsymbol{x}_i \in \mathbb{R}$. The dynamical benchmark network can be represented by the following continuous state-space model [125, 21]:

$$\dot{\boldsymbol{x}}_i = \omega_i + \rho \sum_{j=1}^{N} a_{ij} \sin(\boldsymbol{x}_j - \boldsymbol{x}_i), \quad i = 1, 2, \ldots, N, \tag{4.6}$$

where $\boldsymbol{x} = \begin{bmatrix} \boldsymbol{x}_1 & \boldsymbol{x}_2 & \ldots & \boldsymbol{x}_N \end{bmatrix}^\mathsf{T}$, N is the network size (and number of states n, in this case), ρ is the coupling strength, and $\omega_i > 0$ is the oscillator natural frequency. Note that the coupling among the oscillators is additive, diffusive and proportional to ρ.

In simulations $\rho = 0.1$, $\omega_i \sim \mathcal{N}(1, 0.03)$ and initial conditions $\boldsymbol{x}_i(t_0) \sim \mathcal{U}(-\pi, +\pi)$, $\forall i$, where $\mathcal{N}(\mu, \sigma^2)$ denotes a Gaussian distribution with average μ and variance σ^2, and $\mathcal{U}(a, b)$ denotes a uniform distribution within limits $[a, b]$. Numerical integration is performed using a fourth-order Runge Kutta algorithm for simulation time of 500 s, with time step 0.1 s.

The output vector is obtained as follows:

$$\boldsymbol{y}_k = C\boldsymbol{x}_k + \boldsymbol{v}_k, \tag{4.7}$$

where $C \in \mathbb{R}^{q \times n}$ is the output matrix, q is the number of sensor nodes, $\boldsymbol{v}_k \sim \mathcal{N}(0, \Sigma_v)$, $\Sigma_v = \sigma_v^2 \cdot I_q$ is the covariance matrix of $\boldsymbol{v}_k$, $\sigma_v = 0.1$ and I_q is an identity matrix of dimension q. It is assumed that measures are taken independently. The set of sensor nodes is $\mathcal{S} = \{s_1, s_2, \ldots, s_q\} \subseteq \mathcal{V}$. A node v_j will be listed as a sensor node s_i if $c_{ij} = 1$, where c_{ij} is an element of C. If measures are taken on all nodes, then $\mathcal{S} = \mathcal{V}$.

The goal is to investigate how the selection of sensor nodes affects the PF performance. Other important aspects such as robustness to model parameter variation, noise level and dimensionality have been investigated elsewhere [23, 109]. Thus, in the simulations the true values of ω_i will be used.

The bootstrap PF is implemented as follows. Particles are propagated through a discrete numerical approximation $f(\boldsymbol{x}_{k-1}^{(p)}, \omega)$ of the continuous model (4.6), obtained analytically via the backward Euler method with time step 0.1 s. We introduce an additive process noise $\boldsymbol{w}_k \sim \mathcal{N}(0, \Sigma_w)$—where $\Sigma_w = \sigma_w^2 \cdot I_n$ is the covariance matrix of $\boldsymbol{w}_k$ and $\sigma_w = 0.1$—so that the filter particles have a better coverage of the state-space, as well as avoiding sample impoverishment in few steps. We set $\hat{\boldsymbol{x}}(t_0) = \boldsymbol{x}(t_0)$ for fast convergence and $N_p = 500$.

Based on Algorithm 1, we summarize the implemented PF framework for the Kuramoto network in the following Algorithm 2.

Algorithm 2 Particle filter for the dynamical networks of Kuramoto oscillators and Rössler systems

For time steps $k = 1, 2, \ldots$

1. Draw N_p samples from $p(\boldsymbol{x}_k^{(p)} | \boldsymbol{x}_{k-1}^{(p)})$:

$$\boldsymbol{x}_{i,k}^{(p)} \sim \mathcal{N}\left(f(\boldsymbol{x}_{k-1}^{(p)}), \Sigma_w\right), \quad p = 1, \ldots, N_p. \tag{4.8}$$

2. Given a likelihood distribution $p(\boldsymbol{y}_k | \boldsymbol{x}_k^{(p)}) \sim \mathcal{N}(\boldsymbol{y}_k, \Sigma_v)$, calculate the importance weights $W_n^{(p)}$ accordingly to

$$\begin{aligned} W_k^{(p)} &= W_{k-1}^{(p)} \cdot \frac{\exp\left\{-\frac{1}{2}(C\boldsymbol{x}_k^{(p)} - \boldsymbol{y}_k^{(p)})^{\mathsf{T}} \Sigma_v^{-1} (C\boldsymbol{x}_k^{(p)} - \boldsymbol{y}_k^{(p)})\right\}}{(2\pi)^{\frac{q}{2}} \det(\Sigma_{\mathrm{v}})^{\frac{1}{2}}} \\ &= W_{k-1}^{(p)} \cdot \frac{1}{(2\pi)^{q/2}\sigma_v^q} \cdot \exp\left\{-\frac{1}{2}\left\|\frac{C\boldsymbol{x}_k^{(p)} - \boldsymbol{y}_k}{\sigma_v}\right\|^2\right\}, \forall p. \end{aligned} \tag{4.9}$$

3) Follow steps (3)-(5) from Algorithm 1, using a systematic resampling for $N_{\mathrm{t}} = 0.5$.

4.3.2 Network of Rössler systems

Consider a network of Rössler oscillators, in a chaotic regime, coupled by the y variable [96, 11]. Hence, in each node $v_i \in \mathcal{V}$ there is a system with three state variables $\boldsymbol{x}_i = \begin{bmatrix} x_i & y_i & z_i \end{bmatrix}^{\mathsf{T}}$. The dynamical network can be represented by the following state-space model:

$$\begin{cases} \dot{x}_i &= -y_i - z_i \\ \dot{y}_i &= x_i + a_i y_i + \rho \sum_{j=1}^{N} a_{ij}(y_j - y_i), \quad i = 1, 2, \ldots, N \\ \dot{z}_i &= b_i + z_i(x_i - c) \end{cases} \tag{4.10}$$

where N is the network size, $n = 3N$ is the number of state variables of the network system, and (a_i, b_i, c_i) are the parameters of the i-th Rössler system. Numerical integration is performed using fourth-order Runge Kutta algorithm for a total simulation time of 500 s, with time step 0.01 s. Simulation parameters were set to $\rho = 0.1$, initial conditions $\boldsymbol{x}_i(t_0) \sim \mathcal{N}(0, I_3)$, $(b_i, c_i) = (2, 4)$, and N equidistant values within interval $a_i \in [0.388, 0.408], \forall i$.

Measures are taken linearly on the network of oscillators as follows:

$$\boldsymbol{y}_k = C \cdot \begin{bmatrix} \boldsymbol{x}_{1,k} & \boldsymbol{x}_{2,k} & \dots & \boldsymbol{x}_{N,k} \end{bmatrix}^{\mathsf{T}} + v_k \tag{4.11}$$

where $C \in \mathbb{R}^{q \times n}$, $\boldsymbol{v}_k \sim \mathcal{N}(0, \Sigma_v)$ and $\sigma_v = 0.1$. Note that the observation matrix C defines the network sensor nodes as well as which variables are measured at each oscillator. In this case, a sensor node can be composed of all variables $s_i = (x_i, y_i, z_i)$, only one variable (e.g. $s_i = y_i$) or by a combination of two variables.

Algorithm 2 summarizes the implemented PF for the Rössler network. The true values of (a_i, b_i, c_i) are used. We set $N_p = 500$, $\boldsymbol{w}_k \sim \mathcal{N}(0, \Sigma_w)$ and $\sigma_w = 0.1$ for the reasons mentioned in Section 4.3.1. Function $f(\boldsymbol{x}_k^{(p)}, a, b, c)$ is a discrete numerical approximation of the continuous model (4.10) via the backward Euler method, with time step 0.01 s.

4.4 Numerical Results

In the following numerical studies, consider the dynamical network models and PF frameworks detailed in Section 4.3, where measures are taken independently in each state (node) and the network graph of interest is a *chain graph* of N nodes.

4.4.1 Particle filter framework as a validation benchmark

The quality of a Bayesian filter estimate depends on the observability conveyed by the measured variables. In other words, the higher the observability rank of a network system observed by a particular set of sensor nodes, the better the PF performance, that is, the smaller is the difference between its estimates and the true value. In this section, we analyze the PF framework effectiveness as an alternative mean to assess observability properties of a network system by comparing its performance with the results yielded by the well-consolidated observability rank in (3.20). Since δ_o is quite unfeasible for systems over fifth dimension, we investigate the PF framework on a Kuramoto dynamical network of $N = 4$ nodes.

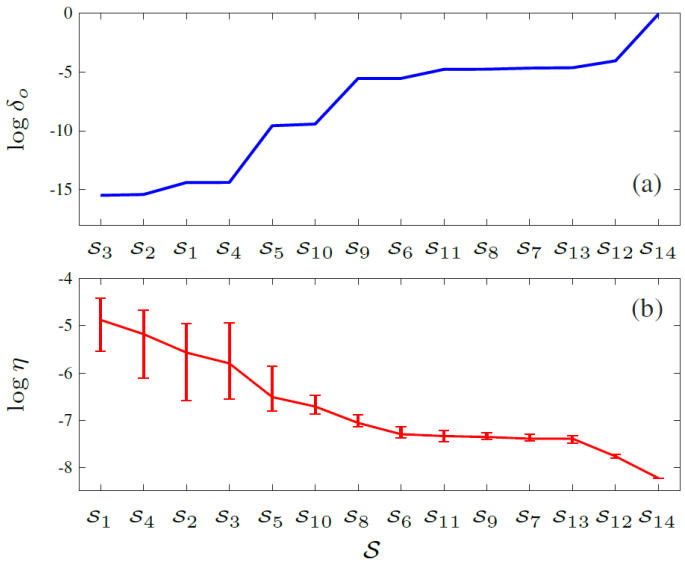

Figure 4.1: For every possible set of sensor nodes in a four-node network of Kuramoto oscillators, (a) the observability rank δ_o and (b) the performance index η, in logarithmic scale. Error bars show the interquartile range. Sets $\mathcal{S}$ are sorted in crescent and decrescent order for δ_o and η, respectively. Simulations were performed with $\omega = [1.0155 \;\; 0.9648 \;\; 1.022 \;\; 1.0476]^\mathsf{T}$. The sensor sets cardinalities are $|S_{1-4}| = 1, |S_{5-10}| = 2, |S_{11-13}| = 3$, and $|S14| = 4$.

Moreover, it is important to notice that, unlike the observability metrics presented in Section 3.1 and 3.2, the PF is not a deterministic tool since its results heavily depend on the particles realizations. A statistical analysis is required. Thus, in the following numerical simulations, the applied performance index η_i is the median of the normalized root-mean-square error (NRMSE) per node v_i over 200 Monte Carlo simulations:

$$\eta_i = \text{median}\left\{ \frac{1}{200 \cdot \Delta \boldsymbol{x}_i} \sqrt{\frac{1}{N} \sum_k \left(\boldsymbol{x}_{i,k} - \hat{\boldsymbol{x}}_{i,k|q} \right)^2} \right\}, \tag{4.12}$$

where $\hat{\boldsymbol{x}}_{i,k|q}$ refers to estimate $\hat{\boldsymbol{x}}_{i,k}$ of the qth Monte Carlo simulation (with different process noise realizations), and $\Delta \boldsymbol{x}_i = \max \boldsymbol{x}_i - \min \boldsymbol{x}_i$ is the measured data range. Note that median is preferred rather than the mean since the PDF of $\hat{\boldsymbol{x}}_{i,k}$ is non-Gaussian. The PF overall performance in a dynamical network is defined as $\eta = \frac{1}{n} \sum_{i=1}^{n} \eta_i$.

Fig. 4.1 presents the computed observability ranks δ_o and the PF framework performance index η for every possible combination of sensor nodes in this network. Firstly, it is interesting to note that *all* choices of sensor nodes are observable (i.e. $\delta_o > 0$ for all sets $\mathcal{S}$). This is in line with Liu *et al.* structural approach [70, 73] since the whole graph is a root-strongly connected component (SCC). Nevertheless, from a

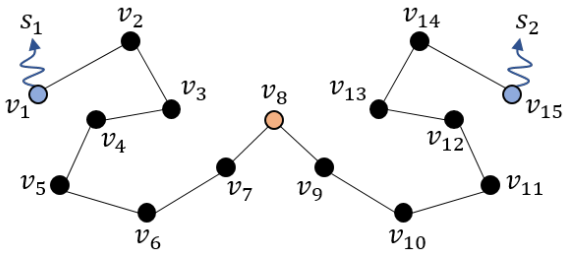

Figure 4.2: Chain graph of Kuramoto oscillators, with measures taken on network ends. Sensor nodes are marked in blue and the node with highest path length from all sensor nodes is marked in orange.

practical aspect, as pointed out by δ_o metric, some choices of sensor nodes (specially where $|S| = 1$) are *almost unobservable*.

It is evident that the PF performance η is not an *exactly* equivalent metric to δ_o. Specially for $|\mathcal{S}| = 1$, there is low correlation between η and δ_o. A possible justification is that, since systems of poor observability compromises the PF update stage efficacy, the PF realizations exhibits large interquartile ranges in its estimates which, in turn, also compromises the statistical relevance of η for $|\mathcal{S}|$. However, when $|\mathcal{S}| \geq 2$, we note that the standard deviation of the PF estimates η reduces considerably and results become statistically relevant. Indeed, for $|\mathcal{S}| \geq 2$, there is a high correlation between η and $\delta_o bs$, except in two occasions ($\mathcal{S}_8$ and $\mathcal{S}_9$ are switched in Figs. 4.1a,b). We argue that although the PF is not effective to quantify or rank the observability of dynamical systems of very poor observability indexes, it is quite robust when the observability index is a little bit better. The application of the PF framework as a validation benchmark to study observability issues in networks is explored in Section 4.4.2 and 4.4.3.

4.4.2 Network of Kuramoto oscillators

Consider a Kuramoto dynamical network of $N = 15$ nodes where measures are taken independently on the chain extremities ($\mathcal{S}_1 = \{v_1, v_{15}\}$, see Fig. 4.2). Thus:

$$C = \begin{bmatrix} 1 & 0 & \dots & 0 & 0 \\ 0 & 0 & \dots & 0 & 1 \end{bmatrix} \tag{4.13}$$

where $C \in \mathbb{R}^{2\times 15}$. Following Section 4.4.1 results, it is expected that a node (state) with the worst estimation (highest η_i)) by a Bayesian filtering implies that this node is the least observable node from a particular set of sensor nodes. Hence, the optimal

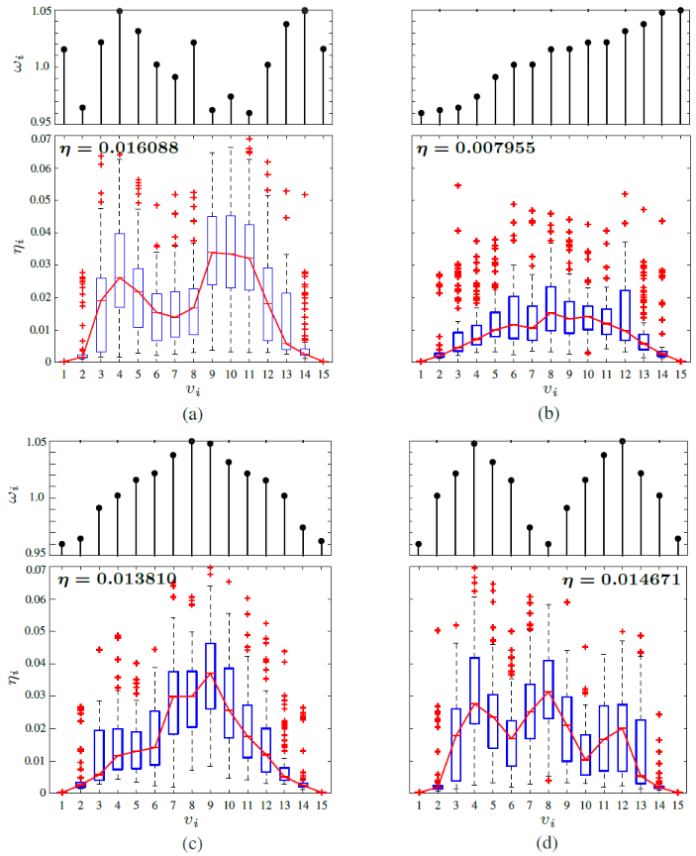

Figure 4.3: Boxplot of η_i per node (left) and the corresponding natural frequency of the Kuramoto oscillator (right), considering the chain graph in Fig. 4.2. (a) Random draw from $\omega_i \sim \mathcal{N}(1, 0.03)$; (b) random draw in (a) sorted by ascending order; (c) an unimodal arrangement of random draw in (a); and (d) a bimodal arrangement of random draw in (a). The η_i median is traced by a red line to guide the eyes.

selection of sensor nodes is actually the one that provides minimum overall estimation error η when compared to all other options with a same number of sensor nodes.

If no dynamics are considered at the nodes (i.e. each node is modeled as an unidimensional dynamical system with nonlinear interactions disregarded), this selection will be based entirely on the network graph. For instance, consider Fig. 4.2. Indeed, one might argue that, since the central node v_8 is, topologically, the farthest away from both sensor nodes, it might be the least observable node from $\mathcal{S} = \{v_1, v_{15}\}$. But if nodal dynamics were considered, i.e. the nonlinear interactions between the oscillators and their individual natural frequencies of oscillations ω_i, would v_8 still be the least observable one? It is known from [11, 29] that the location of oscillators (with different ω_i) in a network affects the synchronization process, but how does it affect the observability of a dynamical system? References [128, 48], in turn, showed through

small motifs that the optimal $\mathcal{S}$ is dependent not only of the ordinary differential equations that governs the system behaviour but also from its specific parameters.

It is here argued that this can be understood assessing the performance of the PF estimates along different networks that share a same topology, but different locations of oscillators. Figure 4.3 presents the attained filter estimates η_i for different distributions of ω_i over the chain network in Fig. 4.2.

Despite all networks in Figs. 4.3a-d being composed of the same Kuramoto oscillators, we see that their *placing order* along the chain graph affects the PF performance in different manners. Depending on the oscillators location, the PF worst estimate shifts away from v_8, presenting different η_i distributions over the network. For instance, in Figs. 4.3a,d we see, respectively, a bimodal and trimodal distribution of η_i, while in Figs. 4.3b,c there is a somewhat unimodal distribution. There is an implication between the degree of observability and the graph topology and dynamic interactions that seems to be, likewise in synchronization analysis [11], related to the degree of mismatch between the dynamics of an oscillator and its neighbours. In the case of a Kuramoto network, the nodal dynamics differ exclusively by the oscillators natural frequencies. Adopting [11] convention, we refer as *soft transition* if there is a relatively small frequency mismatch in a neighbourhood, or as *hard transition* otherwise.

Consider Fig. 4.3a. Note that the frequency mismatch among the pairs of nodes (v_2, v_3), (v_5, v_6), (v_8, v_9) and (v_{12}, v_{13}) can be considered as hard transitions. These hard transitions gives rise to *cluster* synchronization behaviours, where nodes $\mathcal{C}_1 = \{v_3, v_4, v_5\}$, $\mathcal{C}_2 = \{v_6, v_7, v_8\}$ and $\mathcal{C}_3 = \{v_9, v_{10}, v_{11}\}$ form distinct synchronous manifolds. Cluster $\mathcal{C}_1$ is topologically closer to the sensor node s_1, cluster $\mathcal{C}_3$ is closer to s_2 and cluster $\mathcal{C}_2$ is central. Consequently, the estimates in $\mathcal{C}_1$ are more affected by observations in s_1, while estimates in $\mathcal{C}_3$ are more affect by s_2 and estimates in $\mathcal{C}_2$ are somehow affected by a combination of both sensor nodes. The mean frequency of clusters $\mathcal{C}_1$ and $\mathcal{C}_3$ deviate from those of both sensor nodes, resulting in worst filter estimates in these clusters—hence the selected sensor nodes might not be optimal to observe these clusters states. Note, however, that $\mathcal{C}_1$ mean frequency is closer to s_1 frequency than $\mathcal{C}_3$ mean frequency is closer to s_2, which in turn is reflected on better estimates in $\mathcal{C}_1$ than in $\mathcal{C}_3$. Furthermore, cluster $\mathcal{C}_2$ has a mean frequency closer to that of both s_1 and s_2, which might justify the better estimates in $\mathcal{C}_2$ than in $\mathcal{C}_1$ and $\mathcal{C}_3$. Interestingly, there is a hard transition between (v_1, v_2) and η_2 is quite low. This might be attributed to the close topological proximity of these nodes on the network, relieving the dynamic difference effects.

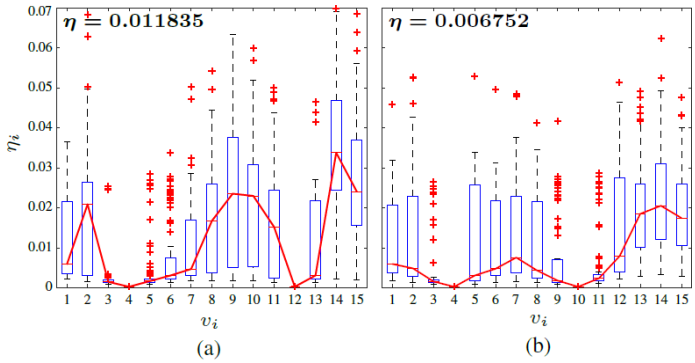

Figure 4.4: Boxplot of η_i per node using the oscillators locations in Fig. 4.3a, but with different pairs of sensor nodes. (a) $\mathcal{S}_2 = \{v_4, v_{12}\}$; (b) $\mathcal{S}_3 = \{v_4, v_{10}\}$.

Figures 4.3b-d support this analysis with different arrangements. In Fig. 4.3b, the frequency mismatch over the network chain is relatively low, pointing to soft transitions. This arrangement favours global synchronization behaviour in the dynamical network [11]. Thus, the tendency to form a single synchronous manifold for the whole network, rather than isolated clustered manifolds in Fig. 4.3a, might lead to observations of better quality for the sensor nodes and, hence, a lower overall η as seen in Fig. 4.3b. Moreover, being the natural frequencies arranged in a homogeneous manner, the central node might have the worst estimates due to its large topological distance from both sensor nodes as well as the high dynamic behaviour differences between v_8 and s_1 or s_2. The η_i is mostly unimodal, although some slight peaks in η_6 and η_{10} might be attributed, respectively, to relative soft transitions on pairs (v_6, v_7) and (v_{10}, v_{11}).

The unimodal and bimodal arrangement of natural frequencies of the Kuramoto oscillators in Fig. 4.3c,d shows interesting relation. Once again, in Fig. 4.3c, the worst estimates are central, due to high topological distance to sensor nodes and high dynamic behaviour differences. The worst estimate is actually in node v_9, although this might be attributed to a relative soft transition on pair (v_8, v_9). The filter estimates in Fig. 4.3d presents a trimodal distribution along the network nodes, where the second and third highest errors η_4 and η_{12} are due to dynamical differences in these node behaviours compared to the sensor nodes one. Node v_8, although having similar natural frequency to sensor nodes s_1 and s_2, has the worst estimate and is the least observable state from the selected pair of sensor nodes—which might be attributed to the fact that these sensor nodes do not share the same synchronous manifold of state v_8.

Using the oscillators location along the chain graph of Fig. 4.2, we show in Fig. 4.4 how the PF performance changes with the sensor locations. For instance, in Fig. 4.4a, we set a pair of sensor nodes which provide the smallest path length from all other nodes

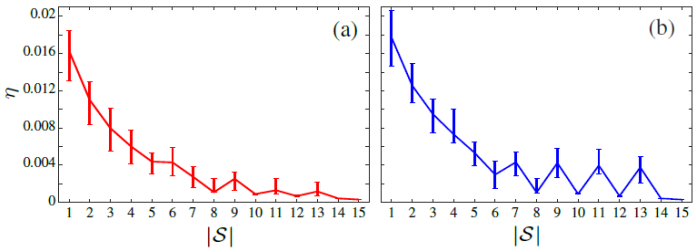

Figure 4.5: PF overall performance index η per number of sensor nodes (allocated as detailed in text), for oscillators locations displayed in: (a) Figs. 4.3a, (b) Figs. 4.3d. Error bars show the interquartile range.

in the network, while, in Fig. 4.4b, we set the central nodes of "clusters" $\mathcal{C}_1$ and $\mathcal{C}_2$. Since η is smaller in Fig. 4.4b, we argue that choosing a set of sensor nodes that is not only central to the network topology, but also "dynamically central" (representative of its neighbourhood dynamics) seems to convey better degrees of observability. At least for the Kuramoto dynamical network, presence of synchronous manifolds, dynamical correlations and topological proximity seem to affect the network system observability. The interplay between synchronization, observability and dynamics has already been addressed in [64], with systems of lower dimensionality. The work pointed to a *not exclusive* dependence between synchronization and observability, a remark that seems to be also relevant in high-dimensional systems.

Finally, in Fig. 4.5, we investigate the improvement in the PF performance η by gradually increasing the number of sensor nodes. Sensor nodes are allocated in such a way that the sum of the path lengths between every single node and the closest sensor node is minimum. As the number of sensors increase, the PF usually benefits from more valuable information and, consequently, η has a tendency to decrease in an exponential manner. This is related to Haber *et al.* [48] conclusion that there is an intrinsic obstacle when trying to infer the network states from a small number of sensors. Interestingly, in some instances, η increases after adding a sensor node. Due to the sensor nodes allocation method, from an even number of nodes to an odd number, not only the number of sensors increase but their positions change as well. Thus, increasing the number of sensor nodes do not guarantee a better observability. For instance, Fig. 4.5b shows clearly that the PF performance, and the network observability, are better when not including the central node as a sensor node, which always happens when there is an odd number of sensors. Interestingly, the higher the observability, the lower the median and interquartile range of η—indicating that the PF estimates are more reliable.

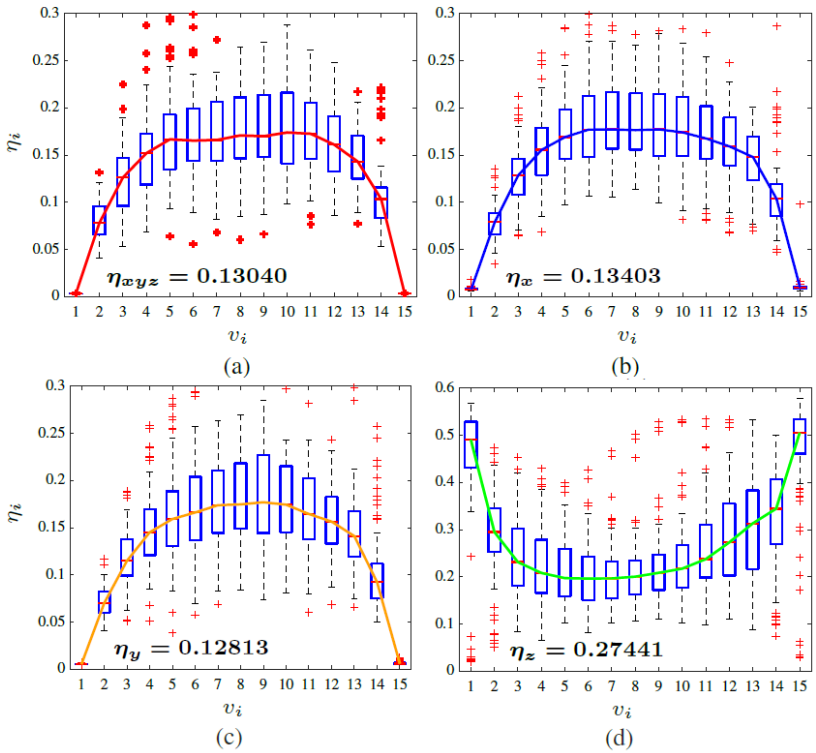

Figure 4.6: Boxplot of η_i per node, for a chain graph of Rössler systems with different sets of sensor nodes: (a) $\mathcal{S}_1$; (b) $\mathcal{S}_2$; (c) $\mathcal{S}_3$; (d) $\mathcal{S}_4$. Numerical setup is described in Section 4.3.2.

4.4.3 Network of Rössler systems

Consider a Kuramoto dynamical network of $N = 15$ nodes ($n = 3N$ states) where measures are taken independently on the chain extremities ($\mathcal{S} = \{v_1, v_{15}\}$, see Fig. 4.2). In this network system, each node is composed of three state variables whose observability rank is $y \rhd x \rhd z$, with y and x being good variables to reconstruct the dynamics, and z a poor one [65]. In this section, based on the PF performance, we investigate how the observability of nodal dynamics affects the network observability. Thus, we compare the numerical results for the following sets of sensor nodes: (i) the sensor nodes measures all states of a node, i.e. $\mathcal{S}_1 = \{(x_1, y_1, z_1), (x_{15}, y_{15}, z_{15})\}$; and (ii) the sensor node measures only one state per node, i.e. $\mathcal{S}_2 = \{x_1, x_{15}\}$, $\mathcal{S}_3 = \{y_1, y_{15}\}$ and $\mathcal{S}_4 = \{z_1, z_{15}\}$.

Fig. 4.6 presents the attained filter estimates η_i for each of the described sets of sensor nodes. As described in Section 4.3.2, the implemented Rössler system network has a soft transition in parameter a_i along the network chain. Although it is not our goal to evaluate the effects of dynamics in network observability in this section, we

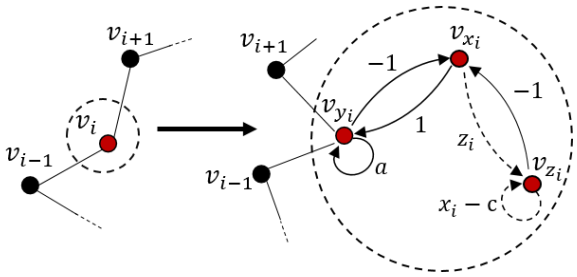

Figure 4.7: Chain graph, and the corresponding graph representation when a given node v_i is an individual Rössler system coupled by the y variable. Linear and nonlinear interactions are traced in solid and dashed lines, respectively.

note that the central node v_8 has the highest η_i in every occasion, just as seen in Fig. 4.3b.

Clearly, the observability rank of Rössler system is carried over to its high-dimensional network, as $\eta_y < \eta_x < \eta_z$. Interestingly, η_{z_i} shows worst performance to node estimates next to the sensor nodes, than in the farthest node. The z variable has little information regarding the system cyclic behaviour, which compromises the state reconstruction, specially when $z_i \to 0$. However, as the path length from a node estimate to a sensor node increases, η_{z_i} reduces, suggesting that the sensor node might retain more information regarding its distant neighbours than from its closer ones. Nonetheless, η_{z_i} in Fig. 4.6d is always inferior compared to the others.

The attained effects of a multidimensional node over the network observability in this study can be studied under a graph optic [4]. A single multidimensional node can be decomposed in multiple additional and interconnected nodes (states) as illustrated in Fig. 4.7. In the case of a Rössler system, based on system model (4.10), a single node v_i can be decomposed into three nodes: $(v_{x_i}, v_{y_i}, v_{z_i})$, where their interconnections can be deduced from the system equation following the Lin's structural controllability approach [70]. The reader is referred to [4] for further details. Nevertheless, notice that v_{z_i} has a direct path to v_{x_i} that is weighted by the state z_i. Thus, when $z_i \to 0$, this path vanishes and v_{z_i} loses information of v_{x_i} and, consequently, of all network. This behaviour is probably one way of understanding the loss of performance in Fig. 4.6d.

4.5 Conclusion

In a network of high-dimensionality, it is not feasible to measure every single node. Thus, an important topic of research is to define the optimal choice of sensor nodes in which the network system trajectories in the state-space can be reconstructed trustworthy.

This is a problem of network observability. Recently, several papers proposed novel metrics to determine this optimal selection of sensor nodes [73, 136, 95, 115, 61, 48]. However, a benchmark framework to compare and validate the efficacy of novel metrics in literature is still absent.

In this paper, we develop a particle filtering framework as a way to assess observability properties of a dynamical network, where each node is composed of an individual dynamical system. This is motivated by the fact that the quality of the filter estimation depends on the "level" of observability provided by the signal. Firstly, we show the PF effectiveness to quantify the observability level in a network by comparing this framework to a traditional observability metric in a system of lower dimensional order. Secondly, we show, in a network of 15 and 45 states (composed of Kuramoto oscillators and Rössler systems, respectively), that a good choice of sensors is related not only to the topological position of a sensor node in a graph, but also to its dynamic behaviour—that is, the precise values of the model parameters. These results corroborates with [48]. It seems that the sensor node dynamics must share some dynamical affinity to its neighbours in order to be representative of their behaviour and, thus, carry relevant information to the measurement signals. Thirdly, we investigate how the choice of an internal measured variable of a sensor node can affect the overall network observability. As shown in a Rössler network, the PF performance, and thus the observability, is better when measures are taken on variables of higher observability.

This work might provide insight for future researches of dynamical networks and the interplay between topology and dynamics. The detailed framework of Bayesian filtering as a performance measure of observability can be used as a validation platform over different benchmarks of networks in order to compare novel observability metrics in literature. As future work, it might be worth to investigate if the *ensemble Kalman filter*, a combination of Kalman filter methodology with a sequential Monte Carlo approach, is more robust or precise than the proposed PF framework for high-dimensional systems [34, 35].

Chapter 5

Phase Synchronization Analysis of Bridge Oscillators between Clustered Networks

Recent works aim to establish necessary and sufficient conditions to guarantee phase synchronization between clusters of oscillators, usually requiring numerous and stronger intra-cluster connections compared to the inter-connections between isolated clusters. In this context, our analysis takes a different approach of studying the synchronous manifold stability of inter-cluster connections, whithout relying on full information on the adjacency matrix describing the specific connections among oscillators in each cluster, since this information can be unavailable in some applications. This approach allows us to reduce the clustered network interactions to a simplified problem where we focus only on inter-cluster relations, modelling intra-cluster effects as perturbations. Based on Lyapunov direct method, we provide a framework to derive sufficient conditions so the interconnected oscillators phase difference is ultimately bounded. The framework is presented in a case study of two inter-connected clusters of Kuramoto oscillators. The theoretical conditions are compared to numerical simulations where we show the results effectiveness, but also conservativeness accordingly to the network available information. This framework could be generalized to different networks and oscillators.

This chapter is organized as follows. We review the literature regarding cluster synchronization in Section 5.1 and provide some background on synchronization and stability analysis in Section 5.2. Section 5.3 defines the statement of the problem, while Section 5.4 describes the main results. The theoretical results are compared

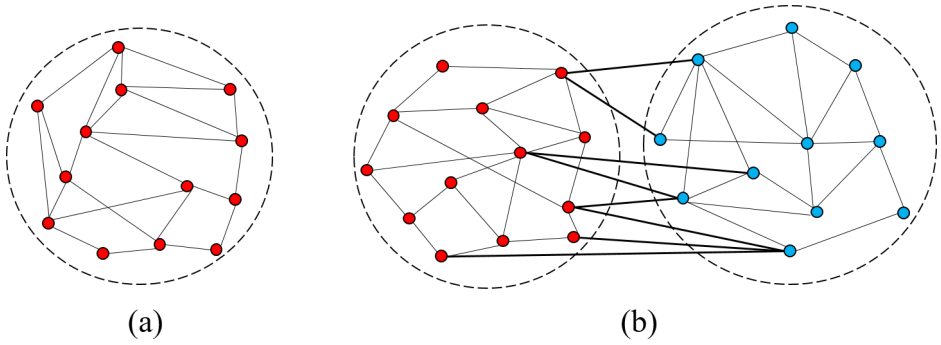

Figure 5.1: (a) Hypothetical cluster formation in the whole network. (b) Full cluster synchronization between two different networks. A common problem is the investigation of the conditions under which red oscillators are PS among themselves, and blue oscillators could either be unsynchronized or PS among themselves but not with the red cluster. Another related problem is to find under which conditions all oscillators get synchronized.

to numerical simulations in Section 5.5. Finally, Section 5.6 concludes this work by summarizing the main results and possible future research directions.

The contents of this chapter are similar to the manuscript [80].

5.1 Introduction

This work is concerned with phase synchronization in a network of oscillators [98, 67]. Some pioneering studies considered just *a pair* of coupled oscillators. In that scenario the conditions to achieve synchronization are mainly related to the oscillators dynamical properties, such as natural frequencies, and coupling methods [42, 96]. However, when studying *a network* of oscillators, the nodes individual characteristics and dynamics must be analysed along with the network topology. For instance, phase synchronization conditions have been provided for specific complex networks of phase oscillators, such as small-world networks [51, 9] and scale-free networks [125, 84].

Different approaches have been provided to describe cluster formation in the synchronization of networks, that is, conditions under which the oscillators in Fig. 5.1a become phase synchronized (PS). To this end, the network clustering coefficient was used in [78] and stability properties were used in [27]. Symmetries and topological patterns are explored in [97, 110]. Schaub et al. [104] point out that cluster synchronization is directly related to the Laplacian matrix. Dorfler and Bullo [29] present a survey summarizing the literature main achievements on complex networks synchronization of phase oscillators.

A different line of investigation involves the study of synchronization of two interconnected clustered networks (Fig. 5.1b). Reference [68] derives conditions under which the red oscillators synchronize with the blue ones, assuming that both isolated networks share the same (inner) topology. This result was extended to interconnected networks of different topologies [118] in the context of generalized synchronization [130, 131]. In particular, works [75] and, more recently, [36] investigate the impact of *intra- and inter-cluster connections* (also known as inner and outter connections) on the stability of the clusters synchronous manifolds. According to the reported results, intra-cluster synchronization is achieved by an intuitive combination of strong intra-cluster and weak inter-cluster connections.

The studies reported in the literature use a wide range of models, from the basic Kuramoto oscillator [58, 113, 29] to more sophisticated models, such as the Hodgkin-Huxley neurons [100] and chaotic systems [11]. In this study, Kuramoto oscillators will be used, mainly for the rich dynamic behaviour that can be attained using such a system in network nodes and the wide range of possible applications [29], with the added advantage of being described by rather simple equations.

In this chapter, *sufficient conditions* are derived under which the interconnected nodes of otherwise isolated clusters (the orange nodes in Fig. 5.2) become PS —without assuming that all oscillators of a cluster are PS, as usually found in the literature [68, 118, 130, 131]. To achieve this goal, the theory of stability analysis of perturbed systems, based on Lyapunov's direct method, is used in the same spirit of [56, Chapter 9]. It is suggested that, under certain conditions, all but one oscillators of a cluster can be modelled as an aggregated perturbation for the purposes of stability analysis. Hence, the red cluster in Fig. 5.2a can be modelled as a single phase oscillator with phase ϕ_1 plus a perturbation δ_1, and likewise for the blue cluster. This greatly facilitates stability analysis and permits investigating conditions under which both clusters will PS.

The approach is presented for pairs of interconnected networks of Kuramoto oscillators (Fig. 5.2a). Nevertheless, the developed framework can be further extended to address more complex and generalized networks, such as the one illustrated in Fig. 5.2c, comprised by more than 2 clusters, provided – as it will be shown – that a Lyapunov function of the simplified model is known. For complex networks of phase oscillators, Ref. [29] briefly discusses appropriate Lyapunov functions for synchronization stability analysis.

Former studies of network synchronization usually assume that the whole network topology (and its corresponding adjacency matrix) is known [104] —which might not

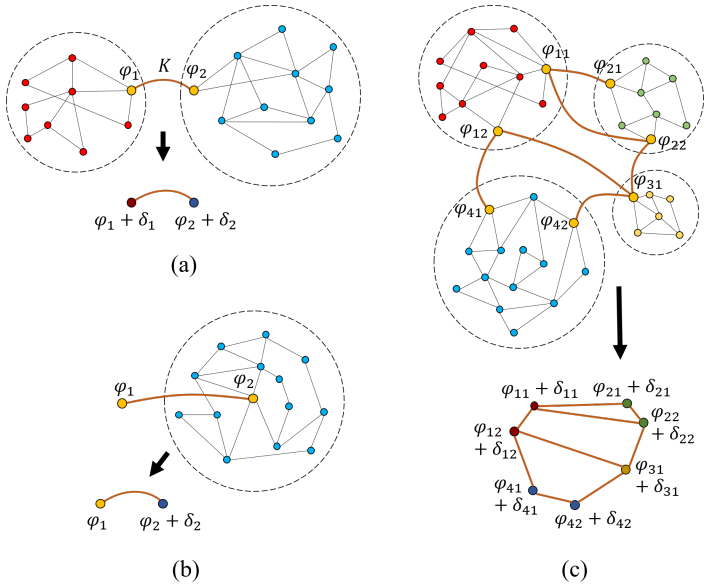

Figure 5.2: Examples of interconnected clustered networks and their respective simplified model added by a bounded perturbation. (a) Two interconnected clusters simplified to a single pair of coupled oscillators – which will be called "bridge oscillators" – added by the respective perturbation δ of its intra-cluster connections. (b) A particularization of (a), where one cluster is replaced by a single oscillator. (c) A generalization of (a), with further clusters and interconnections.

be true in real applications. In this chapter, sufficient conditions for inter-cluster PS, in Theorem 5.5, are obtained without assuming perfect knowledge of the complete network interconnection topology, and they depend only on prior information on the neighboring connections of the so-called "bridge oscillators" (defined in Section 5.3).

5.2 Background

This section provides some background in synchronism of oscillators and network systems. A control approach is given in this work to study the synchronism phenomenon, grounded on the stability theory of Lyapunov. We state the main definitions and results of Lyapunov theorem as well as the stability of perturbed systems in the following sections.

5.2.1 Synchronism

Synchronization is the *"adjustment of rhythms of oscillating objects due to their weak interaction"*, said Pikovsky *et al.* [98]. It is known as synchronization if two

or more *autonomous* (self-sustained) oscillators (defined in Section 2.1.1) with an intrinsic *frequency mismatch* and interconnected by a relatively weak *coupling strength* experience an adjustment of their natural rhythms, driving it to a *frequency entrainment* or *locking*. Naturally, the higher the frequency mismatch, or the smaller the coupling strength, the harder it becomes to synchronize two or more oscillators.

Note that to define a coupling strength as relatively weak or strong is not a trivial concept. One might argue that if the coupling strength is strong enough to "interrupt" the oscillator natural behaviour and force a new dynamic, then this is rather a control phenomenon than a synchronization one. In synchronism, the oscillators sustain their respective intrinsic behaviour even when coupled, adjusting only their rhythms and cycles.

Synchronization is achieved by different means. For instance, two or more oscillators submitted to a same external input are apt to synchronize with their driving force and, consequently, with each other. A usual driving force in engineering systems are the *clock signals*, as seen in many telecommunication, power and digital systems. Biological clocks are also intrinsically present in nature, such as how the daily and seasonal rhythms of living beings are synchronized with Earth's rotation and related aspects, e.g. illuminance. A less trivial example of synchronism by external force is the noise-induced synchronism, which is reported [98, 11] to increase statiscal correlation among the coupled system, inducing synchronism.

On the other hand, synchronization can be also achieved in interconnected systems of autonomous oscillators, or – as addressed in this work – dynamical networks. In this case, each dynamical network is an autonomous oscillator which is interconnected with other oscillators according to the network distribution and a given coupling method. These interactions can be interpreted as transmission lines in power systems, chemical pheromones in fireflies populations, the air in telecommunication systems, and so on. Indeed, in many examples, the coupling strength is indirectly related to the geographic distances between the network oscillators. Nonetheless, the interconnected network of oscillators develop complex interactions in which all oscillators "feel" directly or indirectly the dynamics of each other. The network disposition, the oscillators dynamics (rhythms) and the coupling strength are impact factors to determine if there is or not synchronization phenomenon. This is the topic of interest in this chapter.

Mathematically, the synchronism of two dynamical systems $\boldsymbol{f}_1(\boldsymbol{x}_1) : \mathbb{R}^{n_1} \to \mathbb{R}^{n_1}$ and $\boldsymbol{f}_2(\boldsymbol{x}_2) : \mathbb{R}^{n_2} \to \mathbb{R}^{n_2}$ can be assessed if their dynamic error

$$\|\boldsymbol{e}(t)\| \equiv \|\boldsymbol{x}_1(t) - \boldsymbol{x}_2(t)\| \leq \epsilon \tag{5.1}$$

is bounded by a finite threshold ϵ for $t \geq t_0 + T$. If $\boldsymbol{e}(t) = 0$, for $t \geq t_0 + T$, then both oscillators are said to be in *complete synchronization* (CS). Less strict states of synchronization have been depicted in [11] as follows:

1. *Lag synchronization* (LS): $\|\boldsymbol{e}(t)\| \equiv \|\boldsymbol{x}_1(t) - x(t + \tau_{\text{lag}})\| \leq \epsilon$, for some finite τ_{lag}.

2. *Generalized synchronization* (GS): $\|\boldsymbol{e}(t)\| \equiv \|\boldsymbol{F}(\boldsymbol{x}_1(t)) - \boldsymbol{G}(\boldsymbol{x}_2(t))\| \leq \epsilon$, where $\boldsymbol{F} : \mathbb{R}^{n_1} \to \mathbb{R}^{n_1}$ and $\boldsymbol{G} : \mathbb{R}^{n_2} \to \mathbb{R}^{n_2}$ are vector fields.

3. *Phase synchronization* (PS): $\|\theta(t)\| \equiv \|\phi_1(t) - \phi_2(t)\| \leq \epsilon \leq 2\pi$, where $\phi_i \in (-\pi, \pi]$ is the defined phase[1] of system $\boldsymbol{f}_i$ and $\theta \in (-\pi, \pi]$ is the phase difference between both oscillators.

4. *Intermittent PS* (IPS): $\|\theta(t)\| \equiv \|\phi_1(t) - \phi_2(t)\| \leq \epsilon \leq 2\pi k$, for $t_1 \leq t \leq t_2$ and $k = 0, 1, 2, \ldots$, i.e. the oscillators are PS during limited time intervals separated by *phase slips* of 2π.

The aforementioned types of synchronism can be classified with the following ascending order of difficulty (to achieve synchronization): IPS, PS, GS, LS and CS. Indeed, while GS, LS and CS require that the specific state variables of two oscillators are bounded (given a nonlinear transformation or delay in GS and LS cases), PS is achievable by only adjusting the time scales of two or more oscillators. If the interconnected oscillators have a large variation of frequencies, phase slips are bent to occur, leading to IPS [11]. A broader distribution of time scales of periodic orbits might be a consequence of chaotic systems or interconnected sets of oscillators with different natural frequencies.

A common topic of study is to determine the conditions under which two, or more, oscillators synchronize —in other words, the conditions under which the synchronization manifold is stable. In a CS context, the synchronization manifold of a network of oscillators is given by $\boldsymbol{x}_1 \equiv \boldsymbol{x}_2 \equiv \ldots \equiv \boldsymbol{x}_m$, which is directly related to the temporal evolution of the synchronization error $\boldsymbol{e}_{ij} \equiv \boldsymbol{x}_i - \boldsymbol{x}_j, \forall i = 1, \ldots, m$ and $j = 1, \ldots, m$. For this purpose, a control approach based on Lyapunov stability can be introduced to study the synchronous manifold stability, or rather the synchronization error dynamics, as reviewed in Section 5.2.2.

In this chapter, special focus is given to networks of Kuramoto phase oscillators, as presented in Example 2.1. Note that, by definition, the state variable of a Kuramoto

[1]There are several phase definitions that can be applied to nonlinear oscillators [98, 11, 39], although a general consensus in literature points that a phase variable must present the following characteristics: (i) it is a monotonically increasing function, and (ii) it is related to zero Lyapunov exponent (flow direction) [39].

oscillator is the proper oscillator phase angle[2]: $\boldsymbol{x} \equiv \boldsymbol{\phi}$. The reader is referred to survey [29] for details on Kuramoto oscillator and networks.

5.2.2 Lyapunov stability

The following definitions and theorems are further detailed in [56, Chapter 4]. Proofs are omitted. Consider space-state model (2.2), where $\boldsymbol{f} : [t_0, \infty) \times D \to \mathbb{R}^n$ is a piecewise continuous in t and locally Lipschitz in $\boldsymbol{x}$ and $D \subset \mathbb{R}^n$. Suppose that $\bar{\boldsymbol{x}}$ is the equilibrium point of (2.2), i.e. $\boldsymbol{f}(t, \bar{\boldsymbol{x}}) = 0$. Assume, without loss of generality[3], that the equilibrium point is at the origin, i.e. $\bar{\boldsymbol{x}} = 0$. We present the following definitions of stability in the sense of Lyapunov:

Definition 5.1. *[56, Definition 4.1]* ***(Stability in the sense of Lyapunov)*** *The equilibrium point $\bar{\boldsymbol{x}} = 0$ of (2.2) is*

- *stable if, for each $\epsilon > 0$, there is $\delta = \delta(\epsilon) > 0$ such that*

$$\|\boldsymbol{x}(0)\| < \delta \Rightarrow \|\boldsymbol{x}(t)\| < \epsilon, \quad \forall t > t_0; \tag{5.2}$$

- *unstable if it is not stable;*
- *asymptotically stable if it is stable and δ can be chosen such that*

$$\|\boldsymbol{x}(0)\| < \delta \Rightarrow \lim_{t \leftarrow \infty} \boldsymbol{x}(t) = 0. \tag{5.3}$$

The following Lyapunov's stability theorems are of interest in this work:

Theorem 5.1. *[56, Theorem 4.1]* ***(Lyapunov's direct method)*** *Let $D \subset \mathbb{R}^n$ be a domain containing $\bar{\boldsymbol{x}} = 0$ and $V : D \to R$ be a continuous differentiable function such that*

$$V(0) = 0 \text{ and } V(\boldsymbol{x}) > 0 \text{ in } D \backslash \{0\} \tag{5.4}$$

$$\dot{V}(\boldsymbol{x}) \leq 0 \text{ in } D. \tag{5.5}$$

Then, $\bar{\boldsymbol{x}} = 0$ is stable. Moreover, if

$$\dot{V}(\boldsymbol{x}) < D \text{ in } D \backslash \{0\}, \tag{5.6}$$

then $\bar{\boldsymbol{x}} = 0$ is asymptotically stable. ■

[2] Thus, there is no further concern for the applied phase definition in this work.
[3] This can be circumvented by a change of coordinates.

Function $V(\boldsymbol{x})$ is addressed as *Lyapunov function* if it satisfied conditions (5.4) and (5.5). The choice of a Lyapunov function is not trivial. Indeed, there is no straightforward method in literature to derive a Lyapunov function, although an usual class of functions are the quadratic forms $V(\boldsymbol{x}) = \boldsymbol{x}^{\mathsf{T}}\boldsymbol{x}$. A proposal function to serve as $V(\boldsymbol{x})$ is addressed as a *Lyapunov function candidate* until proven that it satisfies (5.4) and (5.5). Since there is multiple Lyapunov functions to each system, Lyapunov's direct method provides only *sufficient conditions* of a system stability[4].

If $V(\boldsymbol{x})$ satisfies condition (5.4), then it is said to be *positive definite*. If $V(\boldsymbol{x}) < 0$, it is a *negative definite* function. If $V(\boldsymbol{x})$ satisfies a weaker condition $V(\boldsymbol{x}) \geq 0$, then it is *positive semidefinite*, and likewise for *negative semidefinite*.

Global and exponential stability can be defined and proven as follows.

Theorem 5.2. *[56, Theorem 4.2]* ***(Global asymptotic stability)*** *Let $V : R^n \mapsto R$ be a continuous differentiable function such that*

$$V(0) = 0 \text{ and } V(\boldsymbol{x}) > 0, \quad \forall x \neq 0, \tag{5.7}$$

$$\|\boldsymbol{x}\| \to \infty \Rightarrow V(\boldsymbol{x}) \to \infty \tag{5.8}$$

$$\dot{V}(\boldsymbol{x}) < 0, \quad \forall x \neq 0, \tag{5.9}$$

then $\boldsymbol{x} = 0$ is globally asymptotically stable. ■

Definition 5.2. *[56, Definition 4.5]* ***(Exponential stability)*** *The equilibrium point $\bar{\boldsymbol{x}} = 0$ of (2.2) is exponentially stable if there exist positive constants k_0, α and c such that*

$$\|\boldsymbol{x}(t)\| \leq k_0\|\boldsymbol{x}(t_0)\|e^{-\alpha(t-t_0)}, \quad \forall\|\boldsymbol{x}(t_0)\| < c, \tag{5.10}$$

and globally exponentially stable if (5.10) is satisfied for any initial state $\boldsymbol{x}(t_0)$.

Theorem 5.3. *[56, Theorem 4.10] Let $D \subset \mathbb{R}^n$ be a domain containing $\bar{\boldsymbol{x}} = 0$ and $V : [t_0, \infty) \times D \mapsto R$ be a continuous differentiable function such that*

$$k_1\|\boldsymbol{x}\|^a \leq V(t, \boldsymbol{x}) \leq k_2\|x\|^a, \tag{5.11}$$

$$\frac{\partial V}{\partial t} + \frac{\partial V}{\partial x} f(t, x) \leq -k_3\|x\|^a, \tag{5.12}$$

[4]It is a common jargon in literature to address a system as stable (unstable) when it is actually its equilibrium point that can be defined as stable (unstable).

$\forall t \geq t_0$ *and* $\boldsymbol{x} \in D$*, where* k_1*,* k_2*,* k_3 *and* a *are positive constants. Then,* $\bar{\boldsymbol{x}} = 0$ *is exponentially stable. If the assumptions hold globally, then* $\bar{\boldsymbol{x}} = 0$ *is globally exponentially stable.* ■

Finally, although there is no method to derive a Lyapunov function, the following theorem provides guarantees of a Lyapunov function existence if the system equilibrium point is exponentially stable:

Theorem 5.4. *[56, Theorem 4.14]* ***(Converse theorem)*** *Let* $D = \{\boldsymbol{x} \in \mathbb{R}^n \mid \|\boldsymbol{x}\| < r\}$*, where* $r > 0$*, and the Jacobian matrix* $[\partial \boldsymbol{f}/\partial \boldsymbol{x}]$ *is bounded on* D*, uniformly on* t*. Let* k_0 *and* α *be positive constants. Let* $D_0 = \{\boldsymbol{x} \in \mathbb{R}^n \mid \|\boldsymbol{x}\| < r/k_0\}$*. Assume that the trajectories of the system satisfy*

$$\|\boldsymbol{x}(t)\| \leq k_0 \|\boldsymbol{x}(t_0)\| e^{-\alpha(t-t_0)}, \quad \forall \boldsymbol{x}(t_0) \in D_0, \quad \forall t \geq t_0 \geq 0. \tag{5.13}$$

Then, there is a function $V : [t_0, \infty) \times D_0 \mapsto R$ *that satisfies the inequalities*

$$c_1 \|x\|^2 \leq V(t,x) \leq c_2 \|x\|^2, \tag{5.14}$$

$$\frac{\partial V}{\partial t} + \frac{\partial V}{\partial x} f(t,x) \leq -c_3 \|x\|^2, \tag{5.15}$$

$$\left\| \frac{\partial V}{\partial x} \right\| \leq c_4 \|x\|, \tag{5.16}$$

where c_1*,* c_2*,* c_3*,* c_4 *are positive constants. Moreover, if* $r = \infty$ *and the origin is globally exponentially stable, then* $V(t, \boldsymbol{x})$ *is defined and satisfies the aforementioned inequalities on* $\mathbb{R}^n$*. Furthermore, if the system is autonomous,* $V(t, \boldsymbol{x})$ *can be chosen independent of* t*.* △

5.2.3 Stability of perturbed systems

The reader is referred to [56, Chapter 9] further details. Consider the state-space model:

$$\dot{\boldsymbol{x}} = \boldsymbol{f}(t, \boldsymbol{x}) + \boldsymbol{g}(t, \boldsymbol{x}), \tag{5.17}$$

where $\boldsymbol{x} \in D$ is the state vector, with $D \subset \mathbb{R}^n$ a subset that contains the origin $\boldsymbol{x} = 0$. The functions $\boldsymbol{f} : [t_0, \infty) \times D \to \mathbb{R}^n$ and $g : [t_0, \infty) \times D \to \mathbb{R}^n$ are piecewise continuous in t and locally Lipschitz in $\boldsymbol{x}$. Equation (5.17) can be interpreted as a nominal system (2.2) perturbed by $\boldsymbol{g}(t, \boldsymbol{x})$. Without loss of generality, it is assumed that $\boldsymbol{f}(t, 0) = 0$. The perturbation $\boldsymbol{g}(t, \boldsymbol{x})$ describes uncertainties such as noise and modeling errors. However, it is assumed some prior knowledge about $\boldsymbol{g}(t, \boldsymbol{x})$ as specified later.

From Theorem 5.1, one might consider searching for a Lyapunov function candidate for the perturbed system from the knowledge of the nominal system (2.2). The search is based on the behavior of $\boldsymbol{g}(t, \boldsymbol{x})$. If $\boldsymbol{g}(t, \boldsymbol{x})$ is a vanishing perturbation, i.e. $\boldsymbol{g}(t, 0) = 0$, then the nominal and perturbed systems equilibrium points are the same. If $\boldsymbol{g}(t, \boldsymbol{x})$ is a nonvanishing perturbation, i.e. $\boldsymbol{g}(t, 0) \neq 0$, then the origin will not be an equilibrium point of the perturbed system. In the former case, we analyze the equilibrium point stability, while in the latter we study the ultimate boundedness of the solutions of the perturbed system.

Because the present study is based on systems affected by nonvanishing perturbations, a Lemma based on Lyapunov direct method theorem [56], will be adapted for this particular case (see Theorem 5.5). First, the original version of the lemma is presented in what follows.

Lemma 5.1. *[56, Lemma 9.2]* ***(Perturbed system stability)*** *Let $\bar{\boldsymbol{x}} = 0$ be an exponentially stable equilibrium point of the nominal system (2.2). Let $\boldsymbol{V}(t, \boldsymbol{x}) : [t_0, \infty) \times D \mapsto R$ be a Lyapunov function for (2.2) that satisfies conditions (5.14) – (5.16), where $D = \{\boldsymbol{x} \in \mathbb{R}^n \mid \|\boldsymbol{x}\| < r\}$ and c_1, c_2, c_3, c_4 are positive constants. Suppose the perturbation term $\boldsymbol{g}(t, \boldsymbol{x})$ is bounded by:*

$$\|\boldsymbol{g}(t, \boldsymbol{x})\| < \delta = \frac{c_3}{c_4}\sqrt{\frac{c_1}{c_2}}\epsilon r, \quad \forall t \geq 0, \quad \forall \boldsymbol{x} \in D, \tag{5.18}$$

where $0 < \epsilon < 1$. Then, $\forall \|\boldsymbol{x}(t_0)\| < r/k_0$, the solution $\boldsymbol{x}(t)$ of the perturbed system (5.17) is bounded by:

$$\begin{aligned} &\|\boldsymbol{x}(t)\| \leq k_0 e^{-\alpha(t-t_0)}\|\boldsymbol{x}(t_0)\| \quad , \quad \forall t_0 \leq t < t_0 + T, \\ &\|\boldsymbol{x}(t)\| \leq b \qquad\qquad\qquad\quad , \quad \forall t \geq t_0 + T, \end{aligned} \tag{5.19}$$

for some finite T, with

$$k_0 = \sqrt{\frac{c_2}{c_1}}, \quad \alpha = \frac{(1-\epsilon)c_3}{2c_2}, \quad b = \frac{c_4}{c_3}\frac{k_0\delta}{\epsilon}. \tag{5.20}$$

■

Remark 5.1. The ultimate bound b of the perturbed system solution is proportional to the upper bound δ of the perturbation. This is a consequence of the nominal system exponential stability, which guarantees robustness against small perturbations.

Remark 5.2. If $f : [0, \infty) \times D \to \mathbb{R}^n$ is continuously differentiable, and $\|\partial f/\partial x\| < \infty$, on D, a converse Lyapunov Theorem 5.4 guarantees the existence of a Lyapunov function for the nominal system (2.2) satisfying properties (5.14) – (5.16).

5.3 Statement of the Problem

The following definitions of phase synchronization (PS), cluster of oscillators, and connection types are used in this chapter:

Definition 5.3. ***(Phase synchronization)*** *Two oscillators with phases (ϕ_i, ϕ_j) achieve PS when their phase difference $\theta_{ij}(t) \equiv \phi_i(t) - \phi_j(t)$ is bounded by $|\theta_{ij}(t)| <$ const $< \pi$, $\forall t \geq t_0$.*

Definition 5.4. ***(Cluster of oscillators)*** *The set of oscillators $\mathcal{C} = \{v_1, v_2, \ldots, v_p\} \subseteq \mathcal{V}$ is a cluster of oscillators if their natural frequencies ω_i are within an arbitrary deviation Δ of the cluster average frequency $\bar{\omega}$, i.e. $\bar{\omega} - \Delta \leq \omega_i \leq \bar{\omega} + \Delta$, for $i = 1, 2, \ldots, p$.*

Definition 5.5. ***(Connection types)*** *If $(v_i, v_j) \in \mathcal{C}$, then if $a_{ij} \neq 0$ there is an intra-cluster connection, that is, an edge between two oscillators within a cluster. In case the oscillators belong to different clusters, the edge is referred to as an inter-cluster (bridge) connection.*

An oscillator $v_i \in \mathcal{C}$ is a "bridge oscillator" if there is at least one edge $a_{ij} \neq 0$ where $v_j \in \mathcal{V} \backslash \mathcal{C}$. The dynamics of its phase, described by (2.9)[5], can be rewritten in terms of inter- and intra-cluster connections as:

$$\dot{\phi}_i = \omega_i + \underbrace{\sum_{j \in \mathcal{V} \backslash \mathcal{C}} a_{ij} \sin(\phi_j - \phi_i)}_{\text{inter-connections}} + \underbrace{\sum_{j \in \mathcal{C}} a_{ij} \sin(\phi_j - \phi_i)}_{\text{intra-connections}} . \tag{5.21}$$

The following statements are illustrated in Fig. 5.2a. Let us reduce our problem to a Kuramoto network composed of two clusters, i.e. $\mathcal{V} = \{\mathcal{C}_1, \mathcal{C}_2\}$ of size (n_1, n_2), respectively. We denote the oscillators from each cluster as $v_i \in \mathcal{C}_1$, for $i = \{1, 2, \ldots, n_1\}$, and $v_j \in \mathcal{C}_2$, for $j = \{n_1 + 1, n_1 + 2, \ldots, n_1 + n_2\}$, with phases ϕ_i and ϕ_j, respectively.

Let $A_k \in \mathbb{R}^{n_k \times n_k}$ be the adjacency matrix of cluster $\mathcal{C}_k$, $k = 1, 2$, then, if there is no inter-cluster connection, the adjacency matrix of the full network is the block diagonal matrix $A = \text{diag}(A_1, A_2)$.

[5] In this chapter, we adopt the notation $\phi_i \equiv x_i$ to refer to the state variable of a Kuramoto oscillator located at the ith node.

Also, suppose that there is only one pair $(v_{\bar{\imath}}, v_{\bar{\jmath}})$, which is undirectedly coupled, whose edge forms a bridge between $\mathcal{C}_1$ and $\mathcal{C}_2$, as shown in Fig. 5.2a; i.e. $\bar{\imath} \in \mathcal{C}_1$, $\bar{\jmath} \in \mathcal{C}_2$. In this case, oscillators $v_{\bar{\imath}}$ and $v_{\bar{\jmath}}$ will be called "bridge oscillators". In addition, the inter-cluster summation in (5.21) reduces to a single term: $a_{\bar{\imath}\bar{\jmath}} \sin(\phi_{\bar{\jmath}} - \phi_{\bar{\imath}})$. Calling $K \equiv a_{\bar{\imath}\bar{\jmath}} > 0$, the phase difference dynamics $\theta \equiv \theta_{\bar{\imath}\bar{\jmath}} \equiv \phi_{\bar{\imath}} - \phi_{\bar{\jmath}}$ is given by:

$$\dot{\theta} = \Delta\omega - \underbrace{2K \sin\theta}_{\text{bridge}} + \underbrace{\sum_{i=1}^{n_1} a_{\bar{\imath}i} \sin\theta_{i\bar{\imath}} - \sum_{j=n_1+1}^{n_2} a_{\bar{\jmath}j} \sin\theta_{j\bar{\jmath}}}_{\text{intra-connections to } v_{\bar{\imath}}, v_{\bar{\jmath}}} \tag{5.22}$$

where $\theta \in \mathbb{R}^1$ and $\Delta\omega \equiv \omega_{\bar{\imath}} - \omega_{\bar{\jmath}}$.

Our goal is to study under which conditions the bridge oscillators PS, i.e. (5.22) is stable. Assuming that A and $\Delta\omega$ are constants, we determine a threshold K_c so that, for any $K > K_c$, PS is guaranteed. Moreover, it is possible to provide the maximum bounds of $\theta(t)$.

5.4 Phase Synchronization Analysis of Bridge Oscillators

This section provides results about the stability of the synchronization manifold between bridge oscillators. Notice that, under certain conditions, (5.22) can be interpreted as (5.17), where the summations of intra-cluster connection terms are the perturbation term, yielding

$$\dot{\theta} = \Delta\omega - 2K \sin\theta + g(t, \theta). \tag{5.23}$$

Note that, for $g(t, \theta) = 0$, system (5.23) describes the coupling of only two Kuramoto oscillators, such that

$$\dot{\theta} = \Delta\omega - 2K \sin\theta, \tag{5.24}$$

which has an equilibrium point $\bar{\theta} = \sin^{-1}(\Delta\omega/2K)$. On the other hand, since the coupling method is diffusive, the intra-cluster connection terms in (5.23) are always bounded for finite (n_1, n_2); i.e. $|g(t, \theta)| \leq g_{\max}, \forall t \geq t_0$.

Based on Lemma 5.1, the following theorem states sufficient conditions under which the perturbed system (5.23) exhibits a solution $\theta(t)$ that is ultimately bounded—guaranteeing PS between the bridge oscillators in Fig. 5.2a.

Theorem 5.5. *Given the perturbed system (5.23), $\forall|\theta(t_0)-\bar{\theta}|<\frac{\pi}{2}$, the solution $\theta(t)$ is bounded by*

$$\begin{aligned} |\theta(t)| &\leq |\bar{\theta}| + e^{-\alpha(t-t_0)}|\theta(t_0)| \quad , \quad \forall t_0 \leq t < t_0+T \\ |\theta(t)| &\leq |\bar{\theta}| + b \qquad\qquad\quad , \quad \forall t \geq t_0+T \end{aligned} \tag{5.25}$$

for some finite T, if the following conditions are satisfied: (i) $\left|\frac{\Delta\omega}{2K}\right| \leq \frac{\sqrt{2}}{2}$, and (ii) $K > K_c = (g_{\max}+|\Delta\omega|)/2\epsilon$, where $g_{\max}$ is the upper bound of perturbation term $|g(t,\theta)|$ in (5.23), and $0<\epsilon<1$. The coefficients are defined as

$$\alpha = \frac{(1-\epsilon)\cdot(2K-|\Delta\omega|)}{r}, \quad b = \frac{r g_{\max}}{(2K-|\Delta\omega|)\cdot\epsilon}$$
$$r = \tan^{-1}\left(\frac{\sqrt{4K^2-\Delta\omega^2}}{|\Delta\omega|}\right). \tag{5.26}$$

■

Proof. Proof is presented in Appendix A. □

Remark 5.3. Theorem 5.5 is valid only for systems in the form (5.23), as it depends on a specific Lyapunov function for the nominal system (5.24). However, it can be reproduced as a framework for networks with different coupling interactions, different oscillators and higher-order scales—provided that a Lyapunov function of the nominal system is known.

In the preceding analysis, we do not necessarily require knowledge of the adjacency matrix A, but if that is the case, explicit, although conservative, upper bounds for $g_{\max}$ can be estimated. For example, since $|\sin x| \leq 1$:

$$g_{\max} \leq \sum_{i=1}^{n_1} a_{\bar{\imath}i} + \sum_{j=n_1+1}^{n_2} a_{\bar{\jmath}j}. \tag{5.27}$$

Similarly, a further refinement can be obtained by considering the following assumption.

Assumption 5.1. Consider that all adjacent connections $a_{\bar{\imath}i} > 0$ and $a_{\bar{\jmath}j} > 0$ to bridge oscillators $(v_{\bar{\imath}}, v_{\bar{\jmath}})$ are known, and that the phase difference between the bridge oscillators and their neighboring connections inside their own clusters are bounded by $|\theta_{i\bar{\imath}}(t)| \leq \gamma_i$ and $|\theta_{j\bar{\jmath}}(t)| \leq \gamma_j$, $\forall t \geq t_0+T$, for some finite T.

If Assumption 5.1 holds, from (5.22) and (5.23), one has that:

$$g_{\max} \leq \sum_{i=1}^{n_1} a_{\bar{\imath}i}\sin\gamma_i + \sum_{j=n_1+1}^{n_2} a_{\bar{\jmath}j}\sin\gamma_j. \tag{5.28}$$

It is interesting to note that if the bridge oscillators *completely synchronize* with their neighbouring oscillators, then $\gamma_i = \gamma_j = 0$, for all $a_{\bar{i}i} \neq 0$ and $a_{\bar{j}j} \neq 0$, yielding $g_{\max} = 0$.

Remark 5.4. If one considers a slightly stronger assumption than Assumption 5.1 of having all pairwise phase differences between oscillators in each cluster bounded by the same constant value associated with that cluster; i.e. phase differences not only between the bridge oscillators and their neighbors, but $|\theta_{i_k j_k}(t)| \leq \Gamma_k < \frac{\pi}{2}$, for $k = 1, 2$, with $i_k, j_k \in \mathcal{C}_k$, another possible conservative upper bound is

$$g_{\max} \leq \sum_{i=1}^{n_1} a_{\bar{i}i} \sin \Gamma_1 + \sum_{j=n_1+1}^{n_2} a_{\bar{j}j} \sin \Gamma_2. \tag{5.29}$$

such that one can directly relate the PS quality inside each cluster, measured by Γ_k, $k = 1, 2$, with the PS quality between bridge oscillators.

5.5 Numerical Results

For the following numerical results, consider the error dynamics (5.23) of the detailed network in Section 5.3—generically illustrated in Fig. 5.2a. Let $\mathcal{V} = \{\mathcal{C}_1, \mathcal{C}_2\}$, where clusters $(\mathcal{C}_1, \mathcal{C}_2)$ have dimension $(n_1, n_2) = (6, 4)$ and are fully connected with edges of strength $a_{ij} = 0.05$. The individual oscillators natural frequencies and initial conditions were randomly distributed as follows: $\omega_i \sim \mathcal{N}(\bar{\omega}_1, 0.01)$, $\omega_j \sim \mathcal{N}(\bar{\omega}_2, 0.01)$ and $\phi(t_0) \sim \mathcal{U}(-\frac{\pi}{4}, +\frac{\pi}{4})$ —where $\mathcal{N}(\mu,\ \sigma^2)$ denotes a Gaussian distribution with average μ and variance σ^2, while $\mathcal{U}(a, b)$ denotes a uniform distribution within limits $[a, b]$. Note that $|\theta(t_0)| < \frac{\pi}{2}$. All numerical integrations were done in Julia programming language, using a 4th-order Runge-Kutta implementation from the `DifferentialEquations.jl` package. In the following simulations, we investigate the stability of the synchronization manifold of the bridge oscillators for different pairs of $(\bar{\omega}_1, \bar{\omega}_2)$ and inter-coupling strength K.

Figure 5.3 shows numerical results of PS for $(\bar{\omega}_1, \bar{\omega}_2) = (1.0, 1.5)$ and different values of K. Let $\Delta\omega = \omega_{\bar{i}} - \omega_{\bar{j}} \approx \bar{\omega}_1 - \bar{\omega}_2$. We compare the numerical examples of Fig. 5.3a with the theoretical results as follows, noting that if solution $\theta(t)$ is ultimately bounded, then the bridge oscillators are PS.

For $K = 0.1$, we have $\left|\frac{\Delta\omega}{2K}\right| \approx 2.5$, which does not satisfy the necessary condition $\left|\frac{\Delta\omega}{2K}\right| \leq 1$ of the nominal system (5.24) [113]. Hence, system (5.24) is unstable and the solution of the perturbed system (5.23) is unbounded. For $K = 0.36$, $\left|\frac{\Delta\omega}{2K}\right| \approx 0.69$, proving that the nominal system (5.24) origin is stable and satisfying condition (i)

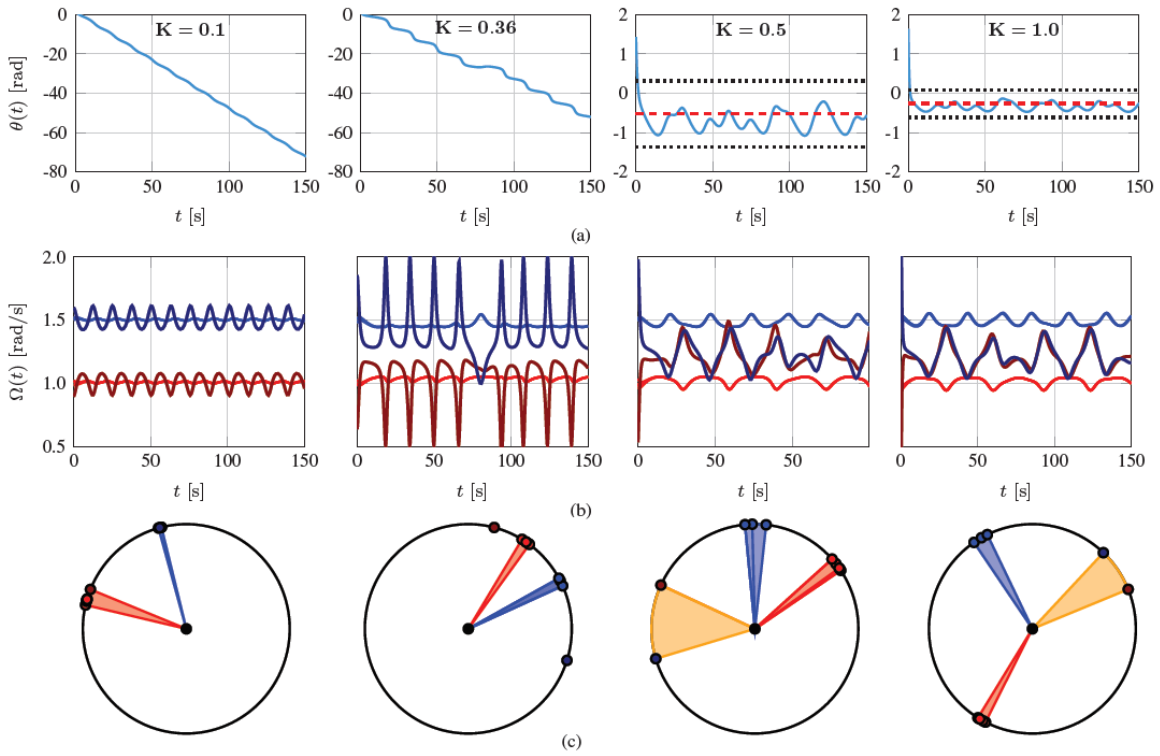

Figure 5.3: (a) Phase difference $\theta(t)$ between bridge oscillators. The equilibrium point and theoretical ultimate bounds are indicated by dashed and dotted lines, respectively. (b) Instantaneous frequency $\Omega(t)$ of coupled (nonautonomous) oscillators. (c) Samples of the oscillators instantaneous phase angles. If a cluster of oscillators are PS, the sector is filled in red or blue colors, accordingly. If the bridge oscillators are PS, then the sector is filled in orange color. In (b) and (c), oscillators from clusters $\mathcal{C}_1$ and $\mathcal{C}_2$ are represented by red and blue colors, respectively, while the bridge oscillators are indicated with the respective darker colors.

of Theorem 5.5. However, it is still necessary to prove condition (ii) regarding the perturbation upper bound. Assuming that only the adjacent connections of the bridge oscillators are known *a priori*, we refer to (5.27) to estimate the network perturbation bound as $g_{\max} = 0.4$, yielding $K_c = (g_{\max} + |\Delta\omega|)/2\epsilon \approx 0.45/\epsilon$. Once again, Theorem 5.5 is not applicable because condition (ii) is not satisfied: $K < K_c$. No formal conclusion can be arrived at regarding the perturbed system (5.23) stability, although numerical results show that the solution is unbounded. This can be expected because the inter-cluster coupling strength is still of the same order of the perturbation bounds.

Assuming that condition (i) of Theorem 5.5 is satisfied, for any $K > K_c$, condition (ii) is also valid and, hence, it is guaranteed that the solution of system (5.23) is ultimately bounded by (5.25). This theoretical result is seen numerically in Fig. 5.3a for $K = 0.5$ and 1. The increase of K suppresses the perturbation term $g(t, \theta)$ in (5.23),

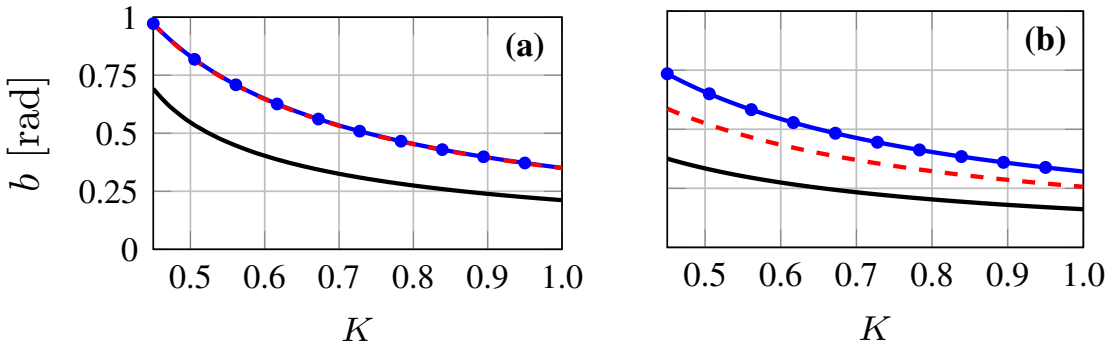

Figure 5.4: Ultimate bound b estimate computed: numerically (black); using (5.27) (circle); and, if Assumption 5.1 holds, using (5.28) (dashed). (a) $(\bar{\omega}_1, \bar{\omega}_2) = (1.0, 1.5)$; (b) $(\bar{\omega}_1, \bar{\omega}_2) = (1.0, 1.1)$.

reducing the ultimate bound b of $\theta(t)$. This can be visually inspected in Fig. 5.3c. As a side note, beware that, for $K = 0.36$, although $\theta(t)$ is unbounded, it is possible to detect an intermittent PS (phase slips) among the bridge oscillators—which is attributed to the proximity of K to the true K_c [11].

In a complementary manner, PS is also related to the instantaneous angular frequencies $\Omega_i(t)$ (see Fig. 5.3b). As K increases, the intensification of PS between the bridge oscillators is accompanied by a rise of perturbation seen in the increase of variance over the red and blue clusters instantaneous angular frequencies. There is, indeed, a twofold perturbation over the network between the bridge oscillators PS and their respective clusters PS. In Fig. 5.3b, note that the increase of K results in an increase of $\Omega(t)$ bounds for clusters $\mathcal{C}_1$ and $\mathcal{C}_2$. Although the clusters oscillators remain synchronized, the fluctuations of $\Omega(t)$ can have deeper impacts over the network. It is interesting to see that bridge oscillators synchronization can be studied as a means to achieve intra-cluster desynchronization [69].

Figure 5.4 compares, for $K \in [K_c,\ 1.0]$, the asymptotic bounds of $\theta(t)$ with the theoretical value of b based on Theorem 5.5 and the ones obtained numerically. Bound b was computed in two different ways. If only the adjacent connections are known, b can be computed based on $g_{\max}$ conservatively estimated from (5.27). If, moreover, Assumption 5.1 holds, it is possible to estimate $g_{\max}$ directly from (5.28).

The bound b decreases rapidly with K (Fig. 5.4). However, an interesting relation is perceptible when comparing Figs. 5.4a and b. For very different natural frequencies (Fig. 5.4a), both theoretical estimations are virtually identical. On the other hand, for more similar natural frequencies (Fig. 5.4b), the lack of knowledge of the adjacent Kuramoto oscillators states (Assumption 5.1) proves to be quite conservative. This is

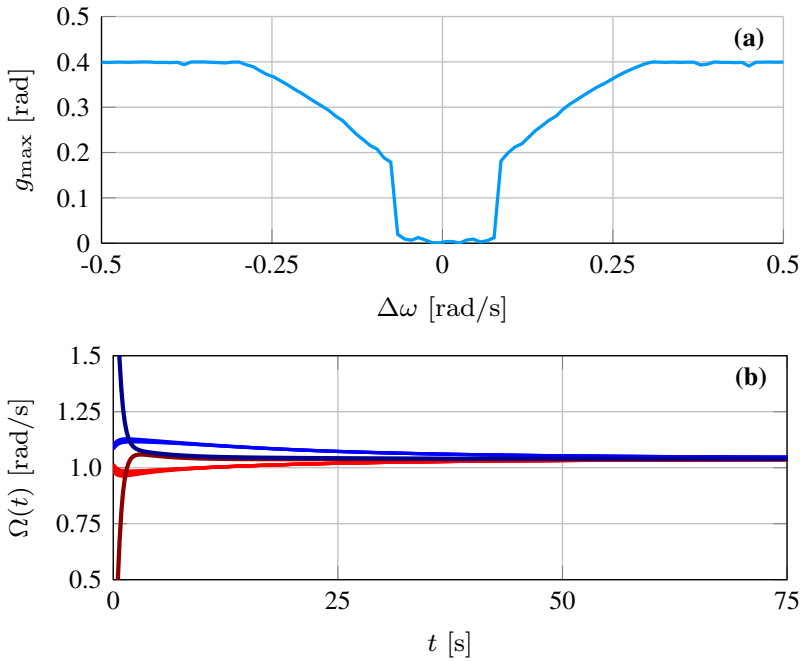

Figure 5.5: (a) Numerical results of the perturbation term $g(t, \theta)$ bound $g_{\max}$ for different values of $\Delta\omega$, considering $K = 0.5$. (b) Instantaneous frequency $\Omega(t)$ of coupled (nonautonomous) oscillators, with parameters $(\bar{\omega}_1, \bar{\omega}_2, K) = (1.0, 1.5, 1.0)$.

a consequence of the difference between the clusters dynamical behavior. Once the clusters are connected by a bridge, the bridge oscillators disengage their respective clusters average frequencies in order to attempt to synchronize with each other. The larger the inter-clusters parametric difference, the stronger the *reaction* of the intra-cluster connections, inducing more perturbations. Thus, the bound of $g(t, \theta)$ tends to (5.27) as $\Delta\omega$ increases. This is further illustrated in Fig. 5.5a. Since the coupling term is a diffusive sine function, the perturbation term is bounded even for high values of $\Delta\omega$.

Indeed, a possible scope of work is to pursue PS of not only the bridge oscillators but also of the two isolated clusters —which we refer to as *full cluster synchronization*. In order to achieve this, the bridge oscillators must PS and retain the (previous) PS with their neighboring oscillators. In this case, all oscillators form up a new single cluster, in which their phase differences are next to zero, yielding $g_{\max} \to 0$, according to (5.28). As seen in Fig. 5.5a, we note that, for a given K, full cluster synchronization is achievable when the clusters average frequency are similar, i.e. $\Delta\omega \approx 0$ (see Fig. 5.5b). Otherwise, full cluster synchronization might not be achievable by only increasing K (see Fig. 5.3b). An alternative is to increase the number of bridge connections among the isolated clusters, although this case is left for future investigation.

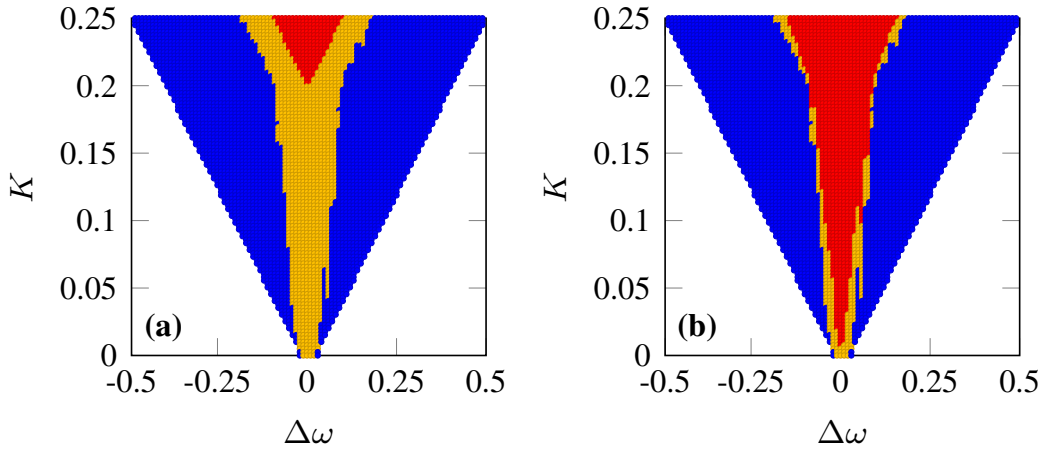

Figure 5.6: Numerically estimated Arnold tongues of the nominal system (5.24) (in blue) and the perturbed system (5.23) (in yellow). The red Arnold tongue corresponds to the theoretically calculated regimes of PS using Theorem 5.5 when the theoretical bounds are estimated: (a) with prior knowledge only of the adjacent connections, using (5.27); and (b) based on Assumption 5.1, using (5.28).

Arnold tongues are a visual representation of PS regimes under different combinations of parameters between two coupled oscillators. A colored dot points that, under a specific combination of parameters (K and $\Delta\omega$, in this case), the coupled oscillators PS. Otherwise, they are not PS. Figure 5.6 illustrates the impact of different combinations of K and $\Delta\omega$ for the PS of bridge oscillators in (5.23). The perturbed system (5.23) will be phase synchronized only if the nominal system (5.24) is synchronized too. The theoretical guarantees of stability provided in Theorem 5.5 when Assumption 5.1 is true are confirmed by the numerical evaluations. It illustrates the fact that if this assumption holds, it is possible to find a less conservative region of PS—specially for smaller $\Delta\omega$ as discussed in Fig. 5.5. Figure 5.6 illustrates the robustness of the theoretical results provided in this chapter.

Finally, it is interesting to note that the interconnection between a single oscillator and an isolated cluster presented in Fig. 5.2b is a particular case of Theorem 5.5, where $n_1 = 1$ and $n_2 > 1$. This single structure, however, fits in a wide scope of engineering applications, such as telecommunication and power systems [37, 30].

5.6 Final Considerations

Many works focus on deriving conditions that guarantee the stability of intra-cluster or full-cluster PS of networks of phase oscillators. In this chapter, we take a different

approach by providing sufficient conditions under which interconnected oscillators from different clusters – here called "bridge oscillators" –, rather than the whole clusters, phase synchronize. To achieve this goal, based on the Lyapunov direct method, we restrict our problem to a simplified version where the studied dynamical system is composed only by the bridge oscillators plus "perturbation terms". The intra-cluster connections, in turn, are modeled as such perturbations under certain conditions. In this context, the full adjacency matrix is not required to derive sufficient conditions for the phase synchronization of the bridge oscillators.

The study is carried out on a network composed of two clusters interconnected by a single bridge. Theorem 5.5 provides sufficient conditions for the synchronization of the bridge oscillators. These conditions are expressed in terms of the bridge oscillators natural frequencies and coupling strength. The theoretical results were validated using a network of Kuramoto oscillators, by means of extensive numerical simulations.

This analysis is expected to be useful in practical applications where the whole network graph is not well known, but a reasonable knowledge of the neighboring connections to the bridge oscillators is available. In addition, the proposed theorem could be generalized as a framework to more complex systems, with different network structures and oscillators dynamics, as illustrated in Fig. 5.2c.

Chapter 6

Conclusion

6.1 Final Considerations

This dissertation presents some numerical and theoretical results in the study of observability and synchronization of dynamical networks.

To motivate the investigation of observability properties in dynamical networks, a thorough review is provided in Chapter 3. Classic linear and nonlinear techniques are presented and explored under a low-dimensional context. The importance of gradually quantifying the observability "level" of a dynamic system is discussed. Thereafter, these notions are explored under a network context, where high-dimensionality issues provides a new obstacle to the classic methods. Pioneer methods in literature based solely on properties of the network topology are reviewed and criticized for its lack of applicability in real networks, where nodal dynamics are involved. This chapter concludes with some interesting guidelines for research of more feasible and applicable methods to classify and quantify observability in network systems.

During the review in Chapter 3, a recurrent issue in literature is the lack of validation of novel observability (controllability) methods to classify the best set of sensor (driver) nodes in a network. This discussion motivated the development in Chapter 4, where we propose a Bayesian filtering inspired framework, based on the particle filtering, as a benchmark to validate the efficacy of novel observability metrics in literature. Moreover, by applying the framework to a network of Kuramoto oscillators and Rössler systems, we investigated the observability relation to the interplay between network topology and nodal dynamics, reaching some interesting conclusions.

Finally, on a synchronization context, we provided a case-study in Chapter 5 of a network composed of two interconnected clusters of Kuramoto oscillators. We provide a

reductionist framework to investigate the sufficient conditions under which the "bridge oscillators" in each cluster phase synchronize. Under certain conditions, we show that the clusters of Kuramoto oscillators can be modeled as a single perturbed Kuramoto oscillator. If perturbations remain within a given bound, then the network analysis reduces to a simple pair of Kuramoto oscillators, whose synchronous manifold stability is now feasible to be investigated through Lyapunov direct method. We suggest that, although the provided framework was conceived to investigate only a particular case-study, it can be generalized to different networks configurations and oscillators models.

6.2 Future Work

Review in Chapter 3 and the investigation in Chapter 4 has given further insights in the study of observability in network systems.

Firstly, Summers *et al.* [115] shows that classic dynamical observability metrics have submodularity properties that, in turn, allows to assess the network observability problem by a set function optimization approach via rather simple greedy algorithms. Interestingly, Haber *et al.* [48] also shows that this approach is robust to nonlinear problems. Although this proposal circumvents the problem of finding among 2^N combinations the best set of sensor nodes, computation of classic dynamical observability metrics might still not be feasible in a N-dimensional network. A possible line of scope is to investigate if there is or not correlation between the best set of sensor nodes provided by a combination of Summers *et al.* framework and some other graph measure of this set, such as centrality, distance or clustering metrics. Since graph metrics are quite robust in high-dimensional systems, it would be quite useful to find a correlated metric. Moreover, Summers *et al.* framework could be investigated with the conditioning number metric δ_o rather than the Gramian-based ones in [115].

Secondly, despite the proposed Bayesian framework assessment showing some possible lines of investigation, the interplay between network topology and nodal dynamics in observability remains unclear. Under a linear context, an interesting approach to analyze how this interplay unfolds in high-dimensional systems is to explore different formulations that take benefits of a network intrinsic presence of redundancy and patterns. Refer to (2.7). This equation can be rewritten as follows by using a Kronecker product notation:

$$\dot{\boldsymbol{x}} = \sum_{i=1}^{m} \left(J_i \otimes A_i\right) \boldsymbol{x} + \sum_{i=1}^{n} \sum_{j=1}^{n} \left(L_{ij}^{\mathsf{T}} \otimes K_{ij}^{\mathsf{T}}\right) \boldsymbol{x}, \tag{6.1}$$

where $\boldsymbol{x} = \begin{bmatrix}\boldsymbol{x}_1 & \boldsymbol{x}_2 & \dots & \boldsymbol{x}_m\end{bmatrix}^\mathsf{T}$, $\boldsymbol{x}_i = \begin{bmatrix}x_{i1} & x_{i2} & \dots & x_{in}\end{bmatrix}^\mathsf{T}$, $A_i \in \mathbb{R}^{n\times n}$ is the dynamical matrix relative to state variables $\boldsymbol{x}_i$ at node v_i, $J_i \in \mathbb{R}^{m\times m}$ is a diagonal matrix where $j_{ii} \neq 0$ and all other elements are zero, L_{ij} is a Laplacian matrix of graph $\mathcal{G} = \{\mathcal{V}, \mathcal{E}\}$ that dictates how the ith state variable of a node couples to the jth state variable of another node, and K_{ij} is a matrix where $k_{ij} \neq 0$ and all other elements are zero. Basically, the first sum is a block diagonal matrix that describes the dynamical behaviour A_i in each node v_i and the second sum is a block matrix that describes the coupling structure among internal variables (vertices) of different nodes. This formulation can also be represented as *Generalized Sylvester Equation*:

$$\dot{X} = \sum_{i=1}^{m} A_i X J_i^\mathsf{T} + \sum_{i=1}^{n}\sum_{j=1}^{n} K_{ij}^\mathsf{T} X L_{ij}, \tag{6.2}$$

where $\boldsymbol{X} = \begin{bmatrix}\boldsymbol{x}_1 & \boldsymbol{x}_2 & \dots & \boldsymbol{x}_m\end{bmatrix} \in \mathbb{R}^{n\times m}$.

Any network model whose nodes are dynamical systems of the same dimension n can be represented by model (6.2). Although the Generalized Sylvester Equation shares some interesting results in literature [33], some specific assumptions recurrent in a network context can reduce significantly (6.2). For instance, assume that all nodes share the same dynamical behaviour, i.e. $A = A_1 = A_2 = \ldots = A_m$, and that any coupling structure among internal variables (vertices) in each node are dictated by the same graph (Laplacian matrix L). Thus, both sums in (6.2) are reduced to a single element each, yielding

$$\dot{X} = AXI_m + K_{ij}^\mathsf{T} X L, \tag{6.3}$$

where I_m is an identity matrix of dimension m. Note that K_{ij} is a matrix that "selects" whether a coupling between the ith and jth vertices exists, if $k_{ij} \neq 0$, or not, otherwise.

If $k_{ij} = 0$, $\forall i \neq j$ (i.e. there is no cross-coupling among internal variables, or vertices), and $k_{ij} = 1$, $\forall i = j$, then $K_{ij} = I_n$, yielding

$$\dot{X} = AXI_m + I_n^\mathsf{T} X L, \tag{6.4}$$

Equation (6.4), known simply as the *Sylvester Equation*, has been studied in [18] under a network context (not a dynamical network context), where interesting stability, controllability and observability properties were derived. However, (6.4) has a fundamental shortcoming: it is a model of a "network of network", a "grid" graph where *all* internal variables from a given node couples to *all* internal variables of another node according to the *same* Laplacian matrix. For a more applicable study in dynamical networks, we have to refer to (6.3) formulation. In a future work, we hope that this formulation

allows us to derive fundamental results in controllability and observability that might give us insight, or even explain, how the interplay between nodal dynamics (dynamical matrix A) and the network topology (Laplacian matrix L) unfolds.

References

[1] Aguirre, L. A. (1995). Controllability and Observability of Linear Systems: Some Noninvariant Aspects. *IEEE Transactions on Education*, 38(1):33–39.

[2] Aguirre, L. A. and Letellier, C. (2005). Observability of multivariate differential embeddings. *Journal of Physics A: Mathematical and General*, 38(28):6311–6326.

[3] Aguirre, L. A. and Letellier, C. (2011). Investigating observability properties from data in nonlinear dynamics. *Physical Review E*, 83(6):1–10.

[4] Aguirre, L. A., Portes, L. L., and Letellier, C. (2018). Structural, Dynamical and Symbolic Observability: From Dynamical Systems to Networks. *Submitted.*, pages 1–22.

[5] Baldwin, T., Mili, L., Boisen, M., and Adapa, R. (1993). Power-system observability with minimal phasor measurement placement. *IEEE Transactions on Power Systems*, 8(2):707–715.

[6] Barabási, A.-L. (2009). Scale-Free Networks: A Decade and Beyond. *Science*, 325(5939):412–413.

[7] Barabási, A. L., Albert, R., and Jeong, H. (1999). Mean-field theory for scale-free random networks. *Physica A: Statistical Mechanics and its Applications*, 272(1):173–187.

[8] Barabasi, A.-L. and Pósfasi, M. (2016). *Network Science*. Cambridge University Press.

[9] Batista, C. A., Lameu, E. L., Batista, A. M., Lopes, S. R., Pereira, T., Zamora-López, G., Kurths, J., and Viana, R. L. (2012). Phase synchronization of bursting neurons in clustered small-world networks. *Physical Review E*, 86:016211.

[10] Bianco-Martinez, E., Baptista, M. S., and Letellier, C. (2015). Symbolic computations of nonlinear observability. *Physical Review E2*, 91:06912.

[11] Boccaletti, S., Kurths, J., Osipov, G., Valladares, D., and Zhou, C. (2002). The synchronization of chaotic systems. *Physics Reports*, 366(1–2):1–101.

[12] Boccaletti, S., Latora, V., Moreno, Y., Chavez, M., and Hwang, D.-U. (2006). Complex networks: Structure and dynamics. *Physics Reports*, 424(4-5):175–308.

[13] Bretas, N. and London, J. (1998). Network observability: the critical measurement identification using the symbolic Jacobian matrix. *International Conference on Power System Technology.*, 2:1222–1226.

[14] Bullo, F. (2016). *Lectures on Network Systems*.

[15] Candy, J. V. (2016). *Bayesian Signal Processing*.

[16] Castillo, E., Conejo, A., Menendez, J., and Jimenez, P. (2008). The observability problem in traffic network models. *Computer-aided civil and infrastructure engineering*, 23(3):208–222.

[17] Chang, B. and Shachter, R. D. (1992). Structural controllability and observability in influence diagrams. In *Proceedings of the 8th Conference on Uncertaity in Artificial Intelligence*, pages 25–32.

[18] Chapman, A., Nabi-Abdolyousefi, M., and Mesbahi, M. (2014). Controllability and Observability of Network-of-Networks via Cartesian Products. *IEEE Transactions on Automatic Control*, 59(10):2668–2679.

[19] Chen, C.-T. (1999). *Linear system theory and design*.

[20] Chen, D. and Qi, H. (2009). Controllability and observability of Boolean control networks. *Automatica*, 45(7):1659–1667.

[21] Chen, G., Wang, X., and Li, X. (2013). *Fundamentals of complex networks*. Wiley.

[22] Chen, G.-R. (2014). Problems and Challenges in Control Theory under Complex Dynamical Network Environments. *Acta Automatica Sinica*, 39(4):312–321.

[23] Chen, Z. (2003). *Bayesian filtering: From Kalman filters to particle filters, and beyond*. PhD thesis.

[24] Ching, J., Beck, J. L., and Porter, K. A. (2006). Bayesian state and parameter estimation of uncertain dynamical systems. *Probabilistic Engineering Mechanics*, 21(1):81–96.

[25] Costa, L. d. F., Rodrigues, F. A., Travieso, G., and Villas Boas, P. R. (2007). Characterization of complex networks: A survey of measurements. *Advances in Physics*, 56(1):167–242.

[26] Cowan, N. J., Chastain, E. J., Vilhena, D. A., Freudenberg, J. S., and Bergstrom, C. T. (2012). Nodal dynamics, not degree distributions, determine the structural controllability of complex networks. *PLoS ONE*, 7(6).

[27] Dahms, T., Lehnert, J., and Schöll, E. (2012). Cluster and group synchronization in delay-coupled networks. *Physical Review E - Statistical, Nonlinear, and Soft Matter Physics*, 86(1):1–10.

[28] Devaney, R. (2003). *An Introduction to Chaotic Dynamical Systems*. CRC Press.

[29] Dorfler, F. and Bullo, F. (2014). Synchronization in Complex Networks of Phase Oscillators: A Survey. *Automatica*, 50(6):1539–1564.

[30] Dorfler, F., Chertkov, M., and Bullo, F. (2013). Synchronization in complex oscillator networks and smart grids. *PNAS*, 110(6):2005–2010.

[31] Doucet, A., Godsill, S., and Andrieu, C. (2000). On sequential Monte Carlo sampling methods for Bayesian filtering. *Statistics and Computing*, 10(3):197–208.

[32] Doucet, A. and Johansen, A. (2011). In *Handbook of Nonlinear Filtering*, chapter A tutorial on particle filtering and smoothing: fifteen years later, pages 656–704. Oxford Univ. Press.

[33] Duan, G.-R. (2015). *Generalized Sylvester Equations: Unified Parametric Solutions*. CRC Press.

[34] Evensen, G. (1994). Sequential data assimilation with a nonlinear quasi-geostrophic model using Monte Carlo methods to forecast error statistics. *Journal of Geophysical Research: Oceans*, 99(C5):10143–10162.

[35] Evensen, G. (2009). The ensemble Kalman filter for combined state and parameter estimation. *IEEE Control Systems Magazine*, 29(3):83–104.

[36] Favaretto, C., Cenedese, A., and Pasqualetti, F. (2017). Cluster Synchronization in Networks of Kuramoto Oscillators. In *20th IFAC World Conference*, pages 1–9.

[37] Filatrella, G., Nielsen, A. H., and Pedersen, N. F. (2008). Analysis of a power grid using a Kuramoto-like model. *European Physical Journal B*, 61(4):485–491.

[38] Fortunato, S. (2010). Community detection in graphs. *Physics Reports*, 486(3-5):75–174.

[39] Freitas, L., Torres, L. A., and Aguirre, L. A. (2018). Phase definition to assess synchronization quality of nonlinear oscillators. *Physical Review E*, 97(052202):1–13.

[40] Friedland, B. (1975). Controllability index based on conditioning number. *Journal of Dynamic Systems, Measurement, and Control*, 97(4):444–445.

[41] Fu, Y., Wang, L., and Chen, M. (2016). Robustness of Controllability for Scale-free Networks Based on a Nonlinear Load-Capacity Model. In *IFAC Proceedings Volumes*, pages 37–42.

[42] Fujisaka, H. and Yamada, T. (1983). Stability theory of synchronized motion in coupled-oscillator systems. *Progress of Theoretical Physics*, 69(1):32–47.

[43] Gao, J., Liu, Y.-Y., D'Souza, R. M., and Barabási, A.-L. (2014). Target control of complex networks. *Nature Communications*, 5:5415.

[44] Gates, A. J. and Rocha, L. M. (2015). Control of complex networks requires both structure and dynamics. *Scientific Reports*, 6(24456):1–39.

[45] Gilarranz, L. J., Rayfield, B., Liñán-Cembrano, G., Bascompte, J., and Gonzalez, A. (2017). Effects of network modularity on the spread of perturbation impact in experimental metapopulations. *Science*, 357(6347):199–201.

[46] Gu, S., Pasqualetti, F., Cieslak, M., Telesford, Q. K., Yu, A. B., Kahn, A. E., Medaglia, J. D., Vettel, J. M., Miller, M. B., Grafton, S. T., and Bassett, D. S. (2015). Controllability of structural brain networks. *Nature Communications*, 6:8414.

[47] Gutiérrez, R., Sendiña-Nadal, I., Zanin, M., Papo, D., and Boccaletti, S. (2012). Targeting the dynamics of complex networks. *Scientific reports*, 2(July 2017):396.

[48] Haber, A., Molnar, F., and Motter, A. E. (2018). State observation and sensor selection for nonlinear networks. *IEEE Transactions on Control of Network Systems*, 5(2):694–708.

[49] Hammond, C., Bergman, H., and Brown, P. (2007). Pathological synchronization in parkinson's disease: networks, models and treatments. *Trends in Neurosciences*, 30(7):357–364.

[50] Hermann, R. and Krener, A. J. (1977). Nonlinear Controllability and Observability. *IEEE Transactions on Automatic Control*, 22(5):728–740.

[51] Hong, H., Choi, M. Y., and Kim, B. J. (2002). Synchronization on small-world networks. *Physical Review E*, 65(026139):1–5.

[52] Jia, T., Liu, Y.-Y., Csoka, E., Posfai, M., Slotine, J.-J., and Barabasi, A.-L. (2013). Emergence of bimodality in controlling complex networks. *Nature communications*, 4(May):2002.

[53] Johnson, C. D. (1969). Optimization of a certain quality of complete controllability and observability for linear dynamical systems. *Transactions of the ASME - Journal of Basic Engineering*, 91(2):228–238.

[54] Kalman, R. (1959). On the general theory of control systems. *IRE Transactions on Automatic Control*, 4(3):110–110.

[55] Kerner, E. H. (1981). Universal formats for nonlinear ordinary differential systems. *Journal of Mathematical Physics*, 22(7):1366–1371.

[56] Khalil, H. K. (2002). *Nonlinear Systems*. Prentice Hall, 3rd edition.

[57] Klema, V. C. and Laub, A. J. (1980). The Singular Value Decomposition: Its Computation and Some Applications. *IEEE Transactions on Automatic Control*, 25(2):164–176.

[58] Kuramoto, Y. (1975). Self-entrainment of a population of coupled non-linear oscillators. In *International Symposium on Mathematical Problems in Theoretical Physics*, pages 420–422. Springer Berlin Heidelberg.

[59] Lakshmanan, M. and Rajasekar, S. (2003). *Nonlinear Dynamics: Integrability, Chaos and Patterns*. Springer.

[60] Laschov, D., Margaliot, M., and Even, G. (2013). Observability of Boolean networks: A graph-theoretic approach. *Automatica*, 49(8):2351–2362.

[61] Leitold, D., Vathy-fogarassy, A., and Abonyi, J. (2017). Controllability and observability in complex networks – the effect of connection types networks. *Scientific Reports*, 7(March 2017):1–9.

[62] Letellier, C. and Aguirre, L. A. (2002). Investigating nonlinear dynamics from time series: The influence of symmetries and the choice of observables. *Chaos*, 12(3):549–558.

[63] Letellier, C. and Aguirre, L. A. (2009). Symbolic observability coefficients for univariate and multivariate analysis. *Physical Review E*, 79:066210.

[64] Letellier, C. and Aguirre, L. A. (2010). Interplay between synchronization, observability, and dynamics. *Physical Review E*, 82:016204.

[65] Letellier, C., Aguirre, L. A., and Maquet, J. (2005). Relation between observability and differential embeddings for nonlinear dynamics. *Physical Review E - Statistical, Nonlinear, and Soft Matter Physics*, 71(6):1–8.

[66] Letellier, C., Maquet, J., Sceller, L. L., Gouesbet, G., and Aguirre, L. A. (1998). On the non-equivalence of observables in phase-space reconstructions from recorded time series. *Journal of Physics A: Mathematical and General*, 31:7913–7927.

[67] Lewis, F. L., Zhang, H., Hengster-Movric, K., and Das, A. (2014). *Introduction to Synchronization in Nature and Physics and Cooperative Control for Multi-Agent Systems on Graphs*. Springer, London, 1st edition.

[68] Li, C., Sun, W., and Kurths, J. (2007). Synchronization between two coupled complex networks. *Physical Review E*, 76:046204.

[69] Li, X. and Chen, G. (2003). Synchronization and Desynchronization of Complex Dynamical Networks: An Engineering Viewpoint. *IEEE Transactions on Circuits and Systems I: Fundamental Theory and Applications*, 50(11):1381–1390.

[70] Lin, C. T. (1974). Structural Controllability. *IEEE Transactions on Automatic Control*, 19(3):201–208.

[71] Lingala, N., Sri Namachchivaya, N., Perkowski, N., and Yeong, H. C. (2012). Particle filtering in high-dimensional chaotic systems. *Chaos*, 22(4).

[72] Liu, Y.-Y., Slotine, J.-J., and Barabási, A.-L. (2011). Controllability of complex networks. *Nature*, 473(7346):167–73.

[73] Liu, Y.-Y., Slotine, J.-J., and Barabási, A.-L. (2013). Observability of complex systems. *Proceedings of the National Academy of Sciences of the United States of America*, 110(7):2460–2465.

[74] Lombardi, A. and Hörnquist, M. (2007). Controllability analysis of networks. *Physical Review E*, 75:056110.

[75] Lu, W., Liu, B., and Chen, T. (2010). Cluster synchronization in networks of coupled nonidentical dynamical systems. *Chaos*, 20(03120):1–13.

[76] Marwan, N., Carmen Romano, M., Thiel, M., and Kurths, J. (2007). Recurrence plots for the analysis of complex systems. *Physics Reports*, 438(5-6):237–329.

[77] Marwan, N., Donges, J. F., Zou, Y., Donner, R. V., and Kurths, J. (2009). Complex network approach for recurrence analysis of time series. *Physics Letters A*, 373(46):4246–4254.

[78] McGraw, P. N. and Menzinger, M. (2005). Clustering and the synchronization of oscillator networks. *Physical Review E*, 72:015101.

[79] Montanari, A. and Aguirre, L. (2018). Particle Filtering of Dynamical Networks: A Benchmark for Observability Studies. *In preparation.*

[80] Montanari, A., Freitas, L., Torres, L., and Aguirre, L. (2018). Phase synchronization analysis of bridge oscillators between clustered networks. *Submitted to Pysical Review E.*

[81] Monteiro, L. H. A. (2011). *Sistemas Dinâmicos.* Editora Livraria de Física, 3rd edition.

[82] Monteiro, L. H. A. (2014). *Sistemas Dinâmicos Complexos.* Editora Livraria de Física, 2 edition.

[83] Monticelli, A. and Wu, F. F. (1985). Network Observability: Theory. *IEEE Transactions on Power Apparatus and Systems*, PAS-104(5):1042–1048.

[84] Moreno, Y. and Pacheco, F. (2004). Synchronization of Kuramoto oscillators in scale-free networks. *Eyrophysics Letters*, 68:33–40.

[85] Moreno, Y., Pastor-Satorras, R., and Vespignani, A. (2002). Epidemic Outbreaks in Complex Heterogenoeus Networks. *European Physical Journal B*, 26(4):521–529.

[86] Motter, A. E. and Timme, M. (2018). Antagonistic Phenomena in Network Dynamics. *Annu. Rev. Condens. Matter Phys*, 9:463–84.

[87] Nacher, J. C. and Akutsu, T. (2013). Structural controllability of unidirectional bipartite networks. *Scientific reports*, 3:1647.

[88] Nakao, H. and Mikhailov, A. S. (2010). Turing Patterns in Network-Organized Activator-Inhibitor Systems. *Nature Physics*, 6:544–550.

[89] Nemhauser, G., Wolsey, L., and Fisher, M. (1978). An analysis of approximations for maximizing submodular set functions-I. *Mathematical Programming*, 14(1):265–294.

[90] Nepusz, T. and Vicsek, T. (2012). Controlling edge dynamics in complex networks. *Nature Physics*, 8(7):568–573.

[91] Newman, M. (2010). *Networks: An Introduction.* Oxford Univ. Press.

[92] Notarstefano, G. and Parlangeli, G. (2013). Controllability and observability of grid graphs via reduction and symmetries. *IEEE Transactions on Automatic Control*, 58(7):1719–1731.

[93] Ogata, K. (2010). *Modern Control Engineering*. Prentice Hall, 5th edition.

[94] Parlangeli, G. and Notarstefano, G. (2012). On the Reachability and Observability of Path and Cycle Graphs. *IEEE Transactions on Automatic Control*, 57(3):743–748.

[95] Pasqualetti, F., Zampieri, S., and Bullo, F. (2013). Controllability Metrics and Algorithms for Complex Networks. *IEEE Transactions on Control of Network Systems*, 1(1):3287–3292.

[96] Pecora, L. M. and Carroll, T. L. (1990). Synchronization in chaotic systems. *Physical Review Letters*, 64(8):821–824.

[97] Pecora, L. M., Sorrentino, F., Hagerstrom, A. M., Murphy, T. E., and Roy, R. (2014). Cluster synchronization and isolated desynchronization in complex networks with symmetries. *Nature Communications*, 5(May):1–8.

[98] Pikovsky, A., Rosenblum, M., and Kurths, J. (2003). *Synchronization: A Universal Concept in Nonlinear Sciences*.

[99] Pósfai, M., Liu, Y.-Y., Slotine, J.-J., and Barabasi, A.-L. (2013). Effect of correlations on controllability transition in network control. *Scientific reports*, 6:23952.

[100] Prado, T. D. L., Lopes, S. R., Batista, C., Kurths, J., and Viana, R. L. (2014). Synchronization of bursting Hodgkin-Huxley-type neurons in clustered networks. *Physical Review E*, 90(032818).

[101] Rahmani, A., Ji, M., Mesbahi, M., and Egerstedt, M. (2009). Controllability of Multi-Agent Systems from a Graph-Theoretic Perspective. *SIAM Journal on Control and Optimization*, 48(1):162–186.

[102] Rössler, O. E. (1976). An equation for continuous chaos. *Physics Letters*, 57(5):397–398.

[103] Ruths, J. and Ruths, D. (2014). Control profiles of complex networks. *Science*, 343:1373–1376.

[104] Schaub, M. T., O'Clery, N., Billeh, Y. N., Delvenne, J. C., Lambiotte, R., and Barahona, M. (2016). Graph partitions and cluster synchronization in networks of oscillators. *Chaos*, 26(9).

[105] Schimit, P. H. T. and Monteiro, L. H. A. (2009). On the Basic Reproduction Number and the Topological Properties of the Contact Network: An Epidemiological Study in Mainly Locally Connected Cellular Automata. *Ecological Modelling*, 220(7):1034–1042.

[106] Sedoglavic, A. (2002). A probabilistic algorithm to test local algebraic observability in polynomial time. *Journal of Symbolic Computation*, 33(5):735–755.

[107] Slotine, J.-J. and Liu, Y.-Y. (2012). Complex networks: The missing link. *Nature Physics*, 8(7):512–513.

[108] Slutsker, I. W. and Scudder, J. M. (1987). Network observability analysis through measurement jacobian matrix reduction. *IEEE Transactions on Power Systems*, 2(2):331–336.

[109] Snyder, C., Bengtsson, T., Bickel, P., and Anderson, J. (2008). Obstacles to High-Dimensional Particle Filtering. *Monthly Weather Review*, 136(12):4629–4640.

[110] Sorrentino, F., Pecora, L. M., Hagerstrom, A. M., Murphy, T. E., and Roy, R. (2015). Complete Characterization of Stability of Cluster Synchronization in Complex Dynamical Networks. *Science Advances*, 2(4):1501737.

[111] Stankovski, T., Pereira, T., McClintock, P. V., and Stefanovska, A. (2017). Coupling functions: Universal insights into dynamical interaction mechanisms. *Reviews of Modern Physics*, 89(4):1–50.

[112] Stigter, J. D., Joubert, D., and Molenaar, J. (2017). Observability of Complex Systems: Finding the Gap. *Scientific Reports*, 7(1):1–9.

[113] Strogatz, S. H. (2000). From Kuramoto to Crawford: exploring the onset of synchronization in populations of coupled oscillators. *Physica D: Nonlinear Phenomena*, 143(1-4):1–20.

[114] Su, F., Wang, J., Li, H., Deng, B., Yu, H., and Liu, C. (2017). Analysis and application of neuronal network controllability and observability. *Chaos*, 27:023103.

[115] Summers, T. H., Cortesi, F. L., and Lygeros, J. (2016). On Submodularity and Controllability in Complex Dynamical Networks. *IEEE Transactions on Control of Network Systems*, 3(1):91–101.

[116] Sun, J. and Motter, A. E. (2013). Controllability transition and nonlocality in network control. *Physical Review Letters*, 110(20):1–5.

[117] Takens, F. (1981). Detecting strange attractors in turbulence.

[118] Tang, H., Chen, L., an Lu, J., and Tse, C. K. (2008). Adaptive synchronization between two complex networks with nonidentical topological structures. *Physica A: Statistical Mechanics and its Applications*, 387(22):5623–5630.

[119] Tang, Y., Qian, F., Gao, H., and Kurthsc, J. (2014). Synchronization in complex networks and its application - A survey of recent advances and challenges. *Annual Reviews in Control*, 38(2):184–198.

[120] Tanner, H. (2004). On the controllability of nearest neighbor interconnections. In *43rd IEEE Conference on Decision and Control*, pages 2467–2472.

[121] Van Leeuwen, P. J. (2015). Aspects of particle filtering in high-dimensional spaces. *Lecture Notes in Computer Science*, 8964:251–262.

[122] Vidyasagar, M. (1978). *Nonlinear Systems Analysis*. Prentice Hall, 2nd edition.

[123] Wang, L.-Z., Chen, Y.-Z., Wang, W.-X., and Lai, Y.-C. (2017a). Physical controllability of complex networks. *Scientific Reports*, 7:40198.

[124] Wang, X., Li, T., Sun, S., and Corchado, J. (2017b). A Survey of Recent Advances in Particle Filters and Remaining Challenges for Multitarget Tracking. *Sensors*, 17(12):2707.

[125] Wang, X. F. and Chen, G. (2002). Synchronization in scale-free dynamical networks: Robustness and fragility. *IEEE Transactions on Circuits and Systems I: Fundamental Theory and Applications*, 49(1):54–62.

[126] Wang, X. F. and Chen, G. (2003). Complex networks: Small-world, scale-free and beyond. *IEEE Circuits and Systems Magazine*, 3(1):6–20.

[127] Watts, D. J. and Strogatz, S. H. (1998). Collectivedynamics of 'small-world' networks. *Nature*, 393(6684):440–442.

[128] Whalen, A. J., Brennan, S. N., Sauer, T. D., and Schiff, S. J. (2015). Observability and controllability of nonlinear networks: The role of symmetry. *Physical Review X*, 5(1):1–18.

[129] Wolfrum, M. (2012). The Turing Bifurcation in Network Systems: Collective Patterns and Single Differentiated Nodes. *Physica D: Nonlinear Phenomena*, 241(16):1351–1357.

[130] Wu, X., Zheng, W. X., and Zhou, J. (2009). Generalized outer synchronization between complex dynamical networks. *Chaos*, 19(1):013109.

[131] Wu, Y., Li, C., Wu, Y., and Kurths, J. (2012). Generalized synchronization between two different complex networks. *Communications in Nonlinear Science and Numerical Simulation*, 17(1):349–355.

[132] Yan, G., Ren, J., Lai, Y.-C., Lai, C.-H., and Li, B. (2012). Controlling complex networks: How much energy is needed? *Physical Review Letters*, 108(21):218703.

[133] Yan, G., Tsekenis, G., Barzel, B., Slotine, J.-j., Liu, Y.-y., and Barabási, A.-L. (2015). Spectrum of controlling and observing complex networks. *Nature Physics*, 11(9):779–786.

[134] Yang, Y. and Motter, A. E. (2017). Cascading Failures as Continuous Phase-Space Transitions. *Physical Review Letters*, 119(24):1–5.

[135] Yang, Y., Nishikawa, T., and Motter, A. E. (2017). Small vulnerable sets determine large network cascades in power grids. *Science*, 358(6365).

[136] Yuan, Z., Zhao, C., Di, Z., Wang, W.-X., and Lai, Y.-C. (2013). Exact controllability of complex networks. *Nature communications*, 4:2447.

Appendix A

Proof of Theorem 5.5

Proof. We follow Lemma 5.1. A change of coordinates $\theta_0 = \theta - \bar{\theta}$, with $\bar{\theta} = \sin^{-1}(\Delta\omega/2K)$, shifts θ_0 to the origin, yielding

$$\begin{aligned}\dot{\theta}_0 &= \Delta\omega - 2K\sin\left(\theta_0 + \bar{\theta}\right) \\ &= \Delta\omega - 2K\left(\sin\theta_0\cos\bar{\theta} + \cos\theta_0\sin\bar{\theta}\right).\end{aligned}$$

In addition, since $\left|\frac{\Delta\omega}{2K}\right| \leq \frac{\sqrt{2}}{2} < 1 < \frac{\pi}{2}$ by assumption[1], then $\cos\bar{\theta} > 0$ and the last expression can be rewritten as

$$\begin{aligned}\dot{\theta}_0 &= \Delta\omega - 2K\left(\sqrt{1-\left(\frac{\Delta\omega}{2K}\right)^2}\sin\theta_0 + \frac{\Delta\omega}{2K}\cos\theta_0\right), \\ &= \Delta\omega - \left(\Delta\omega\cos\theta_0 + \sqrt{4K^2-\Delta\omega^2}\sin\theta_0\right).\end{aligned} \tag{A.1}$$

Let $V(\theta_0) = \frac{1}{2}\theta_0^2,\ \theta_0 \in D_2$, be a positive definite Lyapunov function candidate for system (A.1), where $D_2 = \{\theta_0 \in \mathbb{R} : |\theta_0| < r < \frac{\pi}{2}\}$. It can be shown that

$$\dot{V}(\theta_0) = \Delta\omega\theta_0\left(1-\cos\theta_0\right) - \sqrt{4K^2-\Delta\omega^2}\theta_0\sin\theta_0 \tag{A.2}$$

is definite negative if $\left|\frac{\Delta\omega}{2K}\right| \leq \frac{\sqrt{2}}{2}$ and $\theta_0 \in D_2$. Hence, the candidate function is a Lyapunov function, establishing sufficient conditions for the local asymptotic stability of the origin.

[1]Notice that $\left|\frac{\Delta\omega}{2K}\right| \leq 1$ is a necessary condition for PS stability of a coupled pair of Kuramoto oscillators [113].

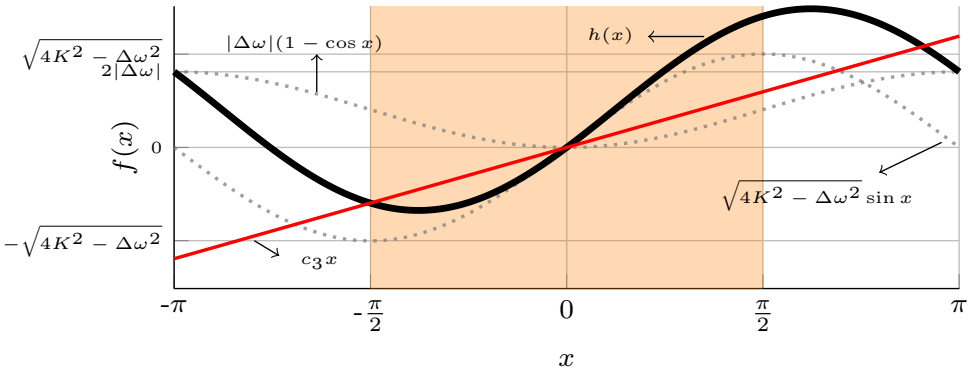

Figure A.1: Illustration of equation (A.3) derivation. The sinusoidal function $h(x)$, where $h(0) = 0$, is a sum of both functions depicted in gray dotted lines in interval $x \in [-\pi, \pi]$. The absolute value of the straight line of slope $c_3 = -h(-r)/r$ is the lower bound of $\text{sign}(x)h(x)$. The region of interest $|x| < r < \frac{\pi}{2}$ is highlighted.

The quadratic Lyapunov function $V(\theta_0)$ satisfies conditions (5.14) and (5.16) for $c_1 \leq \frac{1}{2} \leq c_2$ and $c_4 \geq 1$. Without loss of generality, condition (5.15) is satisfied as follows:

$$\begin{aligned} -c_3|\theta_0|^2 &\geq \left(\Delta\omega(1 - \cos\theta_0) + \sqrt{4K^2 - \Delta\omega^2}\sin\theta_0\right)\theta_0, \\ c_3|\theta_0| &\leq \text{sign}(\theta_0)h(\theta_0), \\ c_3 &\leq -h(-r)/r, \end{aligned} \tag{A.3}$$

where $h(x) = |\Delta\omega|(1 - \cos x) + \sqrt{4K^2 - \Delta\omega^2}\sin x$ and $\left|\frac{\Delta\omega}{2K}\right| \leq \frac{\sqrt{2}}{2}$ is a necessary condition to guarantee a positive c_3, for all $|\theta_0(t)| < r$. Figure A.1 illustrates (A.3) derivation.

By satisfying conditions (5.14)-(5.16), we prove that system (A.1) is exponentially stable. We can finally apply Lemma 5.1 and establish that, for a perturbation satisfying

$$|g(t,\theta)| \leq g_{\max} < \delta = -h(-r)\cdot\epsilon, \quad \forall t \geq t_0, \quad \forall\theta \in D_1, \tag{A.4}$$

the solution $\theta(t)$ is bounded by (5.25), where

$$\alpha = -\frac{(1-\epsilon)\cdot h(-r)}{r}, \quad b = -\frac{r\delta}{h(-r)\cdot\epsilon}. \tag{A.5}$$

Note that δ and b are dependent on r, where $-h(-r)$ is a monotonic function for all $r < \frac{\pi}{2}$ and radius r, in turn, can be chosen arbitrarily small (see Remark A.1). Thus, for a given $\Delta\omega$ and based on an optimal choice of r, one can define a *minimum*

threshold K_c, where condition $\left|\frac{\Delta\omega}{2K}\right| \leq \frac{\sqrt{2}}{2}$ is satisfied, via

$$\begin{aligned} g_{\max} &< \delta = -h(-r)\cdot\epsilon \\ g_{\max} &< \left(-|\Delta\omega| + 2K\cos\left(r - \tan^{-1}\beta\right)\right)\cdot\epsilon \\ g_{\max} &< (2K - |\Delta\omega|)\cdot\epsilon \\ K_c &> \frac{g_{\max} + |\Delta\omega|}{2\epsilon}. \end{aligned} \tag{A.6}$$

where $r = \tan^{-1}\beta$ and $\beta = \sqrt{4K^2 - \Delta\omega^2}/|\Delta\omega|$. It is straightforward to derive (5.26) from (A.4) and (A.5). □

Remark A.1. The states $\phi_i(t)$ of the Kuramoto oscillators and its phase difference $\theta(t)$ (and $\theta_0(t)$) are defined in $\mathbb{R}$, although they are strictly a 2π-periodic phase angle defined in $\mathbb{S}$. This definition is used in order to apply Lemma 5.1, which is only valid for $D \subset \mathbb{R}^n$, to the perturbed system (5.23). As $\phi(t) \in \mathbb{S}^n$, if $\Delta\omega \neq 0$, then there is, inexorably, a time instant t_0 for which $|\theta_0(t_0)| < r$, where r can be chosen arbitrarily small. Moreover, if conditions of Theorem 5.5 are satisfied, then, for all $\theta_0(t_0) < r$, $\theta_0(t)$ converges exponentially to the origin, yielding $|\theta_0(t)| < r, \forall t \geq t_0$. Under these conditions, $\theta_0(t)$ does not leave the interval $\left[-\frac{\pi}{2}, \frac{\pi}{2}\right]$ defined in $\mathbb{S}$. Note, however, that Theorem 5.5 restricts the analysis only to PS ultimately boundedness, not including intermittent PS.

Remark A.2. In Theorem 5.5, the choice of r was defined in order to maximize δ, thus extending Theorem 5.5 applicability to network systems with higher perturbations $g_{\max}$. Moreover, this guarantees that, for a given $g_{\max}$, the theoretical estimate of K_c is minimum. However, this choice of r is not concerned with providing the smallest theoretical estimate of b. Indeed, if it is of interest to obtain a tighter theoretical ultimate bound, the optimization problem in (A.6) can reformulated to find the optimal r for a minimum b subject to $g_{\max} < \delta(r)$.

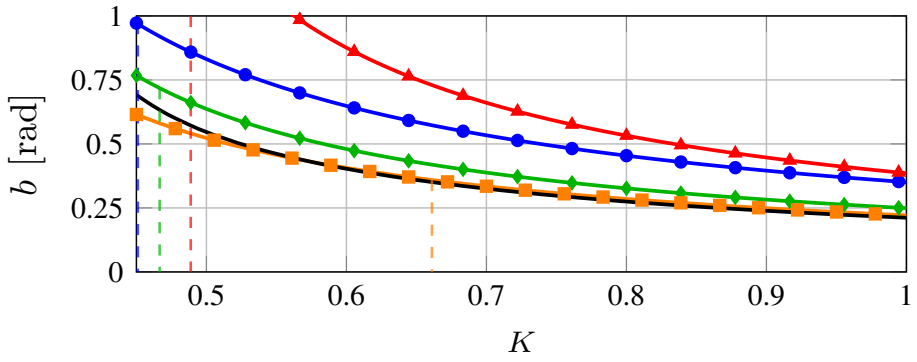

Figure A.2: Theoretical ultimate bound b versus the coupling strength K, for different values of r and $(\bar{\omega}_1, \bar{\omega}_2) = (1.0, 1.5)$. Numerical results are shown in black solid line. Theoretical results are shown for $r = \tan^{-1}\beta$ (circle); $r = \frac{\pi}{2}$ (triangle); $r = \frac{\pi}{4}$ (diamond), and $r = \frac{\pi}{8}$ (square). For each r, the threshold $K_c(r)$ is determined based on (A.4) and traced in the plot by a dashed line of respective color.

Figure A.2 shows how the choice of r is a trade-off between the estimates of b and K_c. If r is a constant for all values of K, the smaller r, the closer the theoretical estimate of b is to the numerical results and the higher the threshold K_c. In Theorem 5.5, we determine an adaptive choice of $r = \tan^{-1}\beta$ in order to acquire a minimum value for K_c—aiming for an increase of applicability of Theorem 5.5 in exchange for precision of b. Nevertheless, we see numerically in Fig. A.2 that its respective K_c is indeed the smallest, with a quite satisfactory estimate of b.